

Two-Photon Polymerization Lithography for Optics and Photonics: Fundamentals, Materials, Technologies, and Applications

Hao Wang, Wang Zhang, Dimitra Ladika, Haoyi Yu, Darius Gailevičius, Hongtao Wang, Cheng-Feng Pan, Parvathi Nair Suseela Nair, Yujie Ke, Tomohiro Mori, John You En Chan, Qifeng Ruan, Maria Farsari, Mangirdas Malinauskas, Saulius Juodkazis, Min Gu, and Joel K. W. Yang*

The rapid development of additive manufacturing has fueled a revolution in various research fields and industrial applications. Among the myriad of advanced 3D printing techniques, two-photon polymerization lithography (TPL) uniquely offers a significant advantage in nanoscale print resolution, and has been widely employed in diverse fields, for example, life sciences, materials sciences, mechanics, and microfluidics. More recently, by virtue of the optical transparency of most of the resins used, TPL is finding new applications in optics and photonics, with nanometer to millimeter feature dimensions. It enables the minimization of optical elements and systems, and exploration of light-matter interactions with new degrees of freedom, never possible before. To review the recent progress in the TPL related optical research, it starts with the fundamentals of TPL and material formulation, then discusses novel fabrication methods, and a wide range of optical applications. These applications notably include diffractive, topological, quantum, and color optics. With a panoramic view of the development, it is concluded with insights and perspectives of the future development of TPL and related potential optical applications.

1. Introduction


Additive manufacturing (AM), also known as 3D printing, offers various advantages over other tooling and manufacturing methods. These advantages include rapid prototyping, free-from morphology fabrication, minimized material waste, and potential cost reduction especially for low-volume production. It has enabled rapid progress in engineering, healthcare, and scientific research.^[1,2] 3D printing has revolutionized manufacturing processes through three categories of approaches: (1) bulk approach that requires printing within a material reservoir, such as continuous liquid interface production, laser stereolithography (SLA), digital projection lithography, two-photon polymerization lithography (TPL) with liquid resins, powder bed fusion, binder

H. Wang, W. Zhang, H. Wang, C.-F. Pan, P. N. S. Nair, Y. Ke, T. Mori, J. Y. E. Chan, J. K. W. Yang
Engineering Product Development Pillar
Singapore University of Technology and Design
8 Somapah Road 487372, Singapore, Singapore
E-mail: joel_yang@sutd.edu.sg

H. Wang
National Engineering Research Center for High Efficiency Grinding,
College of Mechanical and Vehicle Engineering
Hunan University
Changsha 410082, China

H. Wang
Greater Bay Area Institute for Innovation
Hunan University
Guangzhou 511300, China

D. Ladika, M. Farsari
IESL-FORTH
N. Plastira 100, Heraklion, Crete 70013, Greece

 The ORCID identification number(s) for the author(s) of this article can be found under <https://doi.org/10.1002/adfm.202214211>.

D. Ladika
Department of Material Science and Technology
University of Crete
Heraklion, Crete 70013, Greece

H. Yu, M. Gu
Institute of Photonic Chips
University of Shanghai for Science and Technology
Shanghai 200093, China

D. Gailevičius, M. Malinauskas
Laser Research Center, Physics Faculty
Vilnius University
Vilnius LT-10223, Lithuania

T. Mori
Industrial Technology Center of Wakayama Prefecture
Wakayama 6496261, Japan

Q. Ruan
Ministry of Industry and Information Technology Key Lab of
Micro-Nano Optoelectronic Information System
Harbin Institute of Technology (Shenzhen)
Shenzhen 518055, China

DOI: 10.1002/adfm.202214211

jet with solid particles; (2) extrusion method, where a nozzle dispenses materials, for example, fused deposition modelling, direct ink writing, direct inkjet printing, electrospinning, sacrificial/embedding printing, aerosol jet printing, and (3) laminated object manufacturing, that is, by layer-by-layer slicing, lamination of sheets or rolls.^[3–13] The specific choice of a 3D printing method is determined by the material, structure size, fabrication speed, physical and chemical stability, resolution, accuracy, and cost.^[14] As researchers are reacquainted with stunning optical effects in nature, studies of micro and nanoscale structures in biological specimens reveal clever manipulation of light by exploiting physical, chemical, and biological properties of materials.^[15–20] Accordingly, recent optical and photonic applications showcase high-resolution 3D printing, essential to fabricate structures with feature sizes comparable to the wavelength of light. To achieve high print resolutions, nanoimprinting has been developed as it's suitable for easy and rapid manufacturing with high-resolution features, while it's generally limited to structures with dimensions no more than two and half.^[21–24] Interference lithography also possesses similar advantages and is possible for 3D fabrication, but the pattern is not freely customized, and only limited forms of photonic crystals can be made.^[25,26] 3D self-assembly assisted by nanopipette nozzle is promising for complex 3D printing, nevertheless the slow printing speed, weak mechanical stability of structures, and easy jam of the nozzle, hindering the usage for fast and multiscale fabrication.^[27,28] 3D nanoprinting via charged aerosol jets is also demonstrated, making use of magnetic fields and dielectric masks to control the deposition of charged particles or ions.^[29] Finer structures can also be produced with focused electron/ion beam-induced deposition, but these methods are generally slow and costly, and suffer from the contamination issue during fabrication process.^[30–33]

In general, a method to tightly confine energy is required to induce a localized reaction within a volume close to the resolution needed. Hence, focused beams of charged particles (ions and electrons) and uncharged particles, namely photons, are the clear approaches. Arguably, charged beams are less suited for producing 3D structures at a practicable scale due to the inconvenient charge mitigation strategies with conductive substrate/material, ion induced material damage, and especially, the precise localization of electron-/ion-solid interaction in a 3D volume. Conversely, polymerization with light has been widely investigated as photon-initiated crosslinking is conveniently triggered in many kinds of polymers suited for 3D printing, thus lifting the issues mentioned above.^[34–42] However, the materials illuminated within the optical beam path

will experience some degree of polymerization when using the one-photon absorption (OPA) process, leading to reduced resolution, making fabrication of arbitrary 3D structures impossible.^[43–51] Conversely, bearing on the imaginary part of the third-order nonlinear susceptibility, the nonlinear process of two-photon absorption (TPA) is significantly different from OPA as the absorption cross section (ACS) is typically several orders of magnitude smaller than that of OPA. Practically, polymerization only occurs within a volumetric region where the intensity of light exceeds a threshold, achievable with pulsed (femtosecond) lasers. Here, TPA occurs in photoinitiator molecules, which form free-radicals that induce polymerization and crosslinking of nearby monomers, thus forming solidified crosslinked chains.^[52–57] Under ideal conditions, the rate of TPA is proportional to the square of the local light intensity I , thus the resolution could be a factor of square root two smaller than the diffraction limit. The concept of TPA was first described in 1931 by Goepfert–Mayer,^[58] but the first experimental verification of TPA was realized in 1961,^[59] after Theodore Maiman developed the first working laser in 1960. Another 30 years later in the early 1990s, femtosecond laser technology was developed,^[60] which enabled TPL as the laser energy can be spatiotemporally confined to induce TPA.^[61] In 2001, the “microbull” was fabricated with 120 nm feature size, that is, exceeding the optical diffraction limit at the 780 nm wavelength laser used,^[62] sparking great development in TPL related research and applications. Currently, this technology has been well commercialized into turnkey lithography solutions initially by Nanoscribe GmbH in 2007, and more recently with new companies, for example, UpNano, Multiphoton Optics, Femtika, etc. Their products and equipment have been widely applied to realize complex 3D structures in a variety of fields, for example, optics and photonics, biology, mechanics, acoustics, electronics, materials, etc.^[63–75]

As a direct laser writing (DLW) technology, TPL is well positioned for optical and photonic applications with fabrication capabilities of arbitrary 3D shapes. The polymerized structures are generally transparent in the visible band, with surface roughness < 10 nm, thus this technology has been intensively investigated and used to manipulate light since its inception. Here, we look back at the past development of TPL on optical and photonic applications and pay close attention to major milestones in the field, and envision future trends. The main content includes four sections (**Figure 1**), with fundamentals of the TPL principle and configuration to understand the light-matter interaction and operation process; different materials that can be polymerized in TPL, including organic photopolymers, such as acrylates, commercial IP-series, stimuli-responsive materials (SRM) for 4D printing, hydrogels, epoxy, and materials for non-TPL processes, hybrid polymers, such as metallic containing materials, inorganic dielectric materials, and emitting materials; fabrication technologies with overall process, focus modulation methods, high-quality structure fabrication from voxel to bulk, optimization of surface roughness, fine feature size fabrication methods and post-processing approaches like pyrolysis and calcination, other points like resin flow, resin transparency, and refractive index (RI) measurement, also molding and replication methods; in the application section, we classified the works into diffractive optics, imaging optics, fiber

S. Juodkazis
Optical Sciences Centre, School of Science
Swinburne University of Technology
Hawthorn, VIC 3122, Australia

S. Juodkazis
WRH Program International Research Frontiers Initiative (IRFI)
Tokyo Institute of Technology
Nagatsutacho, Midori-ku, Yokohama, Kanagawa 226-8503, Japan
J. K. W. Yang
Institute of Materials Research and Engineering
A*STAR (Agency for Science, Technology and Research)
2 Fusionopolis Way, #08-03 InnovisSingapore 138634, Singapore

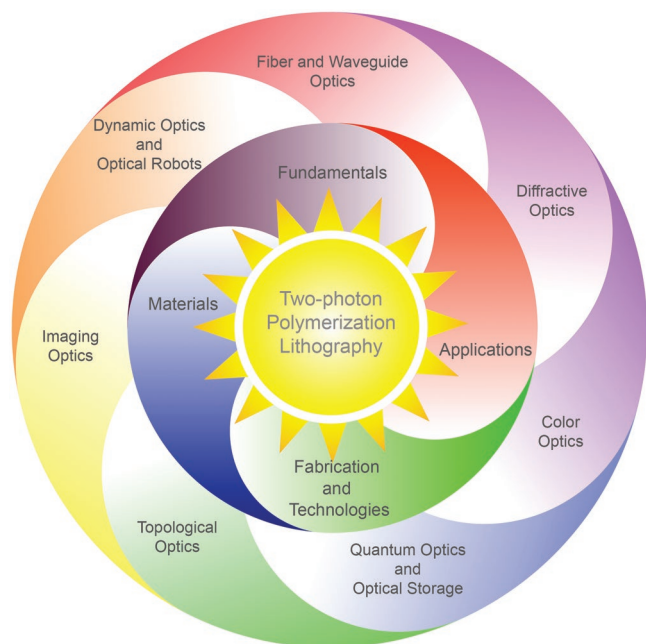


Figure 1. Schematic of two-photon polymerization lithography with different aspects and applications.

and waveguide optics, color optics, topological optics, quantum optics and optical data storage, dynamic optics and optical robots. In the end, we discuss the potential solutions to the current challenges and forecast the prospects of TPL in optics and photonics applications, aiming to promote the fusion of related physics, chemistry, and materials, and deepen our understanding of light-matter interactions.

2. Fundamentals

The basic configuration of a TPL 3D printing system is shown in **Figure 2a**. A femtosecond laser is collimated and propagates through an attenuator and expander, then passing through a shutter, which is generally a high-speed acoustic-optic modulator (AOM) to control the transmitted power of a laser beam

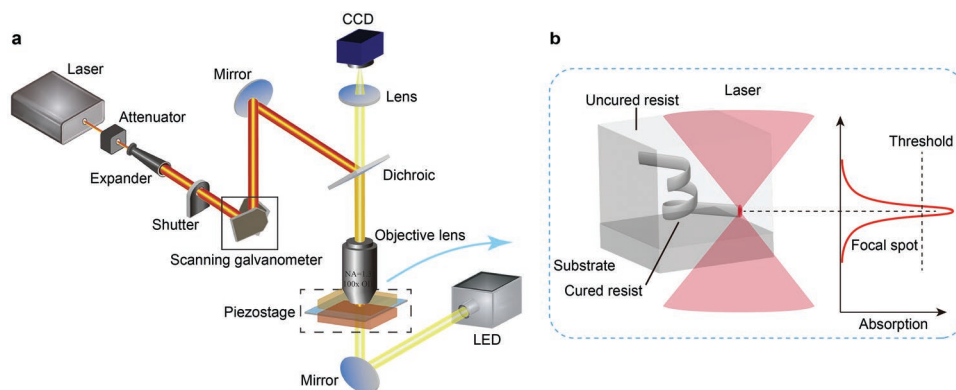


Figure 2. A typical setup of TPL 3D printing fabrication system in a) Adapted with permission.^[76] Copyright 2017, AIP Publishing. b) The schematic of TPA induced solidification of resist at the center of focal spot.

with an electrical drive signal. Afterward, the beam is deflected by a pair of scanning galvanometers (for xy positioning) and reflected into an objective lens. To observe the 3D printing in real time, the field of view (FOV) is illuminated with a light emitting diode (LED) source, and the fabrication process is captured by a complementary metal-oxide-semiconductor (CMOS) or charge-coupled device (CCD) camera with a dichroic mirror in front. In TPL printing, the nonlinear absorption only occurs at the center of the focal spot in which place the intensity of laser power transcends the threshold, hence inducing the curing process of monomers in photoresist with the help of photoinitiators (**Figure 2b**). The uncured resist can be removed by post-development, thus only the designed 3D structures remain on the substrate.

2.1. Moore's Law: Photons Packed in Time Equal Transistors Packed in Space

As the enabling technology for TPL is the ultra-short pulse laser sources, an overview of the progress in laser technology is presented here. In the last 20 years, the average power of ultra-short sub-1 ps laser sources has increased by 10^3 times and table-top lasers with $P_{av} \approx 1$ kW are readily available from several vendors.^[77] From the year 2000, the average power scales as $\text{Power} \approx 2^{N/2}$, in which N represents the number of years.^[78] This trend for photons packed in time (the average power) follows the Moore's law for transistors on a chip,^[78] which is still driving the microelectronics industry for the last 60+ years. The high average power defines an availability of single pulses of high energy at a high repetition rate f , for example, the pulse energy is $E_p = \text{Power}/f \approx 1$ mJ for 1 kW laser at 1 MHz repetition rate.

Ultra-short pulse lasers with $t_p < 1$ ps and power of 1 kW at frequency of 1 MHz made into compact table-top tools^[79] have been increasingly used for large-area material processing,^[80] including applications such as formation of ablation ripples for anti-frosting,^[81] super-hydrophobic,^[82] antibacterial and sensor surfaces, high efficiency solar cells for breaking the Lambertian limit of ray-optics light trapping, which currently defines the efficiency of commercial solar cells.^[83] The laser-textured surfaces with ripples have potential for use in heat-exchangers and

electro-/photo-catalysis applications, for example, hydrogen production. All these emerging large-area applications add to the earlier established laser cutting, dicing, drilling applications, which are becoming increasingly productive and competitive even where large volumes $> 10^2 \text{ mm}^3 \text{ min}^{-1}$ of material should be removed/ablated with high precision, for example, in mechanical machining and tooling of hard materials or in dentistry.^[84] At the fluence of $F_{\text{fast}} = e^2 F_{\text{th}}$, in which the threshold fluence F_{th} is determined by material properties such as mechanical strength, bandgap, evaporation temperature, and melting,^[80] the most efficient ablation rate for volume/time occurs, thus it could be employed to justify the development of high average power ultra-short laser sources. The heat induced ablation would not happen at F_{fast} since the pulse is short, so that the light energy absorption determined heat affected zone (HAZ) is still negligible. By fine tuning material excitation, accumulation of energy deposition based efficient laser ablation at a minimal fluence has been recently demonstrated with MHz-GHz burst mode high-power ultra-short lasers. Typically, the most efficient ablation occurs at fluence per pulse which is by a factor of e^2 larger than the ablation threshold.^[85] The exponential scaling fits well with the Beer–Lambert law determined optical energy absorption, albeit it's extracted from the empirical data on laser ablation rates of different materials. The skin depth absorption is within a region in which the intensity (fluence) decreases with the factor of $e^2 \approx 7.4$. In terms of energy deposition with the ultra-short laser pulse, the same scaling is expected for 3D TPL, as thermalization and transport out of the initial focus is minimal. The smallest energy required for ablation (removal) is evaporation but for the faster ablation it is ionization. Energy deposited into the electronic state during short pulses is coupled to matter which is heated, ionized and ablated afterward. Similarly, in polymerization, the energy in the electronic system couples to the polymer matrix, then heats it up and causes polymerization/crosslinking.

The average laser power defines achievable productivity and fabrication throughput for surface and volume patterning/modification^[86] and can be defined by the rate voxels/time of printing; the volume-element voxel is a convenient unit as it can be applied for both subtractive (–) and additive (+) 3D[±] printing at different focusing conditions (focal spot and volume sizes). The voxels/time can also be interpreted by a useful measure of printing rate in 1 s^{-1} , that is, Hz, which is related to data transfer rate and is increasingly relevant for solution of bottleneck in data transfer rates for continuous 3D printing using controllers for scanners and stages.^[87]

2.2. Light-Matter Interaction: Permittivity at High Irradiance

It is helpful to present basic expressions for evaluation of the light intensity at the focal region and changes of optical properties of material via its permittivity, a square of the refractive index. The average laser power required for 3D printing does not reveal the mechanism of light-matter interaction and energy deposition. The absorption of laser pulse depends on a combination of linear and nonlinear absorption pathways, which are intensity dependent $I_p = F_p/t_p$ as defined by the fluence F_p [J cm^{-2} per pulse] and pulse duration t_p . On

the material side, the permittivity $\epsilon = (n + i\kappa)^2$ determines the reflected R , transmitted T and absorbed A parts of light energy $A + R + T = 1$ (the energy conservation) according to the real and imaginary parts of the RI n and κ , respectively. Importantly, the $\epsilon(t)$ is time dependent and changes during the pulse as will be discussed further. The fluence, or energy per area defined by the focal spot radius r , pulse energy E_p [J], is $F_p = E_p/(\pi r^2)$ and can be very high for tight focusing into focal spots of few micrometers typically used in high resolution 3D TPL. It is convenient to define the focal spot size by the Airy disk, that is, the first minimum of the focused plane wave as $1.22\lambda/NA = 2.44\lambda f_{\#}$, where f-number $f_{\#} \equiv F/D$ expressed via focal length F and diameter of the beam D and the numerical aperture (NA)

$$NA = n \sin \left[\arctan \left(\frac{1}{2f_{\#}} \right) \right] \approx n \frac{1}{2f_{\#}} \quad (1)$$

it is valid as long as $\sin \alpha \approx \tan \alpha$ or $f_{\#} > 1.2$. and n is the RI at the focus. The Airy disk contains 86% of the laser pulse/beam energy. It is comparable with a transmitted power of a Gaussian pulse/beam through the aperture that has radius of the beam waist $1 - e^{-2} = 86.5\%$. When the laser beam is expanded and only its central part is entering the objective lens (clipped on the entrance pupil aperture), the intensity at the focus resembles Airy pattern with a ring. If the Gaussian pulse/beam is closely matching the entrance pupil of the objective lens, the intensity at the focus is Gaussian-like with radial profile

$$I(r) = I_0 e^{-2r^2/w_0^2} \quad (2)$$

where w_0 is the waist (radius). Light localization by a Gaussian-like pulse at $I_0 e^{-2}$ -level is stronger (smaller spot) than the Airy-disk. Here, we use Airy-disk spot size as a conservative estimate of fluence and intensity.

For practical mm-scale applications of 3D TPL, dry-objective lenses with high-NA = 0.9 are used, while for sub-wavelength resolution oil/liquid/resin immersion lenses with NA = 1.3 are typical. Considering typical near-IR wavelength $\lambda = 1 \mu\text{m}$ the focal spot diameter for NA = 0.9 is $2r = 1.22\lambda/NA = 1.36 \mu\text{m}$ ($2r = 0.94 \mu\text{m}$ for immersion NA = 1.3 case). For a $t_p = 200 \text{ fs}$ pulse duration and pulse energy of $E_p = 10 \text{ nJ}$, the fluence and intensity per pulse reads $F_p = 0.69 \text{ J cm}^{-2}$, $I_p = 3.44 \text{ TW cm}^{-2}$ (1.57 J cm^{-2} and 7.86 TW cm^{-2} for oil immersion case). These estimates will be referred to when mechanisms of polymerization will be discussed next since pulses of 0.5–5 nJ are typically used at different overlap and, hence, exposure dose during DLW. The dependence of 3D polymerization at different ultra-short pulse durations (sub-1 ps) and at different wavelengths reveals that high intensity values are required for 3D structuring.^[88] 3D laser polymerization conditions indeed require the high irradiance/intensity that compares with the ablation thresholds.

For comparison, these $F_p \approx 1 \text{ J cm}^{-2}$ and $I_p \approx 5 \text{ TW cm}^{-2}$ values exceeds the ablation threshold of Si for a single pulse at $F_p = 0.2 \text{ J cm}^{-2}$ ($I_p = 1 \text{ TW cm}^{-2}$) for ultra-short laser pulses,^[89,90] while a typical dielectric breakdown (ablation) threshold of transparent materials such as silica glass or crystalline sapphire is higher $\approx 12 \text{ TW cm}^{-2}$. Based on the Drude model, at the dielectric breakdown when a strongly ionized material transfers

into a plasma state, the real part of permittivity becomes $\Re(\epsilon) = 0$ (the definition of dielectric breakdown). The plasma frequency depends on electron density and electrons are following the driving light E -field. At a high intensity and pre-breakdown conditions, the material enters a transient epsilon-near-zero (ENZ) state $\epsilon = (n^2 - \kappa^2) + i2n\kappa$ with $n \approx \kappa$, which can be considered a transition from dielectric-to-metal (Die-Met).^[91]

Remarkable changes in absorbance and reflectance are taking place at the ENZ state (the Die-Met transition). Dielectric material changes from the state with $\epsilon > 1$ to $\epsilon < 1$, or negative, where $n < 1$ and $\kappa > n$, $\Re(\epsilon) \equiv \Re(\epsilon' + i\epsilon'') = \epsilon' < 0$, when it is approaching to the dielectric breakdown conditions $\epsilon \rightarrow 0$. At the ENZ condition $\epsilon \approx 0$, the perfect absorber $A = 1$ is also a perfect emitter $E_{em} = 1$ or $A \equiv E_{em}$,^[92] hence the maximum absorption with ENZ is exceedingly beneficial to the laser fabrication. Energy deposition depth is the skin depth at the conditions of exposure $l_{abs} = c/(2\omega\kappa)$ (for intensity I) and can be sub-wavelength at high (pre-breakdown) intensity, where c is the speed of light and $\omega = 2\pi K$ is the cyclic frequency. Reflected light from the ENZ region experience π -phase shift when permittivity transfers from $\epsilon > 1$ to $\epsilon < 1$. This affects near-field optical energy distribution and deposition in the subwavelength region to the ENZ volume.^[93,94] Since the ENZ-state of material is defined by strongly changing values of $\epsilon \propto n$, κ , it is appropriate to define them by instantaneous permittivity $\epsilon(t)$ and contributing to the light-matter interaction via a linear mechanism via defined $n(t)$ and $\kappa(t)$, rather a nonlinear augmentation to the permittivity via optical nonlinearities. This approach is used in the discussion of energy deposition.

2.3. Energetics of 3D Laser Polymerization/Printing

Typical 3D polymerization is carried out at $I_p = 1 \text{ TW cm}^{-2}$ per pulse applied with scanning speeds v_s for a strong overlap of pulses ($N \approx 10\text{--}100$ along scan) over the diameter of the focal spot $2r$ at repetition rate of f and defines the exposure dose for the resulting modification, for example, degree of crosslinking of photoresist.^[86] Comparison of exposure doses is the most relevant parameter between different materials and irradiation conditions, since the absorbed energy of light is the primary cause of the final state of 3D polymerization, which has also other important contributions from temperature and diffusion of chemical species participating in polymerization and taking place over several orders of magnitude in time, from ps-to- μ s. It is instructive to compare the dose for 3D polymerization using fs-laser pulses with the dose used in photolithography using cw-laser or UV-lamp exposures. This is of particular relevance since the same photoresists and resins developed and photosensitized for UV light exposure become popular for near-IR fs-laser polymerization, hence, linear vs. nonlinear optical exposure. Photoresists (negative and positive tones) produced for UV lamp or laser exposure need 0.1 J cm^{-2} dose for high contrast definition of patterns and a high rate of development $R_D \approx 100 \text{ nm s}^{-1}$.^[95] The development rate R_D vs exposure dose E_D —the Hurter–Driffield ($H\text{--}D$) retention curve—is a step-like function with the slope at its maximum defining contrast of the resist at the exposure wavelength for the direct (linear) absorption

$$\gamma_s = \left. \frac{\partial \ln R_D}{\partial \ln E_D} \right|_{\max} \quad (3)$$

The highest γ_s slopes are at $20\text{--}80 \text{ mJ cm}^{-2}$ dose window. Similar doses have to be accumulated for 3D fs-laser polymerization only via nonlinear energy deposition mode since exposure wavelength is inside a transparency window of photoresist matrix materials as well as photoinitiators doped at mM concentrations ($\approx 0.1\%$ by number density).

2.3.1. Multiphoton vs. Tunneling Ionization: Adiabaticity and the Keldysh Parameter

The dominance of multiphoton vs. tunneling ionization is defined by the adiabaticity or Keldysh parameter γ . It is shown below that classical, multiphoton absorption is more important than tunneling. This analysis assumes free carriers generation in the laser exposed material (photopolymer). The average intensity of the laser pulse is described as

$$I_a = c\epsilon_0 E_0^2 / 2 \equiv cB_0^2 / (2\mu_0) \equiv E_0 B_0 / (2\mu_0) \quad (4)$$

in which ϵ_0 , μ_0 are the permittivity and permeability of free space, respectively, E_0 [V m^{-1}] is the electrical field amplitude, $B_0 = E_0 c^{-1}$ [T] is the maximum magnetic field amplitude. The laser pulses generated electrons are regulated with the instantaneous intensity $I \propto EB$ in time, and for the Gaussian ultra-short laser pulse, the peak intensity is twice the average intensity I_p .

The nonlinear character of light-matter interaction is defined by the adiabaticity or Keldysh parameter γ . It is possible to reach tunnelling ionization threshold of materials at high irradiance/intensity once the surface or a volume of sample receives higher laser pulse intensity without air breakdown. The adiabaticity or Keldysh parameter:^[96]

$$\gamma = \frac{\omega \sqrt{2mE_g}}{eE_{laser}} = \frac{\omega}{\omega_t} \quad (5)$$

in which E_g is the bandgap energy of material, E_{laser} [V m^{-1}] is the electrical field at the peak intensity I_p , e , m are charge and electron mass (the effective mass in material), respectively, $\omega = 2\pi c \lambda^{-1}$ is the central angular frequency of ultra-short laser pulse, and $\omega_t = eE_{laser}/\sqrt{2mE_g}$ is the tunnelling frequency. When the photon energy is smaller than the bandgap $\omega < E_g \hbar^{-1}$, where \hbar is the reduced Planck's constant, Equation 5 is effective. For the classical case, that is, $\gamma \gg 1$, also called as large frequency and moderate (low) field condition, the multi-photon absorption dominates. For the quantum case, that is, $\gamma \ll 1$, also called as low frequency, high-field conditions, the tunnelling ionization dominates. When the required energy for electron tunnelling through the barrier is smaller than the incident photon energy $\omega_t < \omega$, the tunnelling is less efficacious in material ionization. Here, the flight time of an electron through the potential barrier determines ω_t as $\omega_t \propto 1 \text{ time}^{-1}$.

The parameter of γ could also be defined by the electron energy ϵ_e and its variation in one collision $\Delta\epsilon_e$ since $\gamma = \epsilon_e \Delta\epsilon_e (\hbar\omega)^{-2}$. the energy an electron gains by the end of the laser pulse of t_p duration is

$$\epsilon_e = \frac{A}{l_{\text{abs}} n_e} \int_0^{t_p} I_p dt \quad (6)$$

where A is the absorbance ($A = 1 - R$), n_e is the electron density.^[97] In such definition energy exchange between electrons that absorb light and solid state host matrix is evident. The change of electron energy is

$$\Delta\epsilon_e = \frac{2\epsilon_{\text{osc}}\omega^2}{v_{\text{eff}}^2 + \omega^2} \quad (7)$$

that is determined by the electron quiver energy and effective electron-phonon collision frequency as following

$$\epsilon_{\text{osc}} = \frac{e^2 E^2}{4m_e \omega^2} \quad (8)$$

The value of γ will be larger than 1 and the classical multiphoton absorption will dominate the ionization rate, if the electron energy ϵ_e and $\Delta\epsilon_e \approx \epsilon_{\text{osc}}$ are both larger than the photon energy. Therefore, for dielectric breakdown of silica or sapphire at 13 TW cm⁻², it yields $\gamma = 2$ for $E_g = 10$ eV and $\lambda = 1$ μm , hence, the classical rather quantum (tunnelling) case dominates. For 1 TW cm⁻² used in 3D polymerization, $\gamma = 4$ for $\lambda = 1$ μm and bandgap of $E_g = 3$ eV. The multiphoton seeding of electrons and their avalanche ionization that emerges at an irradiance of ≈ 1 TW cm⁻² at room conditions are key mechanisms.^[98] Avalanche is the dominant factor at the longer near-IR wavelengths since avalanche rate scaling as λ^2 (the free carrier absorption).

2.3.2. Nonlinear Energy Deposition in 3D Space

In additive 3D⁺ manufacturing, for example, metal powder sintering by lasers, an energy deposition per volume [J cm⁻³] is the defining parameter. The presented above analysis using fluence and intensity is established in light-matter interaction and surface ablation, however for 3D structuring by polymerization or material modification inside the volume of transparent material, the energy density is arguably the useful parameter.

The next part describes the absorbed energy and corresponding axially spatial localization. Here, The imaginary part of the RI determines the skin depth inside an optically excited dielectric material, because for electric field (E), it's $l_{\text{abs}} = c (\omega K)^{-1} = \lambda (2\pi K)^{-1}$ and for the intensity $I \propto E^2$, it's $l_{\text{abs}}/2$. At the end of the laser pulse, the absorbed energy density is $W_{\text{abs}} = 2AF_p/l_{\text{abs}}$ [J cm⁻³], in which the integral fluence for a pulse is

$$F_p = \int_0^{t_p} I(t) dt \quad (9)$$

Here, R is the reflectance and $A = 1 - R$ is the absorbance. $I(t)$ is the temporal envelope of intensity. The imaginary part variation of permittivity at high excitation inside a dielectric is:^[99]

$$(\Delta\epsilon_d)_{\text{im}} = \frac{\omega_{\text{pe}}^2}{\omega^2} \frac{v_{\text{eff}}}{\omega} = \frac{n_e}{n_{\text{cr}}} \frac{v_{\text{eff}}}{\omega} \quad (10)$$

in which $\omega_{\text{pe}} = e^2 n_e (\epsilon_0 m_e)^{-1}$ is the cyclic electron plasma frequency, ϵ_0 is vacuum permittivity, n_e is the electron density, $n_{\text{cr}} = \epsilon_0 \omega^2 m_e e^{-2}$ is the critical plasma density at the frequency of $\omega = 2\pi c \lambda^{-1}$. For instance, the n_{cr} is 1.05×10^{21} cm⁻³ at the wavelength of $\lambda = 1030$ nm, while the value changes to 4.2×10^{21} cm⁻³ at the second harmonic wavelength of $\lambda/2$; for comparison, the molecular densities of air 2.9×10^{19} cm⁻³ and water 3.34×10^{22} cm⁻³.

In dielectric medium, the permittivity at the ENZ conditions is

$$\epsilon_d = n_0^2 + i \times (\Delta\epsilon_d)_{\text{im}} = n_0^2 + i 2n_0 \kappa \quad (11)$$

where index im represents the imaginary part and n_0 is the real part of an unperturbed RI. The skin depth is expressed as:^[99]

$$l_{\text{abs}} = \frac{\lambda}{2\pi\kappa} = \frac{n_0 \lambda}{\pi (\Delta\epsilon_d)_{\text{im}}} = \frac{2cn_0}{v_{\text{eff}}} \frac{n_{\text{cr}}}{n_e} \quad (12)$$

that determines the energy deposition localization along the axial direction, then the density of absorbed energy is written as:

$$W_{\text{abs}} = A_0 \frac{v_{\text{eff}}}{cn_0} \frac{n_e}{n_{\text{cr}}} F_p \propto \frac{n_e}{n_{\text{cr}}} F_p \quad (13)$$

where $A_0 \equiv 4n_0/[(n_0 + 1)^2 + \kappa^2]$ is the unperturbed absorbance. The above equation shows that the most efficient energy deposition appears when the electron density n_e is close to the critical plasma density n_{cr} . As absorption of fs-laser pulse creates ENZ region at the focus, a positive feedback loop establishes, which further localizes energy deposition at a shallower depth along propagation. When the electron density $n_e \propto I_p^n \approx F_p^n$ generated by n -photon process approaches the critical density, the nonlinear absorption induced electron generation starts to saturate. The volume acts like a metal when the dielectric breakdown $\epsilon_d \equiv 0$ is reached, in which the energy absorption is proportional to the fluence, that is, $W_{\text{abs}} \approx F_p$ at $n_e = n_{\text{cr}}$. In addition, TPA with electron density following a $n_e \propto F_p^2$ power dependence (i.e., slope = 2) would result in $W_{\text{abs}} \approx F_p^3$ energy deposition per volume.

As 3D laser polymerization, nanogratings formation, structural damage, and so on, happens inside a strongly localized volume defined by strongly absorbing ENZ state, and compared with the fluence or intensity $F_p \propto I_p$, the absorbed energy density in the volume W_{abs} is relevant for the definition of optical nonlinearity. A shallow energy deposition into skin depth is important for the 3D laser polymerization as well as ablation. With high repetition rate and small pulse energy of MHz–GHz,^[100] the delivered energy can be optimized for the most precise modification in the burst mode. In this mode of ablation, 3D removal of material approaches a controlled evaporation, which requires the smallest energy required for ablation (removal of material). Interestingly, in respect of the pulse energy E_p (and F_p), the material removal by bursts is with a second order slope = 2,^[100] which is characteristic of the direct absorption by photoexcitation of electrons according to the discussion presented above. It is consistent with $W_{\text{abs}} \propto (n_e/n_{\text{cr}})F_p \propto F_p^2$ since $n_e \propto F_p$ as observed in experiment.^[100]

Importantly, a self-focusing power threshold is usually never reached for 1–10 nJ pulses (powers per pulse 5–50 kW per pulse for 200 fs pulse) and the interaction volume is localized within the focal volume that has depth-of-focus of double Rayleigh length $2z_R = n_0 \pi r^2 \lambda^{-1}$ inside material with RI n_0 . The energy deposition along this length depends on linear and nonlinear absorption as defined by intensity decrease along propagation direction (z -axis)

$$-\frac{dI}{dz} = \alpha I + \beta I^2 \quad (14)$$

where $\alpha = 4\pi K \lambda^{-1}$ is the linear and $\beta = \sigma^{(2)} N_{\text{TPA}} / E_{\text{hv}}$ [cm W⁻¹] is TPA coefficients, respectively, N_{TPA} [cm⁻³] is the density of TPA absorbing molecules, photon energy is $E_{\text{hv}} = h\nu$ [J] and $\sigma^{(2)}$ [cm⁴ s molecule⁻¹] is the TPA cross section in unit of 1 GM (Goepert–Mayer) = 10⁻⁵⁰ cm⁴ s molecule⁻¹. Comparison of α with βI , which both have the same units of absorption coefficient, allows to determine the corresponding contribution of linear and nonlinear absorption in energy deposition. Since photoexcitation at high pre-breakdown intensities ≈ 1 TW cm⁻² leads to permittivity changes and formation of ENZ, the absorption becomes time dependent $\alpha(t) \propto \kappa(t)$ and evolves on an ultra-fast time scale due to its electronic nature. Another factor contributing to an increasing weight of the linear term in absorption is due to the argument of number density of absorbers. A typical doping of a nonlinear TPA absorbing photoinitiator is on order of \approx mM (10⁻³ or 0.1% in terms of the molecular number density), while ENZ evolution is driven by excitation of the host matrix, which has a high molecular number density $\approx 100\%$. It is noteworthy that the here discussed a linear absorption term of αI is changing during the pulse and has a nonlinear character due to free carrier generation while the usual nonlinear TPA βI^2 term is defined nonlinear photoexcitation.

The TPA coefficients β and $\sigma^{(2)}$ are not usually provided by vendors of photoresists/resins and seldom measured. Apparently, $\beta \approx 20$ cm TW⁻¹ is required for TPA polymerization.^[101] This corresponds to $\sigma^{(2)} = 129$ GM considering a 0.1% molecular density of photoinitiator in the host polymer matrix $N_{\text{host}} = \rho N_A / M_{\text{host}}$ [cm⁻³] for typical resist molar mass $M_{\text{host}} \approx 234$ g mol⁻¹ and mass density $\rho = 1.2$ g cm⁻³,^[102] the Avogadro number N_A . At typical $I_p \approx 1$ TW cm⁻² intensities used in 3D polymerization, $\beta I \approx 20$ cm⁻¹, which is not a large absorption contribution via TPA. The strong absorption is defined by $\alpha d > 1$, where d is the length of absorption, for example, for $d = 1$ μ m, $\alpha = 10^4$ cm⁻¹. Moreover, estimates of $\sigma^{(2)} \approx 1$ –10 GM are more realistic^[103] also considering a spectrally narrow resonant TPA band.^[104] The actual contributions to a cumulative absorption coefficient $\alpha_c \equiv \alpha + \beta I$ along the axial depth of focus $\approx 2z_R$, requires knowledge of the fast-changing permittivity (ENZ. i.e., Die–Met state), hence, reflectance and absorbance as well as the axial extent of energy deposition (the skin depth). The required formulae presented above allows for estimation, while the exact values will depend on the irradiation conditions and photoresists. The known energy density in volume W_{abs} [J cm⁻³] is a useful parameter to reveal mechanism of 3D polymerization.

The final note to the described above energy deposition and polymerization is the local heating of the focal volume. Laser repetition rate R_{rep} and the exothermic nature of polymerization

can contribute to modification of polymerization and crosslinking, which needs further investigations. However, the temperature rise at the focal spot can be readily estimated.^[99] The thermal accumulation model was adopted to analyze multi-pulse thermal accumulation in polymerization.^[105] For a single pulse, the size of focal spot d_f , the diffusional cooling time is calculated as $t_{\text{th}} = d_f^2 / D_{\text{dif}}$, where $D_{\text{dif}} = k_T / C_p \rho$ is the heat diffusion coefficient of resist, k_T and C_p are the thermal conductivity and the specific heat capacity of resist, ρ is the density of the resist. For the temperature rise by one pulse T_1 , the temperature accumulation for N pulses is defined as:^[99]

$$T_n = T_1 (1 + \beta + \beta^2 + \dots + \beta^N) = T_1 \frac{1 - \beta^N}{1 - \beta} \quad (15)$$

where, $\beta = \sqrt{(t_{\text{th}} / (t_{\text{th}} + 1/R_{\text{rep}}))}$. This formula allows one to estimate the thermal accumulation effect, which could contribute to polymerization. It is also noteworthy that the energy density has the unit of pressure J m⁻³ = Pa and, at high intensity, the structural failure of photopolymer indeed has signature of expanded focal region.^[88]

3. Materials

Until recently, the majority of materials employed in TPL were developed for classic UV lithography or stereolithography applications. It is only during the last decade or so that materials specifically designed for TPL usage started to emerge. In all cases, however, the main constituents of these materials are the same: (i) a monomer/oligomer mixture, which will cross-link to allow the fabrication of a 3D structure and (ii) a photoinitiator, a molecule that will absorb simultaneously two-photon of the incident light, in order to produce the active species and eventually induce polymerization.^[67,106] Several combinations of monomer/oligomer and photoinitiators have been investigated in TPL.^[107–109]

Like the case in UV lithography, there are both positive and negative TPL photoresists. The most widely used and tested are negatives photoresists,^[110–112] in which two-photon exposure of the photoresist results in a cross-linked or polymerized 3D structure, allowing the uncured photoresist to be washed away after printing. In positive photoresists,^[113] light exposure leads to molecule chains to break apart, following by the creation of shorter chains that will then in the development step be dissolved and washed away. The materials that are used as TPL photoresists can be a liquid, a gel or a solid. Also, they can consist exclusively of organic molecules, or can be organic–inorganic hybrids. Generally speaking, the following requirements should be fulfilled for a suitable TPL photopolymer: (1) containing monomers, oligomers, or a mixture of those, which will connect during the TPL process to form the polymer skeleton making up the structure, (2) being completely transparent to the wavelength of the laser used for TPL, (3) at least one solvent that dissolves the monomer but not the final polymer, which is for development of structure and removal of the non-polymerized resin, (4) for the laser power used for TPL, The ablation threshold of the resin should be higher than its multiphoton polymerization threshold. In the following sections we

will describe the most widely used TPL photopolymers in optics and photonics.

3.1. Organic Photopolymers

3.1.1. Acrylates

Acrylate resins are the first group of materials that was used for TPL.^[126] Acrylate monomers still possess a significant role in the research area of TPL, as well as in industry, as they have a variety of properties that make them attractive. Acrylic monomers are in general low-cost and widely available, existing in a variety of formulations and compositions, thus they can provide functionalization. Additionally, they can be easily processed via spin coating or drop-casting, also transparent at the visible and the near-infra-red wavelengths, using a high polymerization speed and they can be dissolved in common solvents. Concerning the polymerized acrylate structures, they exhibit different shrinkage ratios with different printing parameters, and show mechanical and optical stability.^[127–130]

Commercial IP-Series: The need for more commercial photosensitive materials for TPL leads the Nanoscribe GmbH company to develop a variety of materials called the IP-series. These resins paved the way to the fabrication of structures with extremely large heights with high beam scanning speed, as some of them act as an index-matching liquid during the TPL procedure.^[131] Moreover, due to their specialized properties, fabrication of accurate optical structures with low roughness and 3D-structures with high aspect ratios and low shrinkage, were enabled with favorable mechanical stability.^[132] In addition, these photosensitive materials are capable of bio-photonics applications as they show biocompatibility and low autofluorescence. More applications of these materials have been investigated such as micro-optics,^[133,134] microfluidics,^[135] diffractive optical elements (DOEs),^[136] microelectromechanical systems (MEMS),^[137] and medical sciences.^[138] Except the widely used IP-Dip, IP-L, and IP-S, the newly developed high transparency IP-Visio, high refractive-index photoresin IP-n162, and flexible IP-PDMS, may extend the research field and inspire more interdisciplinary researches. IP-series resins are available exclusively to Nanoscribe GmbH customers.

Stimuli-Responsive Materials: Stimuli-responsive materials (SRMs) are materials that can vary their configuration over time upon external stimuli, such as temperature,^[139–141] humidity,^[142,143] light,^[144–146] electricity,^[147,148] and magnetic field.^[149,150] Recently, SRMs have been introduced to TPL,^[114,151–159] and structures with micron and nanoscale feature sizes have been achieved.

Early works in this field began with shape memory polymers (SMPs). Zhang et al. developed a Vero Clear based SMP resin suitable for TPL.^[114] To tune the mechanical properties of the Vero Clear, an 2-hydroxy-3-phenoxypropyl acrylate (HPPA) based elastomer was added to the photoresist at different ratios. With the customized resin, features at a resolution of ≈ 300 nm was achieved, which is ≈ 10 times higher than traditional high-resolution printing methods such as DLP^[139] and SLA.^[160] The printed structures can switch between the as-printed state and deformed state, due to the switch of geometry between

the as-printed and deformed states (**Figure 3a**). In a following work,^[115] they developed a stiff SMP suitable for TPL, which is an acrylic acid (AAc) and HPPA copolymer SMP crosslinked by dipentaerythritol penta-/hexa-acrylate (DPEPA). By tuning the ratio of the crosslinker, storage modulus as high as 100 MPa in the rubbery state can be obtained, which is one order of magnitude higher than previous reports. Benefiting from the high storage modulus in the rubbery state, the deformed and touched high-aspect-ratio nanopillars can recover to the as-printed state by overcoming the van der Waals force upon heating to 150 °C. Reconfigurable structural color with resolution $\approx 21\ 150$ dpi was demonstrated with these SMP nanopillars (**Figure 3b**).

Contactless programmable materials such as ionogel, liquid crystal elastomer (LCE), and electrically controllable materials can be considered when the mechanical programming process for SMPs is not possible, which is not convenient at micron and nanoscale for tunable optical devices. Delaney et al. developed an ionogel photoresist can be used for printing at submicron resolutions, which can realize reversible response to different vapors under atmospheric conditions.^[116] They dissolved acrylamide monomer, pentaerythritol triacrylate crosslinker, and 7-diethylamino-3-thenoylcoumarin photo-initiator into a tetrabutyl phosphonium chloride ionic liquid. They printed grids with submicron features by this customized ionogel photoresist by TPL. In the presence of water vapor, they observed a rapid change of structural color of the printed photonic arrays (**Figure 3c**).

3.1.2. Hydrogels

Another group of materials that has been studied extensively in TPL are hydrogels, which have been previously used in the realm of drug delivery and tissue engineering, but are still quite new in the optical fields. They possess similar constituents of the cell extracellular matrix (ECM), making them the perfect candidate for mimicking the cell's 3D environment.^[161,162] There are three groups of commonly used hydrogels: natural materials, modified natural materials and synthetic hydrogels. The natural materials are mainly developed by using proteins such as fibrogen, silk, bovine serum albumin (BSA), and collagen.^[163–171] The use of the above-mentioned macromolecules made it possible to synthesize biobased materials without initiators, thus these materials exhibit lower cytotoxicity than the commonly used TPL photoresists.^[172–174] Although natural materials are the closest imitation to the ECM, their mechanical properties are not ready for 3D scaffolds. To deal with this issue, researchers move to the modification of the natural polymers for use in TPL. This was fulfilled by adding acrylate and methacrylate groups to natural polymers such as gelatin,^[175] polylactide,^[176] chitosan,^[177] acrylated epoxidized soybean oil,^[178,179] and vegetable oil epoxy resins.^[180] The hydrogels are suitable for making biocompatible, flexible, degradable, or absorbable optical elements or devices on skin or inside bodies.

3.1.3. Epoxy

SU-8 is a unique epoxy-based photoresist, which can be polymerized via TPL, as it possesses eight epoxy groups per monomer.

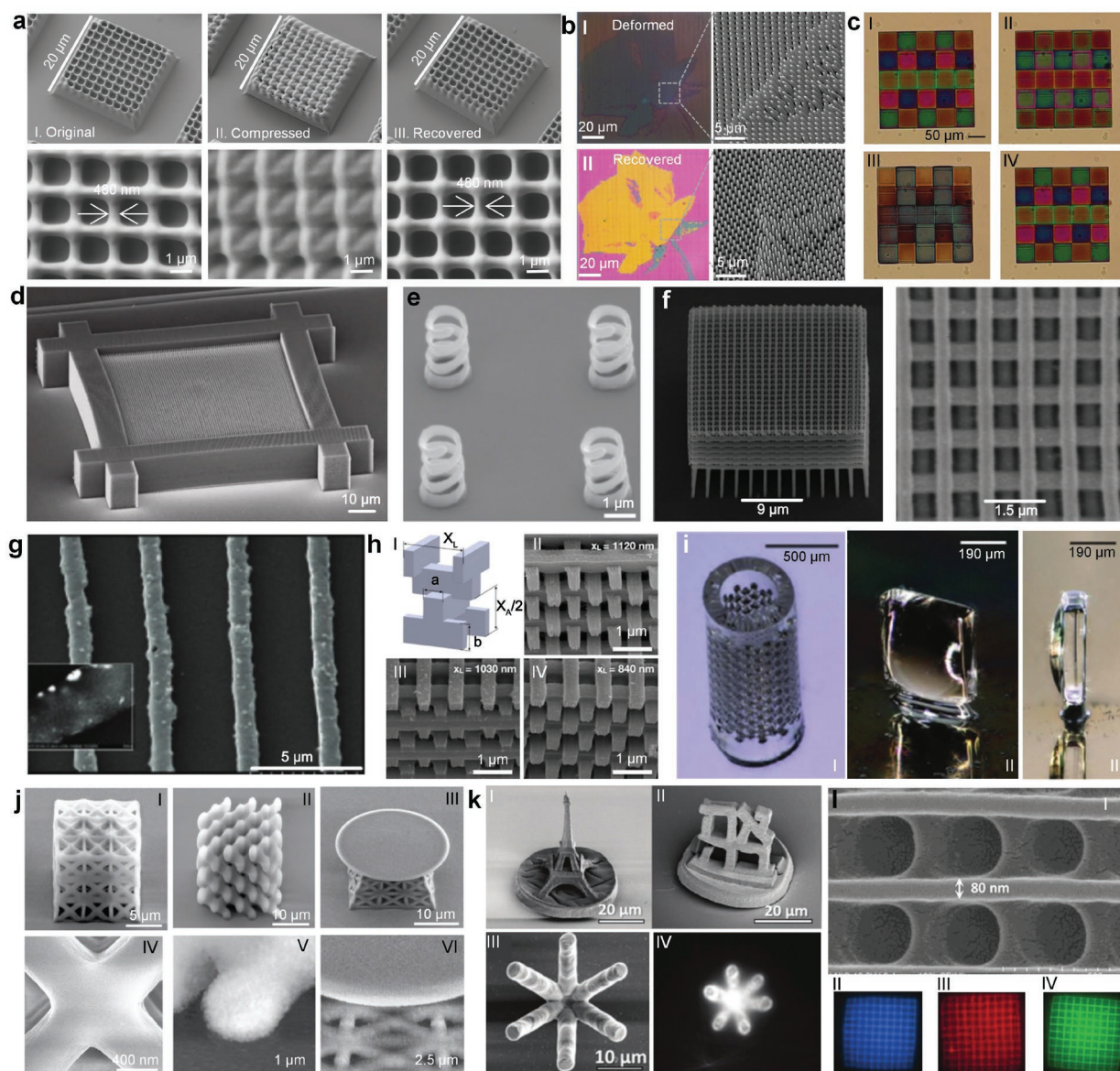


Figure 3. TPL of different materials for optics and photonics. a) Printing SMPs at submicron scale. Scanning electron microscope (SEM) images of SMP structures before and after programming and after recovery, respectively. Reproduced under terms of the CC-BY license.^[114] Copyright 2021, the Authors, published by Nature Publishing Group. b) Stiff SMPs for high-resolution reversible nanophotonics. I,II) The deformed and recovered nanopillars under optical microscope and SEM, respectively. Reproduced with permission.^[115] Copyright 2022, American Chemical Society. c) Vapor-responsive photonic arrays. I–IV) Optical image of a grid array in air, in water vapors ≈ 20 s, saturation with water vapors ≈ 88 s, and after the gas flow stopped, respectively. Reproduced under terms of the CC-BY license.^[116] Copyright 2021, the Authors, published by Royal Society of Chemistry. d) SEM image of a 40-layer face-centered-cubic photonic structure printed by SU-8. Reproduced with permission.^[117] Copyright 2004, Nature Publishing Group. e) SEM image of helices with an axial pitch of 800 nm and a radius of 800 nm fabricated by the two-step absorption photoresist. Reproduced with permission.^[118] Copyright 2021, Nature Publishing Group. f) 3D photonic crystal structures produced by TPL of low shrinkage hybrid photoresist. Reproduced under Optica Publishing Group Open Access Publishing Agreement.^[119] Copyright 2009, the Authors, published by Optica Publishing Group. g) SEM image of a grating structure with pitch size of 4 μm (inset: zoomed backscattered electron image) by TPL of sub-wavelength metallic structures in a polymer matrix. Reproduced with permission.^[120] Copyright 2010, Wiley–VCH. h) AM of high-refractive-index nanoarchitected titanium dioxide. I) A schematic of the woodpile. II–IV) SEM images of the sintered titanium dioxide woodpile structures with 1120, 1030, and 840 nm lateral pitch size, respectively. Reproduced with permission.^[121] Copyright 2020, American Chemical Society. i) TPL of Glassomer materials. I) Micro-filter element of fused silica glass printing by TPL. II,III) Tilt and side view of the printed fused silica glass upright lens. Reproduced under terms of the CC-BY license.^[122] Copyright 2021, the Authors, published by Wiley–VCH. j) 3D-printed silica with nanoscale resolution. I–III) SEM images of 3D-printed fcc lattice truss structure, diamond lattice truss structure and disc-on-truss structure, respectively. IV–VI) Zoomed-in SEM images of the corresponding structures in panel I–III. Reproduced with permission.^[123] Copyright 2021, Nature Publishing Group. k) 3D printing of micrometer-sized transparent ceramics. I–III) SEM images of printed polycrystalline structures after heating to 1500 $^{\circ}\text{C}$. IV) Top view optical image of the splitter heated to 1500 $^{\circ}\text{C}$ while illuminated by a laser in the center. Reproduced with permission.^[124] Copyright 2020, Wiley–VCH. l) TPL of light emitting materials. I) SEM image of woodpile with pitch size of 350 nm fabricated by TPL with quantum dots photoresist. II–IV) Photoluminescence images of printed polymer grids containing quantum dots with emission peaks at 460, 510, and 620 nm, respectively. Reproduced with permission.^[125] Copyright 2019, Wiley–VCH.

It was originally developed for LIGA (Lithographie, Galvanoförmung, Abformung—lithography, electroplating, and molding), a lithographic process for producing high aspect-ratio nanostructures. As radical polymerization is the most common process, the only composite that employs ions to be cross-linked is SU-8. It is from the early steps of the TPL, extensively used in the conventional 3D-laser lithography, due to its good processability, high resolution, and high mechanical strength.^[112,181–185] As it can be easily casted in films up to 500 μm thickness, which leads to 3D structures with high aspect ratios and excellent feature sizes. SU-8 is a low-cost material that needs to be heat-treated after polymerization, improving thermal stability in related applications.^[186–188] Last but not least, it's transparent in the visible and highly resistant to traditional solvents, making it suitable for many applications such as microfluidic,^[163] photonic (Figure 3d),^[117] biomedical structures.^[189]

3.1.4. Materials for Non-TPL Processes

Using some of the above-mentioned group of materials, a new way of fulfilling the TPL process was presented in the work of Vincent et al.^[118,190] Specifically, simultaneous TPA is replaced by consecutive two-photon polymerization, as a way to minimize the laser cost of the 3D printing and maximize the spatial resolution (Figure 3e). Common photoinitiators were used such as the quencher bis (2,2,6,6-tetramethyl-4-piperidyl-1-oxyl) sebacate (BTPOS) and the IP-Dip material to achieve fabrication of 3D printed structures, by a continuous-wave source and two-step absorption.

Another approach for TPL was demonstrated recently,^[191,192] in which triplet–triplet annihilation (TTA) paves the way to sub-micron resolution 3D printing inside the resin using an incoherent and low intensity LED source. Limberg et al. selected pairs of palladium (II) octaethylporphine (PdOEP) as the sensitizer and 9,10-diphenylanthracene (DPA) as the emitter, here the sensitizer was first excited with a green laser, ultimately leading to the triplet energy transfer from sensitizer to emitters, and TTA of closed two triplet emitter molecules.^[191] The resulting high-energy singlet emitter transfers energy to the photoinitiator. As the concentration of TTA shows a quadratic dependence on the excitation intensity, it leads to similar results with the TPL. Therefore, the TTA can also generate spatially confined excitation near the focal point of light. The resolution of their structure is higher than that of 3D printing using lanthanide upconversion nanoparticles that upconvert infrared to UV light because polymerization using those nanoparticles depends on the surface area of the particles in the photoresist.^[193]

Moving on with the non-TPL processes, TPL is a powerful DLW technique, but it lacks in fabrication speed, due to the point-by-point and layer-by-layer printing method.^[194] Volumetric 3D printing has been recently introduced, using tomographic principles.^[195–198] Specifically, tomographical illumination was applied in computed axial lithography to print transparent silica glass with high-viscosity resins.^[199] Besides, the development in different ways of nanofabrication lead to a proposed scenario by Liaros et al.,^[200] where resonance energy transfer in a donor–acceptor pair is presented for writing 3D

features in the far field. In this method, the donor will be a radical-producer molecule upon excitation, that is, acrylate resins, whereas the acceptor will not. Therefore, the population of excited donors will depend nonlinearly on the excitation intensity, which means that this will be a sequential two-photon process that involves real states. The benefit of the sequential two-photon process is that the excitation is resonant, and therefore low-power cost, continuous-wave lasers can be used to localize the generation of radicals within the focal volume, enabling 3D writing.

3.2. Hybrid Materials

One of the most common group of materials used for TPL is the hybrid organic–inorganic photoresists. The combination of the contradictory properties of the organic and the inorganic part of these materials makes them stand out in the competitive area of the TPL materials. Specifically, the organic part can achieve the tuning of the mechanical properties, the controlling of the porosity, and mainly bring extra physical or biological properties to the material. Whereas the inorganic part makes the material thermally and mechanically stable. It is also possible to vary the RI of the hybrid and lastly contributes to electronic, electrochemical chemical, or active photonic properties. These materials are mostly developed via the sol–gel method.^[110]

3.2.1. Metallic Containing Materials

Silicon-based organic–inorganic metallic elements containing materials are widely used as they combine the versatile properties of the hybrid but there are also optically transparent in the visible and commercially available.^[201–204] The generally studied silicate materials is the ORMOCER® (Organic Modified Ceramic), which has been applied in numerous photonic applications, and also as a scaffold for cell growth and biomolecule immobilization applications.^[205–209] Combining silicon alkoxides with monomers and other metal alkoxides makes the modification of the material properties possible for specific TPL applications, such as the silicon–zirconium hybrid SZ2080™, which is a transparent, biocompatible, and mechanically stable hybrid that can be used for complex 3D structures without shrinkage (Figure 3f).^[119,210–216] So far, different variants of silicon–zirconium composites have been investigated. Besides zirconium,^[217,218] other materials have also been employed such aluminum,^[219,220] titanium,^[121,130,221,222] silver,^[223] vanadium,^[224] nickel,^[225] zinc,^[226] germanium,^[227,228] ionogel,^[229] and graphene.^[229]

For other hybrid materials, Baltrukiene et al. investigated on organometallic polymers containing Al and compared them with other metal precursors.^[219] They achieved a high resolution, reaching < 200 nm feature size of the line and 3D structure. These results were comparable to those obtained using other organometallic polymers. The Al-containing structures underwent minimal shrinkage and deformation during the development process. Another approach is to use a metal salt reduction method to form conductive structures by 3D printing.^[230]

An interesting case is the vanadium one, which self-generates radicals by photoinduced reduction of the metal species, and until now it's the only element for redox multiphoton polymerization. Many groups have reported Au precursors (gold(III) chloride trihydrate) because Au is more stable and has higher conductivity than other elements.^[120,231–237] Shukla et al. demonstrated the fabrication of periodic structures comprising Au nanoparticles generated in situ and embedded in a matrix of the negative photoresist SU-8 (Figure 3g).^[120,231] They recently reported that a plasmonic mesh structure using a Au precursor fabricated over a large area, and structural coloration was demonstrated for the optical applications.^[237]

3.2.2. Inorganic Dielectric Materials

It should be noted that, to obtain a structure with almost pure inorganic composites, the post-sintering process is necessary to remove the organic polymers. These inorganic structures have different optical and mechanical properties compared to their organic counterparts. Using this strategy, Vyatskikh et al. developed a process to print 3D woodpiles of titanium dioxide.^[121] They used a ligand exchange reaction to get titanium (IV) acrylate precursor. The precursor was polymerized into complex 3D woodpiles by TPL in the presence of initiator (7-diethylamino-3-thenoylcoumarin) and crosslinker (pentaerythritol triacrylate). After printing, the woodpiles were pyrolyzed and the sintered structures shrunk by 60%. The main composition of the sintered structures is measured to be rutile titanium dioxide with RI of ≈ 2.3 . By varying the period of the sintered woodpiles (Figure 3h), they experimentally obtained band gap centers at 1.8–2.2 μm wavelength. Another extensively investigated material is glass. Kotz et al. achieved the 3D printing of glass, by using a conventional photopolymer mixed with SiO_2 nanopowder.^[238] Moving forward, in order to keep the superior mechanical, thermal and chemical properties of the glass as well as using the convenience of a photopolymer processibility, they introduced the Glassomer later.^[239] Glassomer has been used with a variety of photopolymers such as HEMA, IP-series by Nanoscribe GmbH (Figure 3i),^[122] and poly (ethylene glycol) diacrylate (PEGDA).^[123] Wen et al. developed a photoresist with a mixture of PEG-functionalized colloidal silica nanoparticles (with ≈ 10 nm in diameter) and polymer precursors containing trimethylolpropane ethoxylate triacrylate and PEGDA.^[123] They realized high-quality amorphous glass and polycrystalline cristobalite microstructures (Figure 3j) with sub-200 nm features after sintering, respectively. Using this process, they printed whispering gallery resonator with a quality factor of 1.1×10^4 at 1,554 nm. Furthermore, nanocomposite ink with rare-earth elements can be doped to realize colored glasses with submicrometric resolution. Coorstein et al. developed a particle-free ink to print transparent ceramics.^[124] They dissolved metal salts ($\text{YCl}_3 \cdot 6\text{H}_2\text{O}$ and $\text{AlCl}_3 \cdot 6\text{H}_2\text{O}$) and photoinitiator IRG 369 in water, ethylene glycol to make the photo-curable ink. After printing, the structures were heated to remove the organic parts. By doping the structures with yttrium aluminum garnet (YAG), they demonstrated the printed doped structures to function as laser with high thermal stability (Figure 3k).

3.2.3. Light Emitting Materials

To enhance the optical performance, emitting materials such as quantum dots (QDs), upconversion nanoparticles,^[240] perovskite nanocrystals,^[241] fluorescent molecules,^[181] and dyes^[242] can be doped into the resin to realize 3D photoluminescent structures for micro-optics and imaging.^[125,221,243–247] For example, Jradi et al. investigated the influence of the QDs (CdSe/ZnS, CdSe/CdS/ZnS) and laser power on the resolution of the printed structures.^[125] They found that QDs can improve the printing resolution with linewidth reaching 80 nm (Figure 3l). They show fluorescence images of the QDs-containing 3D grid structures with vivid color emission.^[247] With the high stability of optical, mechanical, thermal, and chemical properties, the TPL printed inorganic doped or pure inorganic structures have a great potential in variety of optical applications.^[122,199,248,249]

4. Fabrication Technologies

The realization of printing designed structures with 3D TPL and the final quality are influenced by plenty of factors, such as the configuration of the setup, including parameters of femto-second laser, NA and FOV of the objective lens, quality of focal spot, speed and stability of galvo scanning mirrors and piezo stages, modulation ability of acousto-optic modulator, etc.; the light-matter interaction with specific types of photoresists and printing parameter chosen; the environment like temperature, substrate, vibration and contamination; the develop methods and post-processing approaches. In the following sections, these factors are discussed starting from voxel modulation, to lines, and volume fabrication, and the optimization methods of bulk quality and surface roughness are reviewed. Furthermore, the recently proposed fabrication technologies are also included, which help to pave the steps forward to high-resolution structures and near-perfect optical elements.

4.1. Optimization of Printing Processes

The structuring success during 3D TPL fabrication obviously depends on the judicious choice of parameters per material used. For femtosecond laser-based polymerization, the determining parameters are wavelength λ ,^[88] pulse duration τ ,^[250] and repetition rate f_r ,^[251] in interplay with the choice of focusing conditions, polarization state,^[105] and scan velocity. The choice of dose parameters determine the minimum achievable 3D feature called “voxel”,^[252–255] and dependent on the scan algorithm and can distort the intended geometry.^[256,257] The difficulty arises in the fact even there is lack of standardization on how to set each combination of viable parameters for each desired practical outcome. Depending on the application compromise might not be allowed. For example, for optics surface roughness and shape fidelity is the most important^[258] but for microfluidic actuators it is the porosity on the molecular level^[209] or for biomedical cell scaffolds it is the throughput.^[212,259,260] Nonetheless, there is a trend that is leading to a potential standardization of how to approach the choice of parameter-to-material problem.

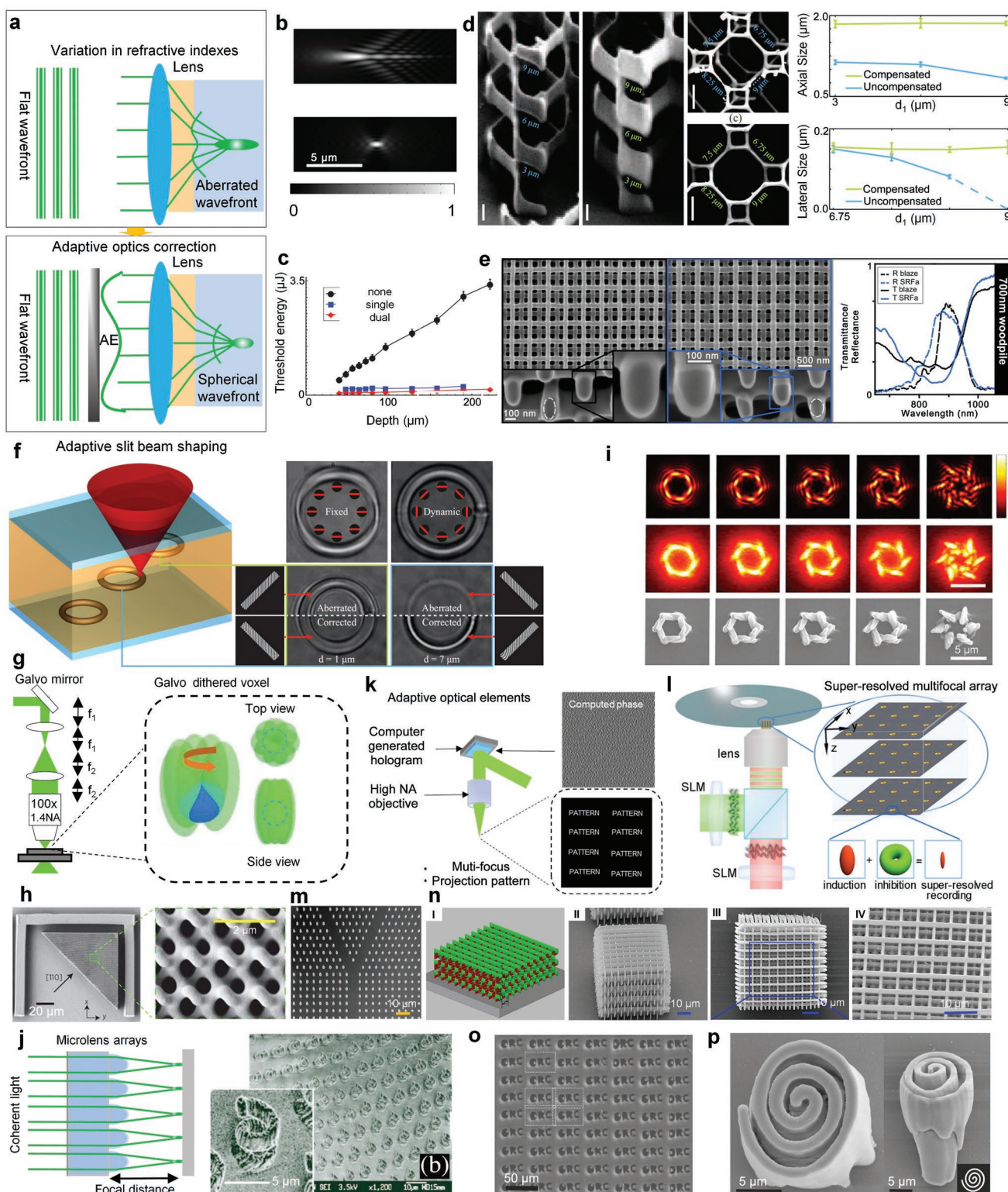


Figure 4. Focus modulation methods. a) Schematic diagram showing the spherical aberration in TPL. b) Simulated focusing with spherical aberration (top) and perfect focusing (bottom). c) The influence of spherical aberration on the TPP threshold energy as a function of depth. Reproduced under Optica Publishing Group Open Access Publishing Agreement with permission.^[273] Copyright 2011, the Authors, published by Optica Publishing Group. d) SEM images of photonic crystals in chalcogenide with high RI enabled by aberration correction. Reproduced under Optica Publishing Group Open Access Publishing Agreement with permission.^[274] Copyright 2014, the Authors, published by Optica Publishing Group. e) Woodpile photonic crystals written with blaze (left) and smoothed PSF (middle) enabled by AOE using amplitude filters and related transmission, reflection spectra. Reproduced under Optica Publishing Group Open Access Publishing Agreement.^[275] Copyright 2012, the Authors, published by Optica Publishing Group.

The approach being adopted is to select a challenge or benchmarking structure and produce 2D arrays of test objects with at least two varied parameters. They are typically used to find the parameter process window. The simplest 3D objects are suspended line objects (resolution bridges).^[102,261] Another type of test is to produce bulk simple geometric shape structures that are useful for measuring the best achievable surface roughness and shape distortions.^[262] The third category are complex shapes encompassing both high resolution and fine infilled bulky features. Usually, a common choice is to produce artistic shapes having a high degree of complexity.^[87,215,216,263]

Most current parameter optimization approaches focus on the increase of throughput via expanding the rapid structuring area. Usually, it is limited to the so-called FOV of microscope-based fabrication systems. To go beyond this area fast galvanometric scanners are employed together with the use of large travel distance translation stages. Usually, stages displace the sample and therefore scan the FOV area, while galvo rapid fabrication scan velocities approaching speed $> 1 \text{ cm s}^{-1}$ in a FOV area of around up to $200 \mu\text{m}$ in diameter for high-NA (1.4) focusing. If it's done step wise in an iterative manner, structures suffer from discontinuities,^[264] where “stitching” is necessary.^[265] This problem is being solved by either using area shape^[266] and dose management approaches,^[267] or algorithmically synchronizing the galvostage system to move in coordinated fashion in real time.^[87] This allowed to perform voxel size and aspect ratio to scan-velocity scaling tests over multi-orders under the same experimental conditions, indicating that the scaling will always be non-linear and require the adjustment of at least one more parameter.

Over the years, the influence of laser wavelength, pulse duration, repetition rate for accuracy, and fabrication throughput was studied quite extensively. However, the studies focused on material, photoinitiating systems, or some sole laser parameters, thus making it difficult to compare or extract the fundamental requirements for photopolymerization. Recently, it was demonstrated that a non-photosensitized resin can be used and photopolymerization can be triggered by non-amplified laser pulses,^[268] where both are necessary requirements by conventional wisdom.^[57] Moreover, current studies reveal that the laser wavelength is not of crucial importance for TPL as long as ultrafast pulses are used, thus enabling various confined photo-excitation mechanism leading “toward perfect polymerization”.^[88]

4.2. Focus Modulation Methods

The technology of TPL is well developed so far to fabricate 3D micro or nanostructures for optics and photonics, including photonic crystals,^[269] metamaterials,^[270] metasurfaces,^[271] and biomedical engineering.^[272] However, due to the diffraction limited nature of the focusing process and the single voxel fabrication scheme in TPL, there exist several technical challenges that hinder TPL in achieving high-quality 3D structures, such as spherical aberration, elongation of the writing voxel, and low fabrication efficiency for volumetric structures. Therefore, plenty of focus modulation methods are developed to tackle these challenges in TPL. This section discusses and summarizes the recent representative strategies of focus modulation in TPL, where the spatial and temporal properties of the focusing profile are modulated for various photonic scenarios.

4.2.1. Focus Modulation for Spherical Aberration Correction

The depth-dependent spherical aberration has a negative impact on TPL, resulting in a high two-photon polymerization threshold, low manufacturing precision, and low laser fabrication efficiency. Spherical aberration, in particular, occurs at the interface between the submersing material and the photosensitive material,^[283–285] and its strength is proportional to the NA of the objective, the RI mismatch between the material interface, and the penetration depth.^[286] The depth dependent spherical aberration primarily causes focus aberration in the optical axis and can significantly restrict the possibility for high-precision 3D fabrication in TPL (As is shown in **Figure 4a,b**).

Adaptive optical elements (AOEs), such as digital mirror devices (DMDs), liquid crystal spatial light modulators (SLMs), and deformable mirrors (DMs), have proved crucial for TPL, allowing for intricate control of the laser focus to eliminate aberration.^[287] These AOEs can be installed before the objective so that the compensation phase can be added on the laser beam, (as illustrated in **Figure 4b**, where the correction phase information is loaded on the AOEs). As a result, the aberration on the focus is canceled, resulting in a spherical phase distribution in the focus. Therefore, optimal laser-material modification and diffraction-limited performance may be accomplished everywhere in a 3D sample.

Based on the above concepts, focus modulation using AOEs has been widely studied and utilized in TPL for depth-dependent aberration correction.^[288] Wilson et al. mapped and

f) Adaptive slit beam shaping in TPL to fabricate curved microstructures. Focus modulation with galvo-dithered (GD) technique. Reproduced under Optica Publishing Group Open Access Publishing Agreement.^[276] Copyright 2013, the Authors, published by Optica Publishing Group. g) Schematic diagram showing the GD method. h) SEM images of miniaturized circular dichroism in gyroid nanostructures achieved by GD technique. Reproduced with permission.^[269] Copyright 2013, Nature Publishing Group. i) TPL fabrication of chiral surface using complex beam shaping with different topological number. Reproduced with permission.^[277] Copyright 2017, AIP Publishing. j) The schematic diagram of parallel focus generation using micro lens arrays and the 3D fabrication of chiral self-standing microspring array using MLA. Reproduced with permission.^[278] Copyright 2005, AIP Publishing. k) Schematic diagram showing the set-up for multi focus TPL and projection TPL. l) Multi-focus enabled super resolution optical data storage. Reproduced under Optica Publishing Group Open Access Publishing Agreement.^[279] Copyright 2015, the Authors, published by Optica Publishing Group. m, n) Photonic crystals fabricated by multi-focus TPL. Reproduced with permission.^[280] Copyright 2004, Optica Publishing Group. Reproduced with permission.^[281] Copyright 2015, Elsevier. o) Projection-based TPL fabrication of nanophotonic devices. p) SEM images of a single laser exposure fabricated 3D spiral pattern. Reproduced under Optica Publishing Group Open Access Publishing Agreement.^[282] Copyright 2013, the Authors, published by Optica Publishing Group.

acquired the analytic formulation of the depth-dependent aberration phase information from the focusing plane to the objective back aperture plane,^[275] and applied the AOE enabled focus modulation in a high NA confocal microscopic system. Booth et al. proposed a wavefront shaping (WFS) method. In this method, iterative optimization is used to compensate the optical scattering-induced distortions,^[286,289–291] or time-reversing the scattering wavefront.^[292–294] Further systematic study of the depth-dependent spherical aberration by Martin J. Booth's group shows that depth-dependent aberration would lead to detrimental elongated focus for TPL, leading to a higher threshold pulse energy for fabrication as laser penetrate deeper into the sample, with an elongated shape of the writing voxel along the optic axis (shown in Figure 4c,d). Through the application of a dual adaptive optics system,^[273] the threshold pulse energy for fabrication, delivered by AOE enabled aberration correction TPL system, becomes independent of the penetration depth in the photosensitive material, as is illustrated in Figure 4b, making larger depth TPL fabrication possible. For instance, with a NA of 0.95, the theoretical maximum penetration depth maintaining diffraction limited performance is estimated to be $\approx 10 \mu\text{m}$. With AOE enabled focus modulation method,^[295] the penetration depth can be extended by approximately two orders of magnitude,^[296] which has approached or exceeded the typical working distance of the high NA objective. By introducing a defocus decoupled adaptive optics approach into TPL, M. Gu's group demonstrated complex 3D photonic crystal with substantially improved the spatial fidelity and uniformity fabricated in the high RI chalcogenide glass As_2S_3 ,^[274] and the significant circular dichroism phenomenon in high agreement with theoretical calculations is demonstrated.

Aberration correction using AOE has also enabled the precise fabrication of high-resolution photonic devices in a wide range of materials and applications. Longitudinal photonic waveguides with the waveguide axis parallel to the substrate motion have been written inside glass.^[297] Laser-written fiber Bragg gratings,^[290] 3D data storage in polymers,^[288] and liquid crystal devices^[298] have also been achieved using TPL strategies with aberration correction. Ultra-large penetration depth $\approx 3 \text{ mm}$ with a NA of 0.45 has been achieved using a feedback system in a phase microscopy.^[297] A combined focus modulation method proposed by G. Freymann, demonstrated a focus modulation method to decrease the aspect ratio of the point-spread-function (PSF) using amplitude filters, which enabled the successful fabrication of the woodpile photonic crystals with high structural and optical quality (Figure 4e).^[275]

4.2.2. Focus Modulation for Complex Beam Shaping

Recent advances in focus modulation in TPL have also proved adaptive optics as an important tool in complex beam shaping, allowing the morphology of features generated by laser manufacturing to be more flexible than the conventional ellipsoid of a diffraction-limited laser focus.^[299–301] For photonic circuits,^[302] 3D chiral structures,^[303–305] and biomedical engineering applications,^[272,306] it is of great significance to develop focus modulation methods to fabricate structures with circular cross

sections. Gu et al. developed a method to generate a disc-like focus by installing an optical slit before the objective, therefore the focus profile can be spread in the direction perpendicular to the slit while maintaining the axial resolution (Figure 4f).^[276,307] The benefits of utilizing AOE to provide slit illumination include the ability to rotate the slit during fabrication, while preserving proper alignment of the focus disk and the curved paths. Additionally, AOE can alter the dimensions of the slit to adjust the profile of cross-section.^[308–310] Alternative techniques to generate circular cross section employ an astigmatic beam to adjust the laser-writing profile,^[311] where both focal position and beam waist in the sagittal and tangential planes are controlled by using an astigmatic beam, achieving symmetric waveguides with a feature size of $1.5 \mu\text{m}$. Adaptive elements such as DMS, SLMs have also been used to control the beam astigmatism and ellipticity for enhanced flexibility.^[312,313]

Another popular strategy in complex beam shaping in TPL is the application of galvo mirrors, or the galvo dithering (GD) technique.^[270] GD technique has been proved to be highly useful for photonic applications, such as optical activity,^[314] fiber-optical microendoscopy,^[315] and circular dichroism.^[316] It contributes to preserving the circular cross-section and smoothness of the micro structure, and thus maintaining the unique photonic properties.

To generate a circular symmetric shape of the fabrication voxel using GD technique in TPL, a 2D galvo-mirror (or a pair of galvo-mirrors) is usually employed to initiate a circular path to the focus, so that the photo-polymerization is constrained in the center of the circular path. As a result, the fabrication voxel in GD-TPL obtains a more circular symmetry than the typical ellipsoid, as is demonstrated in Figure 4g,h. The exact feature size of the fabrication voxel bases on fabrication conditions, including the beam power, the fabrication speed, and the dithering amplitude, an empirically relationship is described in reference.^[317] Through the utilization of GD-TPL, a nanoscale chiral gyroid network is achieved,^[318,319] where the right- and left-handed circularly polarized light operating at the wavelength of $1.615 \mu\text{m}$ can be efficiently separated, providing a new freedom of optical polarization manipulation. In addition, GD technique can also improve the fabrication speed in TPL, as the dithering speed can reach up to 1 mm s^{-1} , while the maximum speed of typical piezo nano-translational stage is $\approx 200 \mu\text{m s}^{-1}$. Therefore, GD technique has also become an important tool in fabrication large scale volumetric photonic devices in TPL.^[315]

Recently, optical beam carrying orbital angular momentum (OAM) has received widely attention in the research fields of holography,^[320] metasurface,^[271] which also excites the research interest in utilizing the OAM to shape the beam focus in TPL.^[321] To generate focus carrying varying states of OAM, AOE are usually introduced in TPL, where the phase information of the OAM is loaded.^[277,322] A series of complex microstructures have been demonstrated with modulated focus with different states of OAM (Figure 4i). Furthermore, donut-shaped depletion beam in stimulated emission depletion (STED) microscopy has also been generated and implemented for TPL fabrication of structures with sub-30 nm feature size,^[323–325] where system aberrations was taken into consideration, and higher-fidelity fabrication is achieved.^[326,327]

4.2.3. Focus Modulation for Parallel Fabrication

Focus modulation methods also help to address another challenge in TPL: the point-based voxel leads to long processing time, especially for 3D structures with large volumes or large scales, as the printing time is the third power of the object size. It may cost hours or even longer time to get a single device.^[328] Introducing focus modulation to achieve parallel fabrication in TPL is of great importance not only to improve the fabrication efficiency, but also can eliminate the drift errors during the fabrication,^[329] as components can be fabricated simultaneously. Therefore, several focus modulation approaches were developed to reduce the fabrication time through the generation of multi-focus or projection-based fabrication, such as introducing microlens arrays (MLA),^[278,330] or AOEes,^[331–333] into the TPL fabrication system.

To generate multi-focus array for parallel fabrication in TPL, a microlens array is first used as the focal objective.^[334] A schematic figure of MLA fabrication system is shown in Figure 4j. The feature size of this 2D focal array pattern is $\approx 2 \mu\text{m}$, and spots have been fabricated in parallel with this system.^[278] The advantage of the MLA fabrication system is the ability to fabricate a large area ($10 \text{ mm} \times 10 \text{ mm}$) at the same time. The 2D spot array pattern with a feature size of each spot is $\approx 2 \mu\text{m}$ can be parallel fabricated with this system. While it is convenient to use an MLA for parallel fabrication with large area, there are still three disadvantages related to the MLA method. First, the short working distance (in the range of several tens microns) limited by the focal length of each lens makes it not preferable in the achievement of the intrinsic 3D ability of the TPL. Additionally, the uniformity in the transmission of each micro lens prevents the MLA from fabricating functional photonic devices. Second, the aberration related to each lens makes the spatial resolution provided by the MLA incompatible to the widely used high NA objective. Third, as the arrangements of the MLA are limited to be triangle or square, it is impossible to generate arbitrary intensity patterns and intentional defects.

Another popular strategy to generate an array of foci for TPL is to display a computer generated hologram (CGH) on AOEes, such as DMDs and SLMs, using phase or amplitude modulation method (Figure 4k).^[281] To generate the CGH phase or amplitude modulation pattern, computational algorithm including the Gerchberg–Saxton method,^[335,336] optimal rotation angle (ORA) method,^[337,338] direct binary search, or multiplexing Fresnel lenses are usually used.^[279,339] As shown in Figure 4k, an array of focus spots is created in the focal plane since the CGH displayed on the AOEes is projected onto the pupil plane of the objective. The multi-focus array can be applied in TPL to simultaneously modify the photosensitive materials at once to reduce the fabricating time and increase the efficiency by orders of magnitude. This method has been widely used in optical data storage^[279] and photonic crystals fabrication (Figure 4m,n).^[280]

Due to the systematic mismatch in the optical set-ups and the unwanted 'zero order' in CGH, the generation of focus array with uniform intensities remains a challenging task.^[340–343] To increase the uniformity of the multi-focus arrays, various methods have been developed. In some cases, iterative computational optimization algorithm is introduced, but fur-

ther experimental calibration is required to improve the uniformity of the focal arrays.^[344–347] Therefore, large-scale parallelization in TPL can be realized with > 1000 foci demonstrated using a SLM.^[348] The focal array can then perform as a fundamental building block in TPL to make macroscale structures with micron scale features.^[349–352]

However, using multiple focus array in TPL is not the best option for efficient TPL fabrications, as the fabrication still utilizes single writing voxels. For volumetric microstructures, it is better to use intensity distributions with desired patterns in TPL. Therefore, projection-based focus modulation methods have been developed to provide very sharp TPL fabrication with a single time of exposure. Compared with CGH multi-focus method discussed above, projection based TPL utilizes AOE to provide amplitude modulation of the light beam, the modulated light beam then propagates through the objective, as shown in Figure 4l, leading to a large area of exposure in the sample. High speed TPL fabrication has been achieved using DMD devices,^[282,353] and more applications have been developed for surface processing.^[354] Simultaneous spatio-temporal focusing (SSTF) has also been readily developed by combining the project TPL with spatio-temporal method.^[355,356]

4.3. High-Quality Fabrication from Voxel to Bulk

The quality of 3D TPL printed polymer structures is mainly evaluated by the preservation of designed shape and uniformity of RI, which are vital for the performance in optical or photonic applications.^[63,357] Generally, the structures are deformed due to temperature changes, optical irradiation, or post-processing methods. The primary reason for the shrinkage and deformation in the fabricated structures is due to the low degree of conversion (DC) of resin,^[66,132,358–360] and nonuniformity of RI is caused by the inhomogeneous DC values in the volume. For typical TPL resins, differential scanning calorimetry (DSC), coherent anti-Stokes Raman scattering (CARS) spectroscopy, Raman microspectroscopy, and Fourier transform infrared (FTIR) spectroscopy etc. can be used to detect the DC value of polymerized resins with the following function^[361],

$$\text{DC} = \left[1 - \left(\frac{A_{\text{C}=\text{C}} / A_{\text{C}=\text{O}}}{A'_{\text{C}=\text{C}} / A'_{\text{C}=\text{O}}} \right) \right] \times 100\% \quad (16)$$

where, $A_{\text{C}=\text{O}}$, $A_{\text{C}=\text{C}}$, $A'_{\text{C}=\text{O}}$ and $A'_{\text{C}=\text{C}}$ are the C=O and C=C bonds corresponded integrated peak intensities of Raman peaks in the polymerized and the non-polymerized resins. They provide molecular details about the monomer/oligomer photo-conversion. However, 100% DC is not physically possible because of the formation of highly cross-linked networks that restrict functional group mobility, for example, the maximum DC values of IP-series photoresists are between 45 and 75%,^[362] and for polymerized IP-Dip, the maximum Young's modulus is $\approx 4.5 \text{ GPa}$.^[363] The incomplete photoreaction of the resin is also related with the intrinsic energy distribution at the focal spot of the Gaussian beam, and the subsequent removal of the unreacted resin during development also further deteriorate the final mechanical properties.^[363]

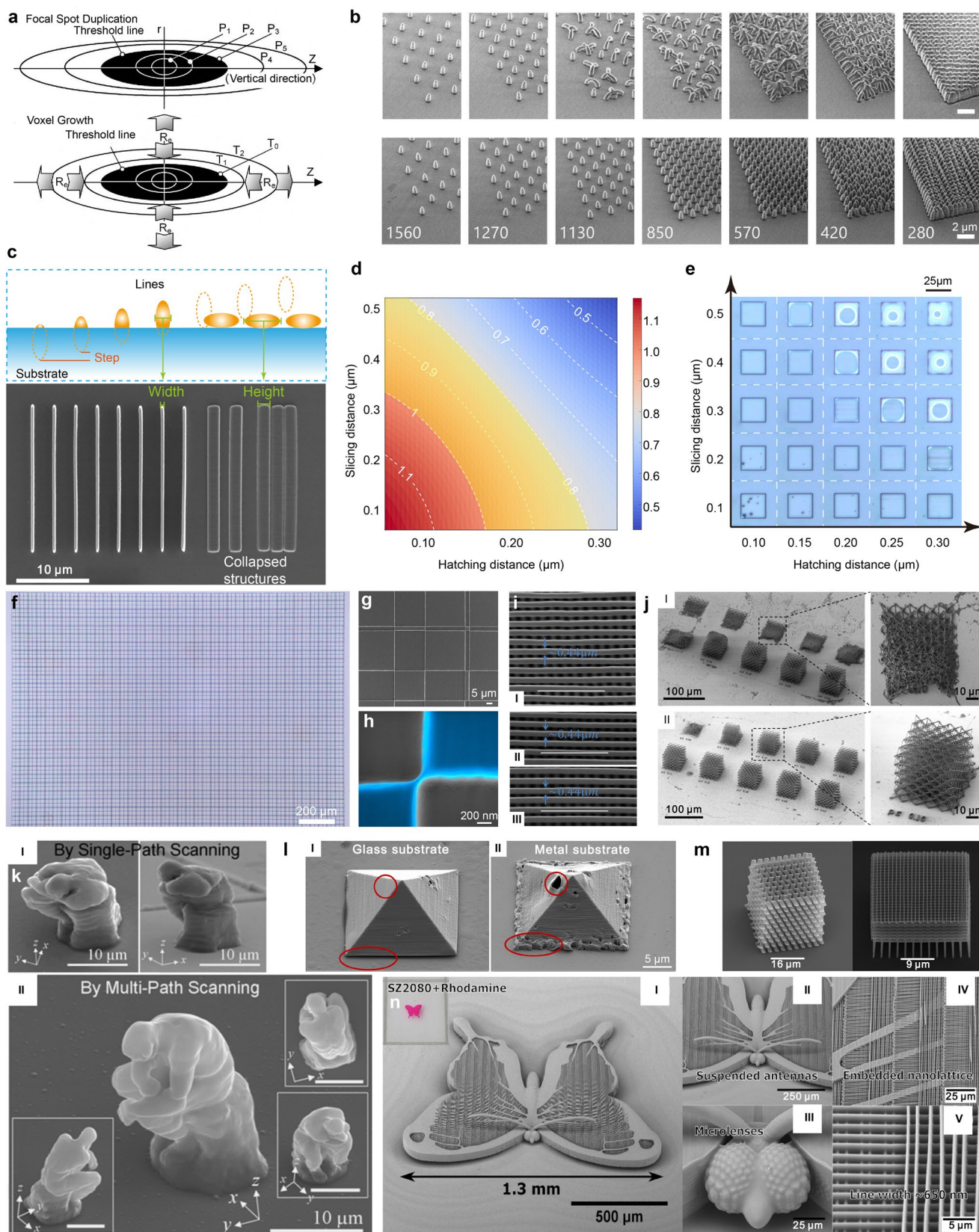


Figure 5. High quality structure fabrication with TPL. a) Models for initial voxels formation and growth. Reproduced with permission.^[253] Copyright 2003, AIP Publishing. b) Nanopillar arrays developed by the traditional (top) and UV curing method (bottom). Reproduced with permission.^[389] Copyright 2018, Elsevier. c) Side view plot (top) and top view SEM images (bottom) of the lines fabricated with ascending scan method. Reproduced with

To optimize the printing parameters and thus get a fine structure with desirable DC value and uniform RI, we can start with the 3D printing unit-voxel. The scaling law of voxel can be obtained by considering the polymerization kinetics with highly confined spatiotemporal scales to investigate the time and energy required for voxel with different laser irradiation (Figure 5a,b).^[252–255,364,365] Generally with short exposure time, the laser power is scaled with the inverse square root of the exposure time at the polymerization threshold, while for longer exposure time, Schwarzschild effect needs to be considered regarding of the diffusion of photoinitiator molecules and oxygen.^[366] The proximity effect of voxel arrays can be calibrated by considering the point spread function overlap and diffusion processes.^[256] When multiple voxels form into lines, the dimensions of width and height can be estimated,^[265,367] thus we can predict the optical damage threshold with the proximity effect of lines (Figure 5c).^[368,369] A lumped TPL parametric model with parameters of beam scan speed, laser power, slicing distance, and hatching distance based on single-photon absorption model was built to realize near-perfect 3D printing (Figure 5d–h),^[370] in which, the effect of employed microscope objective, printing configuration, substrate, and resin also should be included.^[371–375] The generally used substrate is glass, when silicon or metal substrate being employed, the interaction between pulsed laser with substrate should be described by the two-temperature model to get the electron and phonon temperatures. Increased temperature will reduce the heat conduction thus decreasing the reflectivity at the interface and vary the local refractive index. Furthermore, the accumulated heat and changed local laser power will alter the radical concentration and diffusion process, bringing significant influence on the polymerization results (Figure 5l).^[376] It has been demonstrated that due to the low polymerization threshold, resins with high viscosity are good for a large range of the pulse energy, with more freedom to control line width and height, fabrication velocity, and to achieve a more robust fabrication process.^[377] The absorption of resins also affects the range of printing parameters, for example, compared with SU8, pure SZ2080TM is ≈ 20 times more resistant to high irradiance,^[262] IP-S has highest transmittance with low scaffold density shell mode printing while IP-Visio is the best choice for broadband applications. OrmoCompTM has lower absorption but longer printing time is required.^[378] Additionally, with synchronization of the linear and galvanometric scanners, stitch-free mesoscale

structures with centimeter size but retaining micro- or nano-features can be obtained (Figure 5n).^[87] Recently, an algorithm considering physical quantities as simulation parameters to account for the main physical–chemical processes during fabrication is developed to predict the topography.^[379] Based on a spatial-temporal machine learning (ML) model, automated detection of part quality during fabrication with deep learning in millisecond with accuracy $\approx 95.1\%$ becomes possible.^[380]

To further enhance the mechanical properties and maintain the designed shape, fabrication methods like shape precompensation,^[381] multipath scanning method,^[382,383] and 2D slicing method^[384] were proposed. However, modifying the 3D model to compensate for the expected shrinkage needs complex and nonlinear shape compensation processes.^[381] Multipath scanning method can be used to reinforce the contour of 3D structures but with the increase of threshold region for polymerization, radicals diffuse outside of the initially formed voxel, thus the voxel size increases gradually, making it not suitable for an ultraprecise DOE fabrication (Figure 5k).^[385] One suggested method is to use resins that yield polymers with greater strength. For example, custom resins, such as sol–gel resins, with high ratio of Zr–O and/or Si–O content have been used to strengthen printed structures.^[210] Blending nanoparticles into resin could help to increase the DC value thus enhance the mechanical properties.^[386,387] The intrinsic high mechanical strength of the particles, or frames formed by nanowires and nanotubes can further strengthen the toughness of the printed structures. However, they should be uniformly mixed with the photoresist and will not cause local hot spots leading to bubbling during exposure procedure. Besides, the nanowires, nanotubes, and nanoparticles may cause strong light scattering, reducing the transmittance significantly if not index-matched to the resist or the size is large thus the effective medium theory not applicable. Furthermore, they may also induce greater surface roughness, hence lower the refraction or diffraction efficiency.^[388] Considering the general practicality and effectiveness, the unreacted groups can be post UV treated after the TPL process to further enhance the cross-linking density. In this way, the resistance against mechanical deformations and mechanical stability of structures are improved, with reduced number of defects and collapsed structures (Figure 5j).^[264,362,389,390] To increase the mechanical properties, thermal post-curing is also a simple but effective way to significantly eliminate the part functionality, characteristic coupling of processing parameters

permission.^[370] Copyright 2020, American Chemical Society. d) Normalized single-photon absorption (unit: α_s) of 3D-printed blocks calculated with printing parameters of laser power 25 mW and scan speed 40 000 $\mu\text{m s}^{-1}$. Orange yellow area represents the high-quality block with single-photon absorption value between ≈ 0.8 and ≈ 1.0 . e) Optical micrograph of fabricated blocks with printing parameters in (d). f) Optical micrograph of the high-quality large-area 3D-printed DOEs and corresponding SEM images in (g,h). Reproduced with permission.^[370] Copyright 2020, American Chemical Society. i) Top-view micrographs of log-pile structures with the same dimension while written by different laser power and beam scan speed combinations. Reproduced with permission.^[367] Copyright 2016, IOP Publishing. j) comparison of collapsed (top) and UV cured (bottom) octet-truss cubes printed with increasing laser peak intensities. Reproduced under Optica Publishing Group Open Access Publishing Agreement.^[362] Copyright 2016, the Authors, published by Optica Publishing Group. k) SEM images of deformed “micro-Thinker” printed with single-path scanning method (top) and precise fabrication with double-scanning path (bottom). Reproduced with permission.^[382] Copyright 2007, AIP Publishing. l) Pyramid written on a glass substrate (left) and on a metal substrate (right). Reproduced under Optica Publishing Group Open Access Publishing Agreement.^[376] Copyright 2019, the Authors, published by Optica Publishing Group. m) Photonic crystal structures printed with zirconium sol–gel material with negligible shrinking. Reproduced with permission.^[210] Copyright 2008, American Chemical Society. n) Synchronized galvanometric scanners and linear stages for a mesoscale butterfly fabrication. Reproduced under Optica Publishing Group Open Access Publishing Agreement.^[87] Copyright 2019, the Authors, published by Optica Publishing Group.

and material properties, by self-initiated thermal curing reaction with no thermal initiator.^[391] It is noteworthy that the non-uniformity of mechanical property could be used for dynamic optical applications, and structures with nonuniform RI, such as directionally controlled printing generating birefringence effect, gradient RI lens, waveguides in volume structure, and phase separation based printing resulting in inherently nanoporous structures for scattering manipulation.^[392]

Furthermore, during post-development, capillary forces above the elastic limit can cause significant defects when the solvent evaporates.^[363] Liquids with low surface tension and viscosity have been used to reduce capillary forces, such as hexamethyldisilazane and nonafluorobutyl methyl ether.^[377,389,393–396] In addition, critical point drying with liquid CO₂ can also mitigate capillary force effects during drying to help prevent shrinkage and deformation.^[397]

4.4. Surface Roughness

Apart from the ultrahigh quality of 3D TPL printing, surface smoothness is also essential for practical applications, especially for high performance optical and photonics devices.^[370,398,399] Both reflective and transmissive photonic devices inevitably request nanoscale surface roughness for efficient and accurate purposes,^[370,398] which is also suitable to fiber based optics.^[399] To evaluate the smoothness and quality of the 3D TPL printed surface, the surface roughness is usually defined as following,^[63]

$$Ra = \frac{1}{lr} \int_0^l |Z(x) - Z_0| dx \approx \frac{1}{n} \sum_{i=1}^n |Z_i| \quad (17)$$

where, l is the scanning length across the surface, $Z(x)$ is the surface height at each spot, while Z_0 is the averaged surface height, and Z_i is the surface height at the sampling point i . To minimize the surface roughness, three different strategies are commonly adopted individually or in combination: (1) increasing the voxel overlap or reducing the voxel size, (2) customized slicing and scanning strategies, (3) post processing such as thermal reflow.

In 3D TPL printing, the gaussian laser beam is usually focused by the objective lens tightly, resulting in a voxel resembling a spinning ellipsoid, as shown in **Figure 6a**. The overlap of such ellipsoid voxels plays an important role in fabricating nanostructures and controlling the surface roughness. The definition of the overlap can be given as following,^[63,400]

$$\delta = \frac{d-dx}{d} \times \frac{l-dz}{l} \quad (18)$$

where, δ is the overlapped section, d is the diameter and l is the length of the ellipsoid voxel, dx and dz are the hatching and slicing distances, respectively (**Figure 6a**). With the increase of overlap and the decrease of the voxel diameter, not only the precision of the fabricated structures will be increased,^[357,401] surfaces roughness will also be reduced into nanometer level (**Figure 6b**).^[63,267] Experimentally, the surface roughness can

be reduced to ≈ 10 nm by appropriately choosing the voxel and scanning parameters (**Figure 6a–c**).^[370,402] These results have been verified using characterization methods like optical profilers, atomic force microscopy, and scanning electron microscopy. Furthermore, in such overlap of voxels, the self-smoothing and self-polymerization effects contribute to minimize the surface roughness.^[228,403–405]

In fabrication of applicable 3D structures, such as microlenses and micro 3D objects, the slicing and scanning strategies are essential in smoothing the surface and saving the fabrication time.^[406] As shown in **Figure 6d–f**, the micro jar can be divided into six regions according to the slope angle.^[407] In the region of gentle slopes, the slicing distance is required to be small to prevent the separations of voxels and keep those voxels well overlapped. While in the region of steep slopes, the slicing can be loose to save the fabrication time. Owing to the optimized slicing distance at different regions, this slicing strategy is called subregional slicing method (SSM). Compared with a constant rough slicing distance, SSM clearly shows a smoother surface while keeping the fabrication time almost the same (**Figure 6g**). When the object to be fabricated is cylindrically symmetric, annular scanning mode (ASM) holds technical superiority over linear scanning methods, as shown in **Figure 6h,i**. When combined with a dynamic slicing distance (**Figure 6h**)^[408] or a shell fabrication method (**Figure 6i**),^[264,409] the surface roughness and fabrication time can be further minimized. Specifically, the surface of the microlens becomes more and more gentle when it reaches the lens top, thus an equal-arc scanning (EAS, **Figure 6j**) together with a shell fabrication method would precisely control the surface roughness and accelerate the fabrication.^[404,410]

As a post processing, thermal reflow is often used in microlens fabrication and controlling surface topography and surface roughness.^[411–414] This long-standing technique has been proven successful both in experiments and theoretical analysis. However, a burgeoning method provides more capability in the form of conformal selective surface smoothening, when combined with 3D TPL printing and nanoimprint lithography (NIL).^[415–417] In the polymeric material, a vertical gradient material contrast, which is expressed by molecular weight M_w /glass transition temperature T_g , can be created through the 172 nm UV light, realizing a selective surface reflow limited in a superficial region without effect on the bulk.^[418–421] As shown in **Figure 6k**, the surface roughness of TPL printed mold can be reduced to 10 nm in its PMMA replica.^[422]

4.5. Feature Size

Except from the high quality and surface roughness of 3D TPL printed structures, the feature size is another vital focus where researchers are concerned about. It relies on not only the intrinsic mechanical properties of the photoresists,^[102,423] but also the configurations of the fabrication system, printing parameters used,^[424] and other techniques applied. The 3D structures with feature size beyond the diffraction limit extend the photonic research toward shorter wavelength, that is, from near infrared, visible band, to the UV range.^[425]

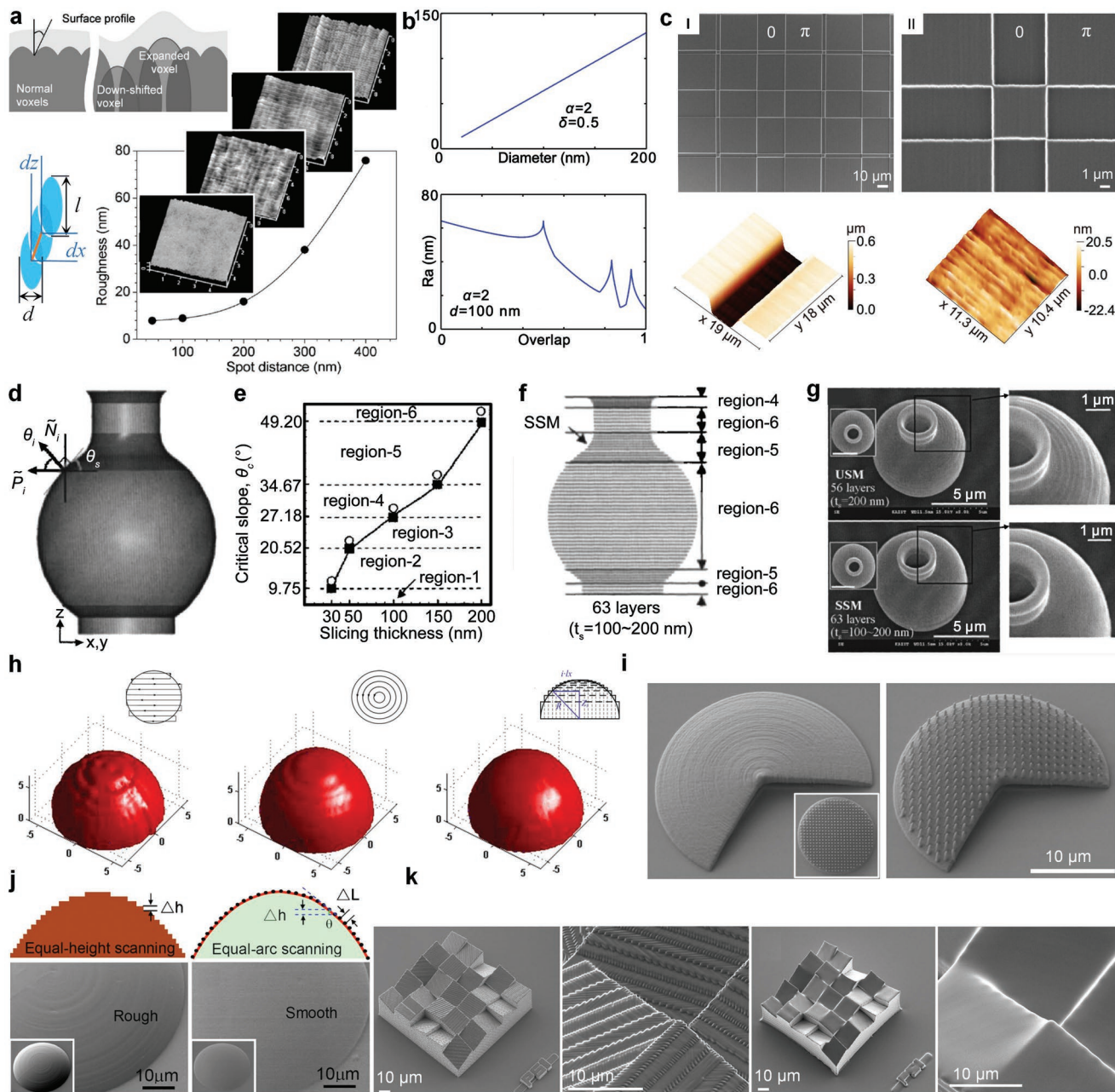


Figure 6. Surface Roughness of 3D TPL printing. a) The effect of voxel overlaps on the surface roughness of TPL printing. Top panel: self-smoothing effect against displacement caused by vibration or voxel fluctuation caused by laser jittering. Bottom panel: schematic figure for voxel overlaps. Right panel: the relationship between surface roughness and spot distance. Reproduced with permission.^[402] Copyright 2005, AIP Publishing. b) Top panel: the relationship between surface roughness and spot diameter. Bottom panel: the relationship between surface roughness and overlap. Reproduced with permission.^[63] Copyright 2015, AIP Publishing. c) SEM and atomic force microscope (AFM) images taken when the voxel diameter, hatching and slicing distance are appropriately chosen. Reproduced with permission.^[370] Copyright 2020, American Chemical Society; d, e) shows the SSM for surface smoothing in 3D TPL printing. Reproduced with permission.^[407] Copyright 2005, AIP Publishing. (d) Schematic figure of the surface slope angle θ . (e) variation of the critical slope angle θ_c . f) Slicing distances of SSM at six different regions. g) fabricated nano jar by using the uniform slicing method (top panel) and SSM (bottom panel). h) Microlenses fabrication by three different scanning strategies. Left: parallel linear scanning mode. Middle: annular scanning mode with a fixed slicing distance. Right: annular scanning mode with a dynamical slicing distance. Reproduced under Optica Publishing Group Open Access Publishing Agreement.^[408] Copyright 2006, the Authors, published by Optica Publishing Group. i) Microlens with nanopillar color-filter fabricated by annular scanning method with calculated microlens heights and core-shell fabrication strategy. Reproduced with permission.^[409] Copyright 2021, American Chemical Society. j) Microlens fabricated by annular and equal arc scanning method. Reproduced with permission.^[404] Copyright 2010, AIP Publishing. k) Selective surface thermal reflow method to minimize the surface roughness as a post processing. Reproduced with permission.^[422] Copyright 2017, Wiley-VCH.

4.5.1. Fabrication Methods

In general, the feature size is related with the wavelength of femtosecond laser, hence it is easier to obtain a smaller feature size with 532 nm laser than 780 nm laser, while the current setups are still limited with the printed linewidth ≈ 150 nm in the horizontal plane. The laser focus position with respect to the substrate can be controlled to realize < 100 nm feature size,^[426] but it's strongly constrained with the substrate, hence the structure is limited to 2D. It is also possible to initiate the polymer growth with hot electrons from plasmon-assisted polymerization,^[427–431] but it is localized adjacent to the metallic resonators. An instinctive method is to reduce the exposure power of laser and simultaneously reduce the pitch, however, the low mechanical stability and proximity effect hinder the further improvement of the feature size for a true 3D structure.^[432] As aforementioned, diffusion-assisted high-resolution TPL approaches and STED have been proposed and the printing resolution can be pushed down to 9 nm (Figure 7a,b).^[325,433–436] These methods requires complex setup modification and precise beam alignment between writing beam and inhibition beam. Leveraging on the high collimation enabled by extraordinary ENZ metamaterial features—a nanocavity in metal/insulator/metal/insulator (MIMI) configuration (Figure 7c,d), ultrathin dielectric hyper-resolution nanostructures are realized with a size reduction of 89% in height and 50% in width respectively, compared with the standard printing method. The height of the structures can be changed between 5 and 50 nm.^[437] When the difference of the refractive indices between the substrate and photoresist is significant, for example, silicon substrate, interference between the incident light and the reflected light occurs. The interference yields a standing wave, making a periodic energy redistribution in vertical direction, thus polymerizes the photoresist with a morphology exactly following the amplitude of the standing wave. The interference-assisted TPL produced structures have feature size ≈ 100 nm and the profiles are like the ridge-lamella configurations in the Morpho butterflies (Figure 7e), which is extremely hard to direct fabricate with conventional TPL method.^[438–441] Currently, the fine structure is constrained just above the substrate with height tuned by laser power, the direction and dimension of the lamella are not freely controlled due to the mechanism. Besides, combining self-assembly with TPL can realize the hierarchical photonic crystal structures with colloidal nanoparticles defined fine feature and 3D model determined profile (Figure 7f). Though sub-10 nm feature size is possible, this method suffers from the intrinsic defects generated during the self-assembly process, and the frame inside is fixed by the lattice, not flexible.^[442] Considering the stability during wet develop, which induces capillary force to deform the printed structures, a reliable way is to post-process the printed objects with shape-preservation methods other than directly fabricating ultrafine structures. Isotropic oxygen plasma etching could easily and quickly reduce the feature size of polymerized 3D structure even down to 25 nm,^[443] at the same time maintain the initial shape, therefore this method can reach to the mechanical limit of the printed structures (Figure 7g). In addition, the elongated laser spot induced high aspect ratio of polymerized lines can be avoided. By writing several lines in an overlapped manner to increase the width first,

then perform plasma etching, aspect ratio of height to width 1:1 is achievable, not the typical value of 3:1.

4.5.2. Pyrolysis/Calcination

In structuring various materials, two main aspects are the most important. The first one is practically achievable feature size (also referred as resolution or spatial accuracy) without critical loss of mechanical stability and fabrication repeatability.^[359] The second one is the achievement of significant improvements to the intrinsic material properties (physical, chemical, and/or biological).^[444,445] Most notable are mechanical stability (like Young's modulus),^[359] chemical inertness, optical transparency,^[262,446] refractive index,^[121,133,228] laser induced damage threshold (LIDT) level,^[368,447] and so forth. A straightforward, simple and widely applied way to achieve improvement of both feature size and material properties is heat-treatment as a post-processing step—it results in increased degree of DC, which in turn influences mechanical and chemical properties.^[391] Different results can be achieved by selecting the specific material and annealing protocol. Materials can include purely organic, hybrid organic–inorganic, and, most recently, colloidal composites, and even specialized inorganic resins (Figure 8a). The treatment method comes down to choosing either oxygen containing atmosphere—calcination, or inert atmosphere—pyrolysis performed in argon, nitrogen gas or vacuum.^[448]

Pyrolysis allows carbonization of structures made from organic resins such as PMMA, PETA based (e.g., IP-Dip) and epoxy class materials like SU-8 (Figure 8b).^[451] They feature the highest downscaling rate reaching 10% as a record value.^[443] The materials are usually carbonized, benefiting from the properties expected from high strength carbon materials.^[452] Calcination can also be used in cases where material inversion is required. Performing atomic layer deposition on top of the organic 3D template and later evaporating it results in production of hollow inorganic structures.^[453] Hybrid resists, in particular, metal–organic network containing resist such as SZ2080,^[210]Ormocomp,^[454] and others can be treated in both types of atmospheres.^[451] Scaling here is less pronounced due to remaining inorganic fraction of the substance as a backbone (Figure 8c).^[215,455] Such materials can remain highly transparent for wide range of spectrum.^[456] They also can be converted to inorganic glasses or even glass–ceramics at above 1000°C.^[216] Currently achieved features dimensions already exceeded < 100 nm barrier needed to be classified as nanotechnology.^[216] Combined with plasma etching before the heat treatment, a nm-scale super-resolution structures can also be produced.^[443] The resulting composition can be foreseen by considering the metal constituents in the initial state.^[216,457] Most commonly, this refers to silicon that, with oxygen in the network, produces SiO₂ glasses as mentioned before in the material sections. Third, the last class of resins are the pure inorganic ones. The most recent demonstration was done with hydrogen silsesquioxane (HSQ).^[450] The thermal treatment step, in contrast with the forementioned cases, is performed as an essential step after single photon exposure or imprinting (Figure 8d). It is a less popular resin, as harsh developers (like fluoric acid) are

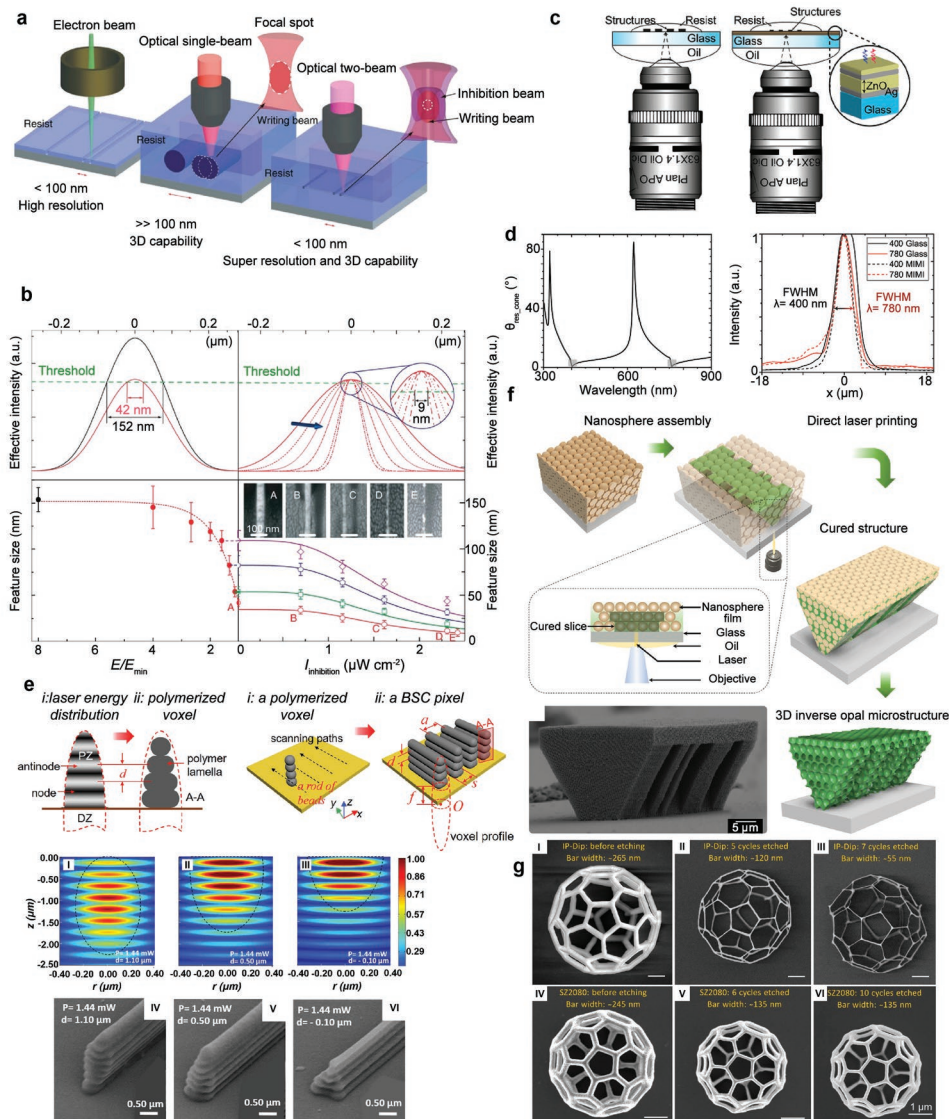


Figure 7. 3D TPL printing technologies for high resolution feature size. a) Comparison between electron beam lithography, single beam, and STED. b) Feature size measurement with STED. Reproduced under terms of the CC-BY license.^[325] Copyright 2013, the Authors, published by Nature Publishing Group. c) Sketch of ENZ assisted DLW process, the resin is on the glass substrate (left) and on the MIMI (Ag/ZnO/Ag/ZnO) nanocavity (right). d) Resonant cone angle of MIMI and experimental point spread function, which shows that the beam shrinks $\approx 36\%$ for MIMI compared with bare glass. Reproduced with permission.^[437] Copyright 2021, Wiley-VCH. e) Schematic illustration of interference assisted TPL. The femtosecond laser is illuminated on the interface between the substrate and photoresist, resulting in a periodic energy redistribution in the z direction thus generating multilayers in the voxel. The ridge-lamella multilayer configuration can be obtained with line scanning method. Reproduced with permission.^[441] Copyright 2021, American Chemical Society. The calculated normalized light intensity distribution and corresponding SEM images of fabricated structures. Reproduced with permission.^[438] Copyright 2021, AIP Publishing. f) Fabrication of 3D inverse opal microstructures with self-assembly assisted TPL fabrication. Reproduced with permission.^[442] Copyright 2021, American Chemical Society. g) Isotropic oxygen plasma etching of 3D printed structures. Initial buckyball and the same one processed after 5 and 7 etching cycles, respectively (top, IP-Dip). Polymerized buckyball and the same one processed after 6 and 10 etching cycles, respectively (bottom, SZ2080TM). Reproduced with permission.^[443] Copyright 2018, Elsevier.

required to be used in its workflow, while it is beneficial where the shrinkage of the structures is required to be minimal to preserve the geometrical rigidity. Lastly, a new class of materials is called (nano-)composites. They were initially developed for the UV SLA approach and are currently being adapted for ultrafast 3D laser nanolithography. They consist of small particles that will fuse from the inorganic material and organic binder that will be decomposed during heat treatment. It is a highly

versatile approach as many transparent materials can be used for the colloid part. However, the resulting resin mix cannot be scattering or absorbent. Thus, the requirements for this method to be applicable are close RI matching between colloidal particles and binder, as well as small particle size in respect to beam spot and the desired object. The particle size sets the feature size resolution limits, such as Glassomer (Figure 8e) that is used for 3D pristine glass fabrication.^[239]

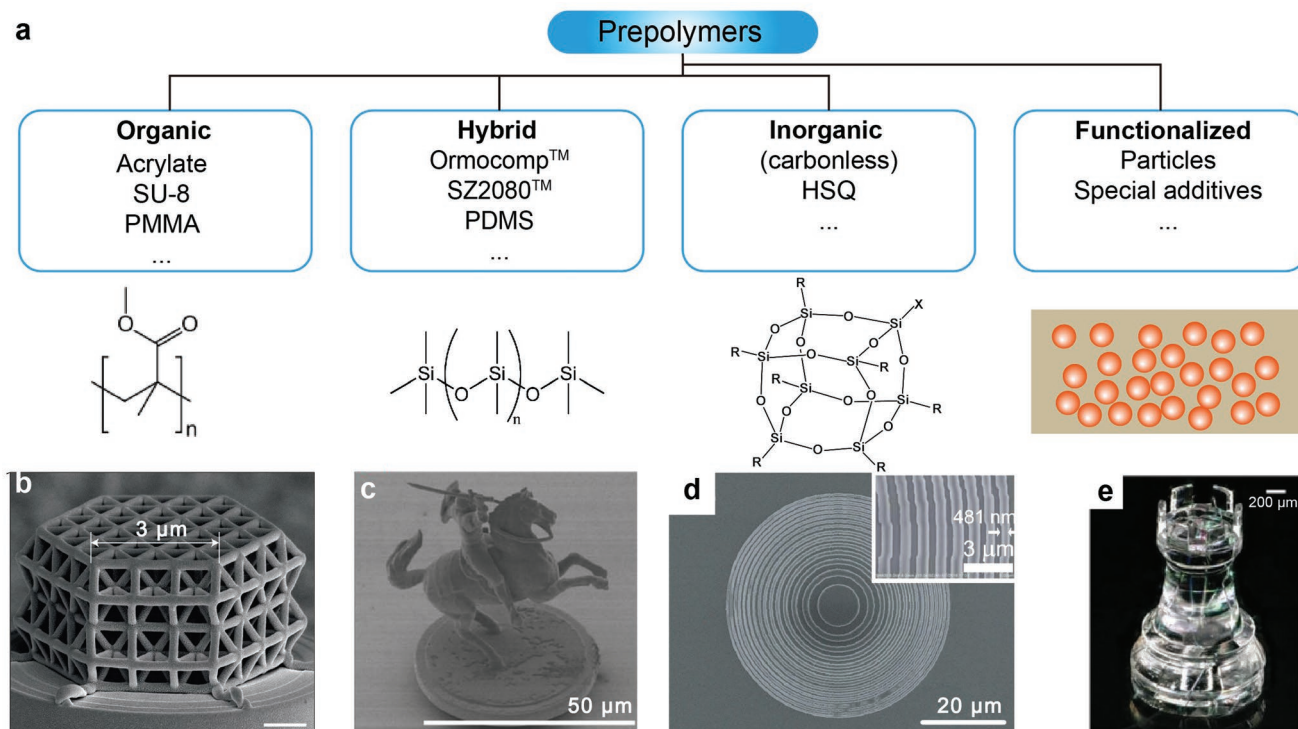


Figure 8. 3D TPL printing with pyrolysis/calcination post-processing. a) Examples of resins with the key components and their post-processed inert structures. b) Organic resist to glassy carbon lattice. Reproduced with permission.^[449] Copyright 2016, Nature Publishing Group. c) Hybrid resin to glass structure. Reproduced with permission.^[215] Copyright 2019, Royal Society of Chemistry. d) Inorganic resin made photonic structure. Reproduced under terms of the CC-BY license.^[450] Copyright 2022, the Authors, published by Nature Publishing Group. e) Composite resin to glass sculpture. Reproduced with permission.^[122] Copyright 2021, Wiley–VCH.

Calcination as a post-processing solution is advantageous due to (1): it is promising for isotropic downscaling of the fabricated features without the loss of geometry. (2): it can help unify the DC to improve and homogenize mechanical and optical properties. (3): It can convert hybrid materials into fully inorganic substances of glass, ceramic, and crystalline or even metallic substances, thus greatly extending the scope of applicable materials for 3D printing with TPL.

4.6. Resin Flow, Transparency, and Refractive Index Measurement

For unique 3D optical elements, both single elements and compound components, some cannot be fabricated using established 2.5 D technologies in a single-step or even multi-step processes.^[458–460] Using the ultrafast laser 3D nanolithography, free-form micro-optics can be additively manufactured and are already proven to be functional in the visible wavelength range.^[461] Usually, this includes suspended structures with functional surfaces separated by air-gaps. The historical examples included suspended lenses,^[133] combined lenses,^[462] hybrid refractive-diffractive elements,^[264] and micro-objectives,^[462] as well as fiber integrated devices.^[399,463]

The first obvious requirement is to mitigate resin flow during the fabrication process.^[67] This means using high-viscosity resins that do not allow flow during fabrication while performing layer-by-layer structuring or limit the per-layer

structuring time and, therefore, the fabricated structures' transverse size.^[464] Most notably, sol–gel materials (SZ2080™) or IP-Dip variants have been used in the aforementioned ways. The second crucially important requirement is transparency.^[131] Although most demonstrations include low absorbance materials transparent above ≈ 400 nm wavelength, photoinitiators increase absorption below this limit.^[259] Practically, this can be observed as a yellowish tint.^[465] The use of photoinitiators also results in the decrease of a very important parameter—the LIDT.^[446] Therefore, optical components made without a photoinitiator should be considered for femtosecond and picosecond high-intensity pulse applications.^[368,466] The non-sensitized resins are also preferred for life sciences due to their increased biocompatibility and reduced autofluorescence needed for imaging.^[467,468]

The third is RI. It is a difficult parameter to measure at the microscale, especially in case of arbitrary structures, and all the optical components designed need the RI to be known a priori. The special problem here is that many resins have their RI characterized for spin-coated samples, exposed in UV. This is done in this way because the classical characterization methods are designed for large samples, notably, centimeter scale thin-film structures.^[469] The problem is that the nature of crosslinking is different and results in RI values that are not necessarily same as the ones observed after multiphoton exposure.^[470,471] For optics, the method for characterizing the RI comes down to downscaling the classical measurement systems, for example, building interferometric systems,^[472] or deducing the RI from

the performance of measured devices using micro measurement approaches, for example, characterizing the focal distance as a function of RI for microlenses.^[473] The same logic can be applied to polymer gratings and other diffractive elements.^[474]

4.7. Molding and Replication

The 3D printed structures can also act as mold to pattern other materials into structures with high resolution, as many categories of materials are not suitable to be directly fabricated with TPL. It also enables low-cost mass production for complex structures with reusable molds. By combining standard processes in nanofabrication such as spin-coating, atomic-layer deposition (ALD), and chemical vapor deposition (CVD), different materials can be deposited onto the fabricated structures. Commonly used materials in deposition based TPL are silicon,^[475–477] titanium dioxide,^[478,479] metals,^[480,481] and other low RI materials.^[482] A simple way to replicate the printed 2D and 2.5D structures is direct molding,^[483] such as electroplating based template fabrication with nickel.^[484] In some cases, it is important to prevent the nickel to enclose the master entirely, thus the master edge can be slightly dipped into a melted wax bath to coat a protective wax layer. To remove the master from the mold, sonication, wet etching, or oxygen plasma can be applied. In addition, with additional depositing nickel at the interior of the mold, a replica with feature size smaller than the master can be obtained. To avoid breaking of the fine features like high aspect ratio structures, soft molds such as PDMS are preferred.^[485] An spin-coated anti-sticking layer such as BGL-GZ-83 will greatly help the master and mold separation process. After the PDMS mixture poured onto the master, a degas procedure is required to further remove air bubbles, hence the as printed polymer pattern can be precisely transferred to PDMS, then reconstructed with other functional materials.^[486] For 3D structures, an isotropic deposition approach is necessary to fully cover the whole printed master. In a typical deposition process,^[487] a layer of SiO₂ was deposited onto the master by CVD and the polymer was then etched away by O₂ plasma. Then Si is sequentially deposited onto the SiO₂ structure and the SiO₂ is again etched away by hydrofluoric acid to get the final 3D Si structure, while mechanical contact between the glass substrate and the structure may be worse during the selective wet etching process. The replication methods significantly extend the choice of applicable materials for 3D structures with complex morphology and fine features for optical applications, which are hardly realizable by the traditional fabrication techniques.

5. Optical and Photonic Applications

5.1. Diffractive Optics

The TPL based 3D printing enables us to fabricate diffractive optical elements (DOEs) with high precision, providing a compact and energy-efficient solution to manipulate the wavefront for different wavelengths thus generating the desired pattern or structural beams (Figure 9). Seiboth et al. fabricated a

tailor-made refractive phase plate to facilitate the aberration correction for a pair of multilayer Laue lenses, resulting in an improved Strehl ratio from 0.41 to 0.81 for X-ray microscopy (Figure 9a). The optical properties, surface quality, and radiation resistance of 3D printed structures can be applied in modern X-ray synchrotron radiation facilities or X-ray free-electron laser.^[488] Sanli et al. also achieved on-chip integration of high-performance kinoform lens for X-ray optics, bringing possibility to precise wavefront control of X-ray and efficiency optimization for harder X-ray.^[489] For DOEs working at longer wavelength, based on the fractional Talbot effect, Jiang et al. realized a flat nanofocalizer to convert the incident laser beam into a uniform subwavelength light spot array, with the full width at half-maximum only 0.82λ for a single focused light spot (Figure 9b).^[490] To realize functions beyond the traditional ones, Wang et al. added blazed facets onto the phase elements of DOE, shifting the laser power into an off-axis direction. With this method, far-field projections from computer-generated holograms are free of the zero-order spot, and the shadowing effects are mitigated thus reaching a diffraction efficiency of ≈ 86% (Figure 9c). The approach of sub-pixel level modification of DOEs can also be utilized in other precise wavefront shaping or detection applications.^[136] Based on the lumped TPL parametric model, they also achieved near-perfect Dammann gratings with millimeter scale and the corresponding diffraction efficiencies close to the theoretical limits, in addition with 0.4% zero-order spot power ratio and 1.4% nonuniformity of the laser spot array.^[370] Kyriazis et al. designed a DOE combined with a mode conversion up-taper onto a single-mode fiber, to realize 1–7 beam splitter and achieved increase of mode-field diameter by a factor of 2 (Figure 9d).^[491] Mark et al. employed the diffraction effect of gyroid photonic crystal to realize chiral beam splitter.^[269] With a hybrid solgel material, which can provide better optical quality, improved mechanical stability, higher damage threshold, and large solvent durability, Lightman et al. printed large scale DOEs that can form the incident beam into a pre-designed manner.^[492] Besides, Porte et al. proposed (3+1)D writing that is a single-step fabrication of graded-index optical elements with varied light exposure during 3D printing, realizing complex 3D RI distribution to manipulate wavefront. They demonstrated volume hologram and photonic waveguide with variation of RI ≈ 5×10^{−3}.^[471]

For structural beam, Zhou et al. realized mid-infrared vortex beam with a spiral phase plate at a wavelength range of 3.1–3.3 μm (Figure 9e).^[493] Wang et al. converted phase distributions of ideal Bessel beams with different topological charges into polymer phase plates, and realized zeroth- and higher order beams propagation-invariant up to 800 mm (Figure 9f).^[494] Yu et al. integrated a spiral zone plate onto the facet of a fiber to realize vortex beam with focusing efficiency over 60% and vortex purity ≈ 86% at the wavelength of 1550 nm (Figure 9g).^[495] Lightman et al. printed two separate elements in one integrated device to realize vortex mode sorters. For both pure and mixed vortex beams with different topological charges in a bandwidth larger than 300 nm, the miniaturized device can distinguish them easily (Figure 9h).^[496] They also realized high-order Bessel beam carrying OAM by fabrication of a twisted axicon and parabolic lens in an adapted fiber configuration.^[497] The advantages of TPL, such as precise fabrication of arbitrary

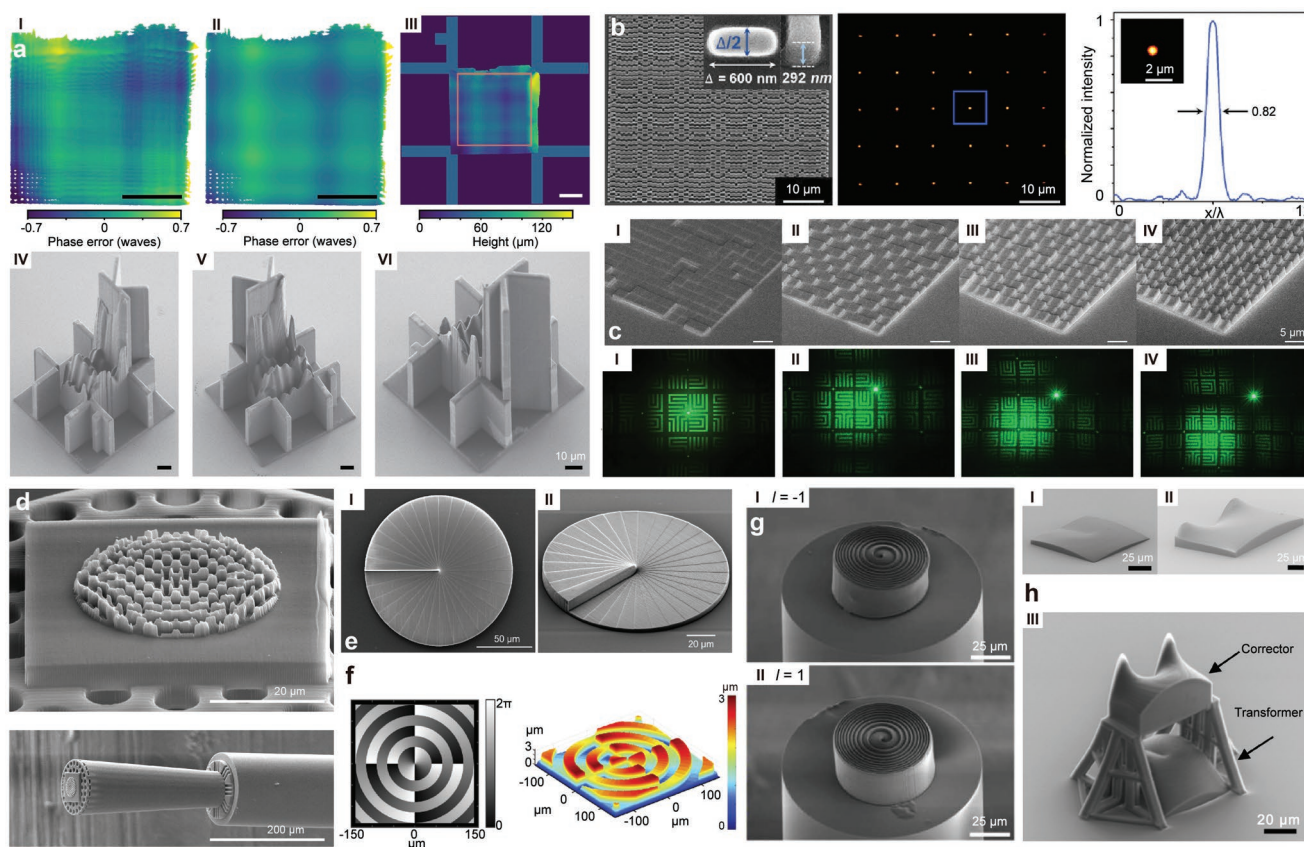


Figure 9. Diffractive structures for wavefront reforming applications. a) Wavefront error and design of the phase plate for X-ray. I. Residual wavefront error. II. Modeled phase error. III. Height profile of the phase plate. IV–VI. SEM images of the printed polymer phase plate. Reproduced under Optica Publishing Group Open Access Publishing Agreement.^[488] Copyright 2022, the Authors, published by Optica Publishing Group. b) SEM image of the 5×6 nanofocalizer, reconstructed intensity distribution at the wavelength of 750 nm, and normalized intensity distribution of one laser spot. Reproduced with permission.^[490] Copyright 2021, Optica Publishing Group. c) Deflection of the energy distribution for different orders in Fourier plane with blazed hologram DOE, SEM images with 50° oblique view and experimental holographic images. Reproduced with permission.^[136] Copyright 2019, Wiley–VCH. d) SEM images of the fan-out fiber beam splitter. Reproduced with permission.^[491] Copyright 2022, SPIE. e) The top and 52° tilted SEM images of a 32 segments spiral phase plate, with a height difference of 6.2 and 120 μm diameter. Reproduced with permission.^[493] Copyright 2022, Elsevier. f) Phase distribution for generating the second-order Bessel beam and measured height profile of the fabricated phase plate. Reproduced with permission.^[494] Copyright 2022, Optica Publishing Group. g) SEM images of the nanoprined kinoform spiral zone plates with topological charge -1 and 1 , respectively. Reproduced under Optica Publishing Group Open Access Publishing Agreement.^[495] Copyright 2020, the Authors, published by Optica Publishing Group. h) SEM picture of the transformer and corrector elements, and a combined mode sorter integrated on a glass substrate. Reproduced under Optica Publishing Group Open Access Publishing Agreement.^[496] Copyright 2017, the Authors, published by Optica Publishing Group.

surface topography, structural stability, compatible with different materials, fast prototyping, and easy cascading different functional elements, make it an ideal tool to explore the diffractive optics ranging from X-ray, visible band, infrared range, and beyond, thus be applied into augmented reality, virtual reality, diffractive neural network,^[498,499] and optical computing.

5.2. Imaging Optics

With the ability to print the demanded complex 3D structures and smooth surfaces, convenient fabrication process, and compatibility with different substrates, TPL is especially applicable for lenses fabrication. Generally, lenses can be categorized into three types by the mechanisms and scales: refractive lens (macrolens, microlens), diffractive lens, and metalens. The performance of TPL fabricated lenses is compatible with the ones

manufactured by traditional methods, and in particular, with micro- and nanoscale features, additional functionalities can be brought in, hence this method has enormous potential for various applications in the area of imaging optics.

For refractive optics, microlens is considered to be the direct migration from macro- to micro- scale. From the regular single concave or convex lens^[408,507,508] to a lens system,^[459,461,509–511] researchers are able to create the miniaturized optical imaging devices and integrated them on to various imaging systems. To demonstrate the advantages of integration and one-shot fabrication, endoscope and fiber imaging system are manufactured with the microlens system to achieve high quality imaging, the unique functionalities exceed the performance of original systems.^[134,500,510,512] For example, Gissibl et al. built the aspherical multi-lens system to help correct the aberration and to provide a wide angle of view as shown in **Figure 10a**.^[134] In **Figure 10b**, similarly, Li et al. explored how to reliably create the side-facing

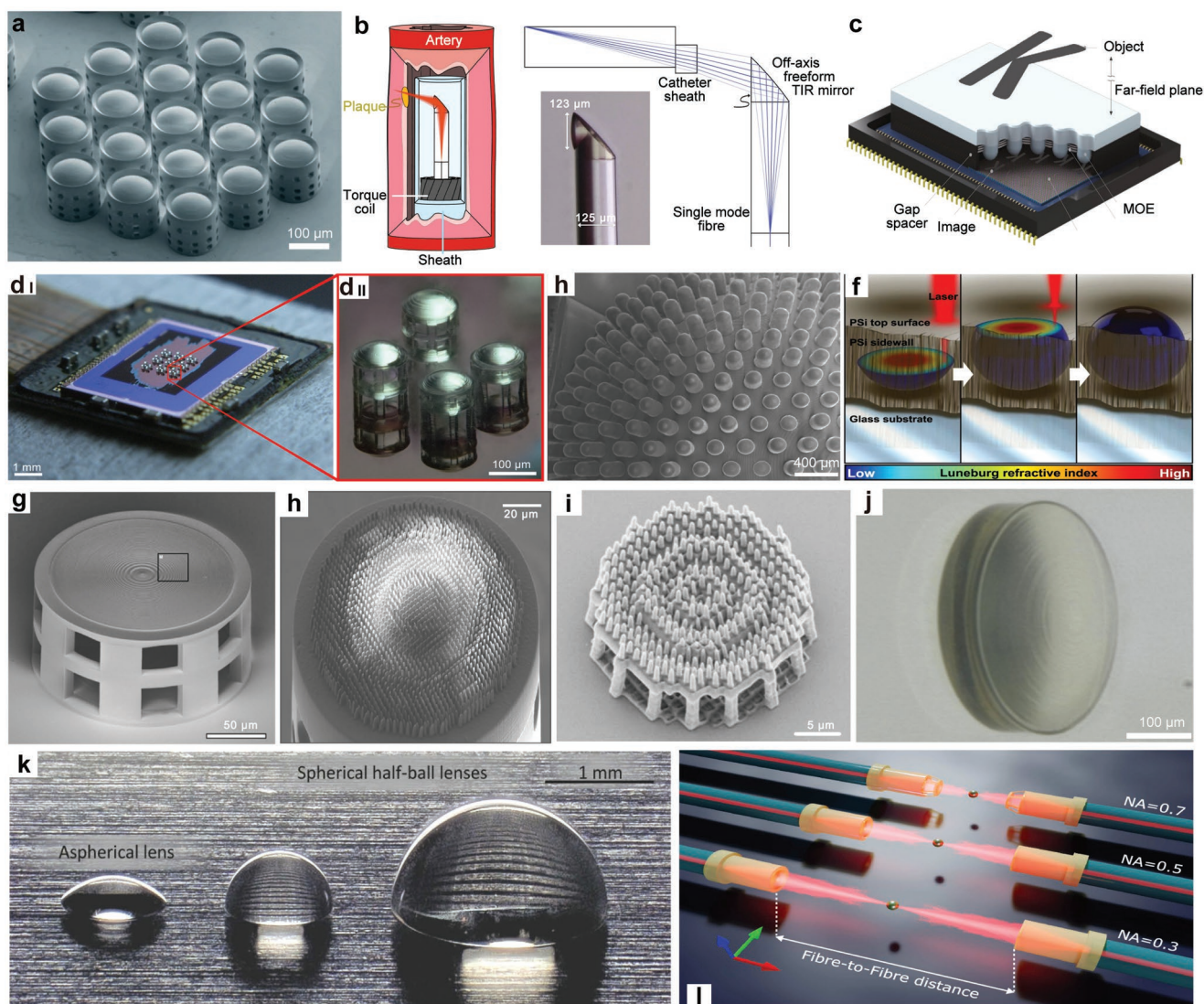


Figure 10. TPL-based 3D printed lens and imaging optics. a) SEM image of triplet lens objective on a fiber. Reproduced with permission.^[134] Copyright 2016, Nature Publishing Group. b) Schematic of OCT endoscope and microscope image of the total internal reflection mirror. Reproduced under terms of the CC-BY license.^[500] Copyright 2020, the Authors, published by Nature Publishing Group. c) Schematic of the ultrathin arrayed camera. Reproduced under terms of the CC-BY license.^[413] Copyright 2020, the Authors, published by Nature Publishing Group. d) CMOS image sensors with compound eye and detail of one of the groups on the CMOS. Reproduced under terms of the CC-BY license.^[459] Copyright 2017, the Authors, published by American Association for the Advancement of Science. e) SEM image of a biomimetic apposition compound eye. Reproduced under terms of the CC-BY license.^[501] Copyright 2021, the Authors, published by Nature Publishing Group. f) Schematic of GRIN lens. Reproduced under terms of the CC-BY license.^[502] Copyright 2020, the Authors, published by Nature Publishing Group. g) SEM micrograph of the stacked triplet diffractive lens. Reproduced under Optica Publishing Group Open Access Publishing Agreement.^[503] Copyright 2019, the Authors, published by Optica Publishing Group. h) SEM image of achromatic metafiber. Reproduced with permission.^[504] Copyright 2022, Nature Publishing Group. i) SEM image of a hybrid achromatic meta-lens. Reproduced under terms of the CC-BY license.^[505] Copyright 2022, the Authors, published by Nature Publishing Group. j) Refractive/diffractive apochromat consisting of IP-n162 (base) and IP-S (top). Reproduced with permission.^[133] Copyright 2021, Optica Publishing Group. k) Aspheric lens with a diameter of 1 mm and half-ball lenses with diameters of 1 mm and 2 mm, respectively. Reproduced under Optica Publishing Group Open Access Publishing Agreement.^[465] Copyright 2020, the Authors, published by Optica Publishing Group. l) Schematic of diffractive lenses at the tips of fibers for counter-propagating optical tweezers. Reproduced with permission.^[506] Copyright 2019, American Chemical Society.

imaging optics as a function of optical coherence tomography (OCT) probe. Different from the single-element lens group, micro lens array plays an important role in the area from enhancement of CMOS and CCD sensors to compact imaging system.^[459,511,513–517] Though, at the beginning, microlens array was essentially bio-inspired,^[518] with the rapid development of TPL based 3D printing, researchers can create more vivid and

more functional compound eyes or microlens array to realize better performance.^[413,461,501,519] In Figure 10c, Kim et al. realized high-contrast and high-resolution imaging system on the CMOS.^[413] Besides, inspired by the eagle eye, Thiele et al. directly 3D printed the multi-lens array onto a CMOS image sensor to achieve a full FOV of 70° with an increased angular resolution as Figure 10d illustrates.^[459] Other compound eye

imaging system were further exploited by Dai et al.^[501] and Hu et al.^[461] as shown in Figure 10e. Dai et al. reported their microfluidic-assisted 3D printed compound eye with full-color wide-angle panoramic views and position tracking. Hu et al. designed the logarithmic profile ommatidia to solve the defocusing problems if people want to integrate the compound eye with a flat CMOS sensor. There are some other interesting works such as microscopy system,^[509] super-resolution imaging,^[520] single molecule imaging,^[521] and color router imaging.^[522] Except from the normal refractive lens, Gradient-index lens can also be fabricated by 3D printing by tuning the printing parameters in the microscale as shown in Figure 10f.^[471,502]

In addition to the traditional refractive optics, researchers have also devoted themselves to the study of micro-level 3D diffractive devices. By stacking micro diffractive lens, Thiele et al. presented doublets and triplets diffractive elements to have a large FOV in the visible range with fabrication time < 15 min.^[503] Not only in the visible, in Figure 10g. Sanli et al. proposed a diffractive lens for on-chip integration of X-ray optics.^[489] Limited to the current available materials, there are less works in other wavelength range except for the visible, infrared and X-rays, while it is quite easy to 3D print a mold thus transfer the lens profile with other suitable materials. In recent days, metalens has become popular due to its advantages like multi-function, ultrathin, and ultra-compact.^[523] With the continuous improvement of high-resolution 3D printing technology, Ren et al. designed a metalens that is located on the fiber end face to work for achromatic focusing,^[504] as shown in in Figure 10h. They 3D printed the fiber tower and metalens together to employ the fiber meta-optics for widespread photonic applications. To determine the design parameters fast, Charles et al. proposed topology optimization to help to inverse design and fabricated a metalens with wide angle of view.^[524] Size, material, and efficiency limitation pushed people forward to seek for higher performance lens groups with the help of stack different type of lens or different material-composed lens. In Figure 10i, Balli et al. combined the multi-level diffractive lens with metalens to create a hybrid achromatic metalens with higher efficiency and broadband performance in the near-infrared band. As depicted in Figure 10j, Schmid et al proposed a refractive/diffractive lens and the first time simultaneously combined the two different photoresists that is known as achromatic doublet in the macro scale.^[133] TPL based 3D printing always has one problem of low throughput that limits the size of the lens. Ristok et al. overcame the previous limitations by use of large writing field and IP-Visio and fabricate a millimeter scale lens with uniform RI inside (Figure 10k).^[465]

From microlens to metalens, from fiber integration to CMOS integrated imaging system, from 2D to 3D, TPL helps to unlock the new door to generate better quality images in various application situations with a convenient fabrication process, which is extremely hard for traditional fabrication methods. It not only enables the miniaturization of optical system, but also helps to improve the imaging quality in medical, integrated circuits, quantum technology, bioanalytic, and so on. In addition, the application of lens not ends in imaging, it also brings more possibilities in collimation optics,^[525] light trapping (Figure 10l),^[506,526] light coupling,^[527,528] structure light,^[529] and auxiliary imaging.^[530]

5.3. Fiber and Waveguide Optics

Optical fibers, due to their compact nature and high optical transmission, are extensively used in a variety of fields like telecommunication systems, imaging, coupling, and sensing applications.^[531–535] Materials and fabrication methods available for manufacturing optical fibers have limited its achievable functionalities. The rapid growth of technology in the fields of communication and sensing has increased the demand for high performing optical fiber devices with multi-purpose functionalities. Multi-core fibers for high efficiency multi-channel transmissions, micro-nano fibers, and fibers with special core shapes were developed to cater for specialized applications.^[536–540] Micro-structures that are fabricated on fiber facets using the conventional subtractive techniques such as laser ablation,^[541] polishing,^[538] and chemical processes^[542] tend to have rough surfaces and low strength. Developments in TPL made it possible to alter the fiber facet with a vivid range of optical components having high precision, flexibility, and a variety of printable polymers as the material choice. Due to its high fabrication accuracy, it has been widely used for various applications in photonics,^[543–546] microfluidics,^[163,547,548] and biomedicine.^[549] Similar to the lab-on-a-chip technology where multiple laboratory functions are achieved on a single chip, the ability to integrate various microfluidic and photonic sensing devices on the facet of an optical fiber with TPL opened the endless possibilities of the lab-on-fiber technology. TPL enables the direct fabrication of fiber on chips with complex configuration and design for communication, hence a full 3D printed chip system is promising with integrated sensing and processing abilities.

Micro-optical components, when fabricated directly on the facet of an optical fiber allow for system integration with minimal signal loss. Conventional methods of integrating optical components on fiber facets like focused ion-beam milling,^[550,551] laser micromachining,^[552,553] and nano imprinting^[554,555] are limited to realizable geometries and resolution. With the advancements in TPL, micro-optical components having complex geometries could be realized with high resolution on fiber facets. Simple microlenses, when printed directly on the tip of optical fibers can render better performance for applications like imaging, particle trapping, illumination, and beam shaping. For example, a simple axicon lens printed on the tip of a single mode fiber (SMF) (Figure 11a) was one among the first demonstrations of printing on the fiber facets.^[463] This axicon rendered a Bessel-like output beam profile from a nearly Gaussian profile of the SMF. Other simple structures like convergent lenses and ring shaped phase masks were also demonstrated with good optical performance.^[529] Figure 11b shows collimating lenses of different diameters fabricated on a SMF that could achieve a transmission efficiency of $\approx 70\%$.^[399] The transparency of the fabricated lenses, and smoothness of the surface is evident from the optical micrograph. The flexibility in printed geometry paved way for the integration of many creative optical designs on the fiber facets for various applications, which are otherwise difficult to fabricate. One such example is the compound lens design shown in Figure 11c. This compound microscopic objective lens consists of five different refractive surfaces. The integrated fiber system is inserted through a

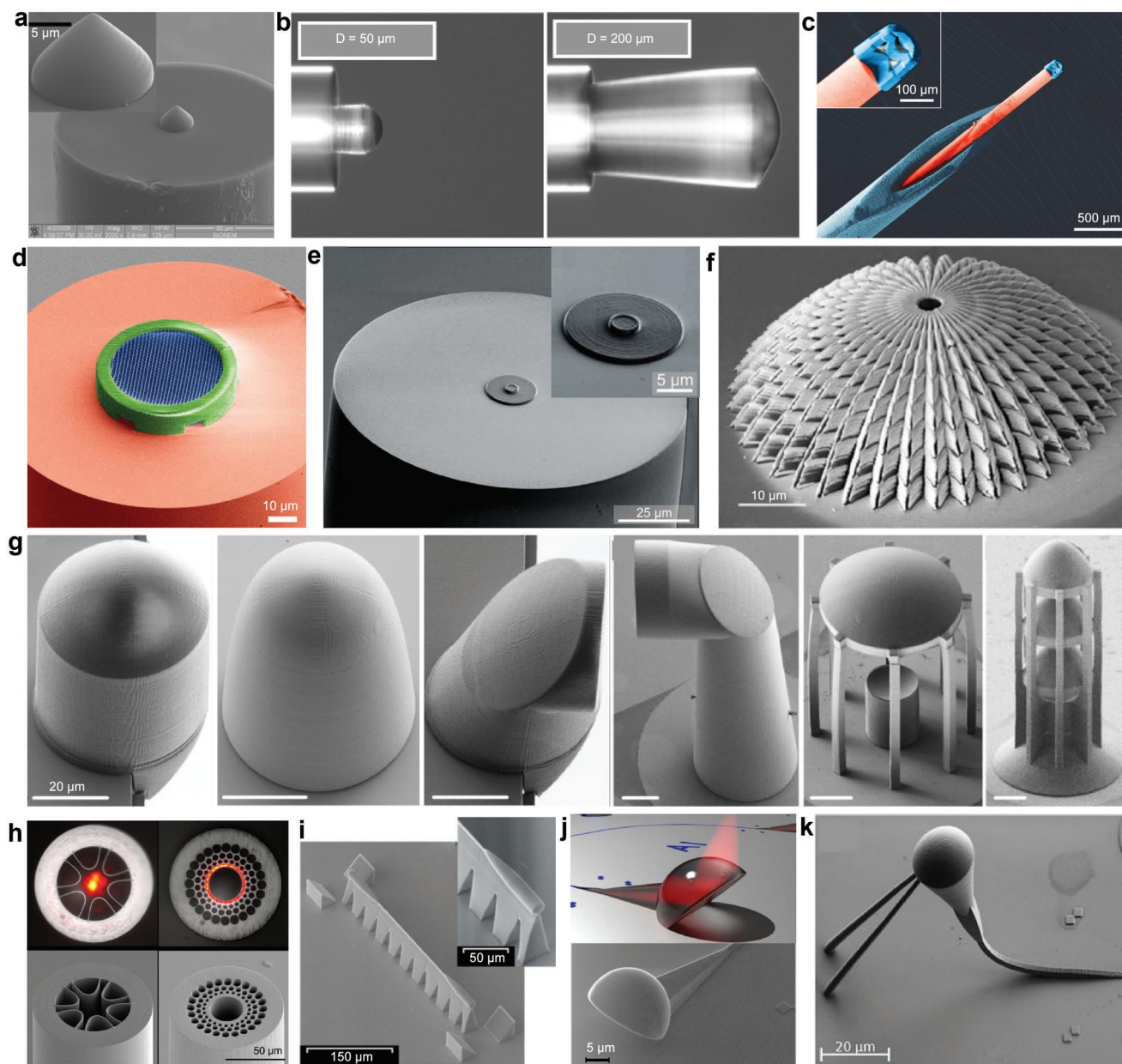


Figure 11. Micro-optical structures with TPL on optical fiber facets. a) An axicon lens printed on an SMF facet. Reproduced with permission.^[463] Copyright 2010, Institute of Electrical and Electronics Engineers. b) Collimating lens with different diameters on a SMF. Reproduced under terms of the CC-BY license.^[399] Copyright 2016, the Authors, published by Nature Publishing Group. c) Colored SEM of compact multi-lens objective (blue) fabricated on SMF (red) and inserted into a cannula. Reproduced with permission.^[134] Copyright 2016, Nature Publishing Group. d) Colored SEM of a twisted woodpile left-hand polarization structure (blue) with a solid supporting ring (green). Reproduced under terms of the CC-BY license.^[399] Copyright 2016, the Authors, published by Nature Publishing Group. e) Diffractive phase plate for spatial intensity redistribution. Reproduced under terms of Optica Publishing Group Open Access Publishing Agreement.^[556] Copyright 2016, the Authors, published by Optica Publishing Group. f) 3D printed SERS structure on an MMF. Reproduced with permission.^[557] Copyright 2015, Wiley-VCH. g) Beam shaping elements (free-form lenses, free-form mirrors, and beam expanders) fabricated on chip and fiber facets. Reproduced with permission.^[528] Copyright 2018, Nature Publishing Group. h) Optical guidance (top) and SEM image (bottom) of TPL printed anti-resonant hollow-core PCF and fractal ring core PCF. Reproduced under terms of Optica Publishing Group Open Access Publishing Agreement.^[560] Copyright 2020, the Authors, published by Optica Publishing Group. i) SEM image of a 400 μm long waveguide with parabolic tapers for adiabatic transition from 15 to 2 μm cross-sections. Reproduced under terms of the CC-BY license.^[561] Copyright 2021, the Authors, published by IOP Publishing. j) Schematic of total internal reflection coupler attached to a nanophotonic circuit (top) and helium ion microscopy image (bottom) of fabricated coupler. Reproduced with permission.^[563] Copyright 2019, Optica Publishing Group. k) SEM image of a polymer coupler attached to a silicon waveguide for angled coupling with optical fiber. Reproduced with permission.^[564] Copyright 2019, AIP Publishing.

small injection cannula for biological imaging applications. The ability of TPL to fabricate 3D structures on fiber facets could

be extended beyond microlens systems. Intricate geometries, like chiral photonic crystal structures, can aid for wavelength

separation and polarization control.^[399] Figure 11d shows a left-handed polarization control structure fabricated on the facet of a SMF for a design wavelength of 1550 nm. Numerous optical elements based on the mechanisms of reflection, refraction and diffraction can be realized using the sub- μm fabrication capabilities of TPL. Figure 11e shows a diffractive phase plate with a base ring and a diffractive element on the end of a SMF for beam intensity shaping.^[556] The structure is fabricated in a ring-by-ring fashion with high resolution that enables the intensity distribution emerging from the SMF to be spatially redistributed. A core area of investigation in the field of lab-on-fiber technology is to realize surface enhanced Raman scattering (SERS) sensing based on optical fibers to achieve robust, flexible, and miniaturized tools for spectroscopic applications. Figure 11f shows a SERS radar structure composed of a spherical SERS body and a parabolic mirror on a multi-mode fiber (MMF).^[557] This SERS device is designed to have microscale trenches for larger surface area to get efficient interaction with analytes. Precise fabrication of these trenches and scales could be achieved due to the superior resolution and process control inherent to TPL.

Besides the ability to realize micro-optical components on individual fiber tips, it has also demonstrated the capability to fabricate optical structures for fiber-chip coupling systems.^[558,559] One such demonstration reported the fabrication of compact beam-shaping optical elements on the facets of both silicon photonic chips and optical fibers for chip-to-fiber and chip-to-chip coupling.^[528] Figure 11g shows a variety of beam shaping elements like free-form mirrors, free-form lenses, and beam expanders fabricated on the chip facet and the fiber tip. The concept of such in situ 3D printing in a hybrid photonic multi-chip assembly system relaxes alignment tolerance and can be used for both edge emitting and surface emitting optical devices. Low loss single mode coupling compatible with passive alignment techniques was demonstrated in this work avoiding bulky on-chip mode converters.

Other than the integration with micro-optical components, in situ fabrication of stacked photonic crystal fiber (PCF) like segments to create an all-fiber integrated devices has also been demonstrated in other works.^[560] Figure 11h shows two such structures: an anti-resonant hollow core PCF and a fractal ring core PCF. The anti-resonant structure with semi-elliptical structures and a central core guidance with a mode field diameter (MFD) of 12.1 μm has been demonstrated. Structures like the fractal-ring core that can support annular ring modes are gaining interest due to their ability to support modes that can carry OAMs. The drawback of traditional PCF fabrication by drawing is that the final fiber cleaving step distorts the fiber structure. As TPL enables direct production of flat, perpendicular, or angled output facets, this drawback is overcome. Other than conventional straight structures for guiding light, air-clad waveguides, tapers, and s-bends have also been investigated to minimize insertion-loss. Parabolic tapers that allow adiabatic transition over a short length (Figure 11i) has been demonstrated with an insertion loss of < -1.7 dB.^[561] Except from in-plane edge and surface coupling schemes that occupies a larger spectrum of the research area, out-of-plane coupling based on total internal reflection of 3D structures have been achieved.^[562] The total internal reflection couplers shown in Figure 11j exhib-

ited remarkable broadband coupling in the visible band with -3.1 dB insertion loss.^[563] A hybrid coupling approach using a near-adiabatic-mode-converter is shown in Figure 11k. With TPL capabilities, continuous bending of the polymer waveguide can be achieved for angled coupling,^[564] which are efficient for quantum source coupling,^[565] fiber array,^[566] even wafer-level test of photonic integrated circuits.^[567] The couplers also can support wide optical bandgap, and have good alignment tolerance, making them a good choice for rapid prototyping of broadband photonic applications like spectrometers, second-harmonic sources.

In addition to the processing on individual fiber facets, the ability to realize multi-fiber integrated optical system was also demonstrated by fabricating a compact scanning probe microscope with integrated optical actuation.^[568] High precision fabrication and processability of a variety of materials are the two key advantages unlocked by TPL process. Optical components fabrication on fiber tips relies on the high resolution of the printing process whereas TPL becomes advantageous for optical waveguide fabrication due to the properties of printable materials. Typical fiber optic devices like grating based sensors pose low sensitivity as the silica material used for the fabrication of such devices has low thermal expansion coefficients.^[569–571] On the other hand, optical fiber sensors fabricated with TPL can ensure improved performance due to the better material properties of polymers used for printing. Investigations have been done mainly on the use of TPL for the fabrication of fiber Bragg gratings. Line type and helical fiber Bragg gratings have been fabricated for the RI measurement of liquids.^[572,573] Devices like multimode interferometers have also been realized for temperature measurements,^[574] and Fabry–Perot interferometer (FPI) with high sensitivity.^[575–577] With complex functionalities evolving, the demand for microscale optical sensing, imaging, and optical manipulation is increasing. Optical fiber integrated with functional devices has great potential in this scenario. With the advancements in the TPL printing method and processable materials, highly complex structures with different sorts of functionalities become possible, giving new dimensions to the concept of lab-on-fiber.^[315,578–583]

Furthermore, direct fabrication of fiber has also been intensively studied as the RI contrast between polymer and air is as high as ≈ 0.5 , similar to the traditional fiber made of silica.^[584] 3D spiral waveguide and suspended air-bridge waveguide have been demonstrated with submicron features and unique coupling interfaces with bandwidth of 3 dB and coupling losses of 1.6 dB. the waveguides support 56 Gb s⁻¹ pulse amplitude modulation 4 high-speed data and 30 Gb s⁻¹ nonreturn to zero.^[585] The fabrication degree from freedom is not limited by spatial dimension, thus it's convenient to make arbitrary non-planar topological photonic integrated circuits.^[586,587] Moreover, fabrication of submicron waveguides through TPL in polymers like PMMA or PDMS is also realized.^[587,588] With the bundle of photonic waveguides, deep neural network based optical image reconstruction has been demonstrated.^[587] Combined with the optical interconnects,^[589,590] and couplers,^[591] along with the rapid development of photonic circuits and chips, all-optical devices capable of in-plane and out-of-plane coupling, signal collection and processing, are possible to be achieved in one 3D printing step.

5.4. Color Optics

TPL is a feasible technique in structural color printing as it uses low-index dielectric materials to fabricate 3D structures that interact with light to produce color. These structures include nanopillars,^[592–597] diffraction gratings,^[598,599] photonic crystals,^[432,600] microscale droplets,^[601] and multi-layer biomimetic structures.^[439–441] Arguably, nanopillars are the most basic structure to fabricate by TPL because their diameters are fixed by the lateral voxel size of the focused laser beam in the material. Varying only the pillar height is able to cover a broad range of hues, serving as color filters in the visible spectrum that have several interesting purposes.^[592] For example, full color and grayscale paintings have been achieved by varying several printing parameters (height, period, laser exposure time) of the nanopillars (Figure 12a).^[593] By integrating the nanopillars onto phase plates, holographic color prints have been achieved (Figure 12b).^[594] Moreover, combining nanopillars with microlenses have also achieved colorful optical moiré effects^[596] and light field prints (Figure 12c).^[597] It is noteworthy that TPL is capable of directly fabricating integrated structures in a single print, which has not been realized in EBL.

The next basic structure in color printing is diffraction gratings, which are commonly used to produce angle-dependent colors. Unlike other fabrication techniques, TPL enables full control over the grating geometry and can create more complex structures. A study on gratings with varying heights, periods, and orientations revealed multiple sets of hidden color information under varying incidence angle and sample rotation angle (Figure 12d).^[598] Moving up in complexity, another study used bigrating structures to examine their color characteristics under varying parameters (Figure 12e).^[599] Most structures have a fixed geometry once they are fabricated, which leads to fixed colors. To overcome this limitation, a study demonstrated color tuning by stretching gratings embedded in a flexible PDMS substrate and revealed distinct images along orthogonal stretching directions (Figure 12f).^[485] Besides, the intrinsic property from the anisotropic nature of liquid crystal can be employed to generate polarization color.^[602] The structural geometry can also be changed by using SRMs. Zhang et al. demonstrated 4D printing of grid-like gratings in a shape memory polymer that appears colorless after heating and mechanical deformation, but the shape and color are recovered after heating.^[114] This ability to tune colors after fabrication has potential applications in concealing secret information and anti-counterfeiting.^[603] TPL can also print colorful arbitrary-shaped 3D objects using woodpile photonic crystals (Figure 12g,h).^[600] However, it is challenging to achieve complete bandgaps in the visible spectrum due to the lateral resolution limit (≈ 500 nm) of TPL in low-index polymers ($n \approx 1.55$). To mitigate this challenge, Liu et al. demonstrated a heat shrinking process that reduces the lattice constant to as small as 280 nm, producing slow light modes in the visible spectrum.^[432]

A less common yet interesting structure that can be fabricated by TPL is microscale droplets. Goodling et al. demonstrated that these droplets produce iridescent colors through multiple total internal reflections at the concave interfaces (Figure 12i). Using interference assisted TPL, other researchers also demonstrated multi-layer biomimetic structures that produce similar

colors found in butterflies (Figure 12j).^[440,441] Related to structural colors are spectrometers that measure reflectance or transmittance as a function of wavelength. Since traditional spectrometers are large and bulky, TPL is a viable solution to fabricate miniature spectrometers ($100 \times 100 \times 300 \mu\text{m}^3$) operating in the visible region (Figure 12k).^[604] Single-photon detectors operating in the infrared region have also been fabricated by TPL.^[605]

As seen so far, TPL offers the capability to fabricate complex 3D structures for color printing. However, it has a drawback of low throughput due to its serial patterning process that takes long hours to print an area spanning a few millimeters. In future works, the throughput can be significantly improved by parallel TPL systems or molding with nanoimprinting for mass production.^[349,606]

5.5. Topological Optics

Originating from quantum physics,^[607,608] bound state in the continuum (BIC) describes the localized states in the continuum of spatially extended states (Figure 13a), however, have no channels coupling to far field radiation.^[609,610] Analogous to electrons, BIC has also been achieved in many photonic system, gratings,^[611] optical waveguides,^[612] photonic crystal slabs,^[613] single dielectric antenna,^[614] and metasurfaces,^[615,616] to name a few. Although the true BIC is optically inaccessible, the real existence of the “true” BIC can be examined by electron energy loss spectroscopy.^[617] Slightly deviating from the ideal condition, the quasi-BIC holds ultrahigh quality factors and finds many applications in lasing,^[618] nonlinear enhancement,^[619] edge detection,^[620] and biosensing,^[615,616] etc.

Limited by low RI contrast and relatively large feature size compared with EBL, TPL is yet to be fully explored in the field of BIC.^[609,621] However, TPL still holds advantages over traditional CMOS compatible fabrication techniques, due to the fast and cost-effective fabrication, large throughput, and especially the extra freedom dimension of height, which makes it easy to break the out-of-plane symmetry.^[622] Currently, TPL related BIC are mostly reported in short and middle infrared ranges, exhibit plasmonic BIC modes when coated with metal.^[622–624] Combining the advantages of both plasmonic structures and dielectric BIC antennas, the plasmonic BIC phenomenon realized high Q-factor and strong field enhancement simultaneously, pave the way for next-generation optical sensing and spontaneous emission.^[615,622,625,626]

As shown in Figure 13b, the quasi-BIC mode gradually appears when nanostructures coated with gold are illuminated with oblique incidence. Similar as the plasmonic nanoantenna, the field enhancement is as high as 10 000 times, meanwhile, the high Q-factor is remained.^[621] The radiation decay rate can be further engineered equal to the intrinsic loss and the perfect absorption condition is achieved, showing a near unity absorption at this quasi-BIC mode. Moreover, such perfect absorbers can be realized under full stokes polarization conditions by fine tuning the parameters of a diatomic metasurface.^[623] To further enhance the light intensity under microscope objectives and break the low-NA limit^[627] to excite surface lattice resonances (SLRs), a hybrid was designed and fabricated using TPL.

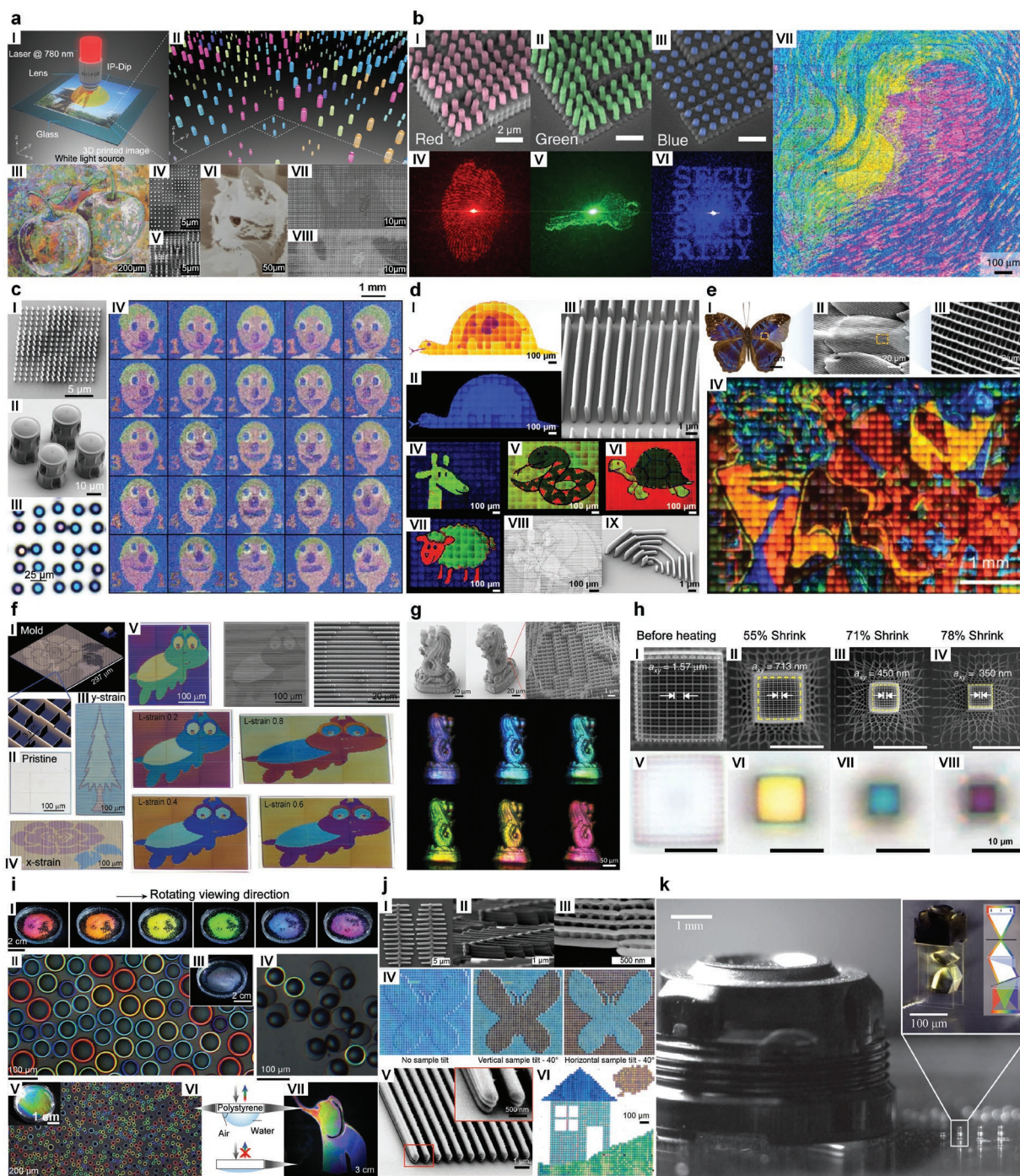


Figure 12. Structural colors and spectrometer fabricated by TPL. a) Full color and grayscale paintings comprising nanopillars. Reproduced with permission.^[114] Copyright 2021, American Chemical Society. b) Holographic color prints comprising integrated nanopillars and phase plates. Reproduced under terms of the CC-BY license.^[594] Copyright 2019, the Authors, published by Nature Publishing Group. c) Light field prints comprising integrated nanopillars and microlenses. Reproduced under terms of the CC-BY license.^[597] Copyright 2021, the Authors, published by Nature Publishing Group. d) Hidden color images in diffraction gratings with varying geometric parameters. Reproduced with permission.^[598] Copyright 2022, American Chemical Society. e) Full color reproduction from bigratings. Reproduced with permission.^[599] Copyright 2022, Wiley-VCH. f) Color tuning by directional stretching of diffraction gratings. Reproduced with permission.^[485] Copyright 2022, Wiley-VCH. g) Colorful 3D object made of woodpile photonic crystals. Reproduced with permission.^[600] Copyright 2022, American Chemical Society. h) Reduced lattice constant by heat shrinking of woodpile photonic crystals. Reproduced under terms of the CC-BY license.^[432] Copyright 2019, the Authors, published by Nature Publishing Group. i) Iridescent colors produced by microscale droplets. Reproduced with permission.^[601] Copyright 2019, Nature Publishing Group. j) Color replication in multi-layer biomimetic structures. Reproduced with permission.^[440] Copyright 2019, Optica Publishing Group. Reproduced with permission.^[441] Copyright 2021, American Chemical Society. k) 3D-printed spectrometer for measurements in the visible region. Reproduced under terms of the CC-BY license.^[604] Copyright 2021, the Authors, published by Nature Publishing Group.

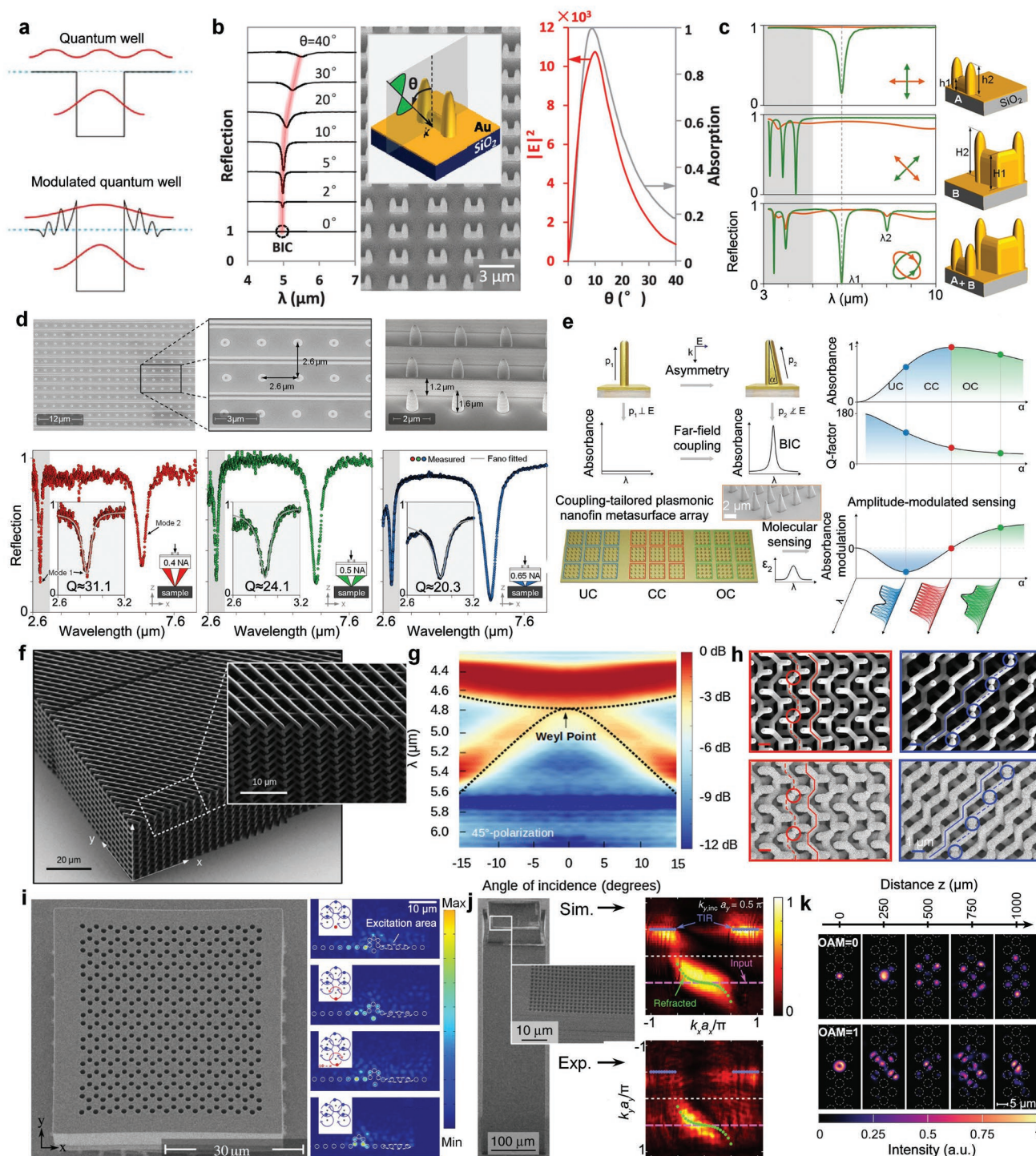


Figure 13. Applications of 3D TPL printing in BIC photonics and topological photonics. a) Schematic figure of bound states in the continuum. Reproduced under terms of the CC-BY license.^[610] Copyright 2019, the Authors, published by De Gruyter. b) Perfect absorbers with plasmonic BIC modes. Reproduced with permission.^[621] Copyright 2020, American Chemical Society. c) Three types of diatomic perfect absorbers under full-stokes polarization illumination. Reproduced with permission.^[623] Copyright 2021, American Chemical Society. d) Angle-dispersion less hybrid anisotropic metasurface with plasmonic BIC modes. Top panels are the SEM figures of the hybrid anisotropic metasurface, bottom panels are reflection spectra illuminated with focused beam with different NAs. Reproduced with permission.^[624] Copyright 2021, American Chemical Society. e) Plasmonic BIC metasurfaces by breaking the out-of-plane symmetry. Right panels: absorption and Q-factors in under-, critical-, and over-coupling regimes. Inset: SEM figures of the plasmonic BIC metasurface. Reproduced with permission.^[622] Copyright 2022, the Authors, published by American Association for the Advancement of Science. f) Fabricated chiral woodpile photonic crystal with charge-2 Weyl point. g) Angle resolved reflection spectrum of the chiral woodpile in (f). Figure 13f,g is reproduced with permission.^[658] Copyright 2020, American Physical Society. h) Fabricated gyroid photonic crystal with type I photonic Weyl point. Red box: SEM images with observation direction of [010], Blue box: SEM images with observation direction of [-10]. Top panels: as printed

Angular dispersion of such plasmonic BIC modes is removed and verified under focused beams with different NAs.^[624] The out-of-plane symmetry can be easily broken by using the 3D TPL and the high Q-factor plasmonic BIC is thus possible under normal incidence.^[622] Through the control of radiative to intrinsic losses ratio, under-, critical-, and over-coupled regimes are explored corresponding to negative, no, or positive modulation induced by the analyte. This breaks the longtime misunderstanding that the optical sensing should be most sensitive at the critical coupled condition, where the electric field enhancement is the highest.^[622]

Similar as optical BIC dates from quantum mechanics, topological photonics are inspired by topological insulators in condensed matter physics.^[628–631] In mathematics, topology deal with continuous deformations of geometric objects and the topological invariant in process.^[632–635] Just as the name suggest, topological photonic system is robust against structural disorders, fabrication imperfections, and scattering losses, unless the topological invariant or topological phase is changed.^[630,633,634] Although topology has been well investigated in various photonic system, such as, photonic crystals,^[636–639] optical waveguides,^[640] metamaterials,^[628,632] particles,^[641] optical cavities,^[642] coupled resonators,^[643] silicon photonics and optomechanics,^[630] 3D TPL printing enable topological photonics exotic and unique properties, which is hard to realize in 2D system.^[632,633,644–657]

Extending topological phenomenon from 2D photonic crystals to 3D version, charge-1 and charge-2 Weyl points are observed experimentally in direct printed photonic crystals (Figure 13f,g)^[658] or coated 3D printed photonic crystals (Figure 13h).^[659] Because of the mathematical analogy between the paraxial approximation of the Helmholtz equation and the Schrodinger equation,^[630,633] photonic waveguide system can be used to examine Floquet topological phenomenon,^[660,661] by introducing artificial gauge fields (AGFs) and treating the waveguide axis z as time varying dimension (Figure 13i). Based on the directly printed waveguides with RI modulation by differing laser powers^[470,472] or the infiltrated waveguides by printing the inverse waveguides array, the robust Floquet edge states (Figure 13i),^[662–664] generalized Snell's law at the boundary between two regions with different AGFs (Figure 13j),^[665] OAM dependent Aharonov–Bohm-caging effect are realized elaborately (Figure 13k).^[643,666,667] Furthermore, the time evolution along the waveguide axis can be directly observed by dissolving fluorescent dye into the infiltration material, exhibiting a quantum-walk like dispersion.^[668] The non-Hermitian physics and PT symmetry can be explored by selectively infiltrating the waveguide holes with gain and loss materials.^[669] Excitingly, topological photonics with real quantum states can also be realized by introducing nanodiamonds with a nitrogen-vacancy

(NV) center in 3D TPL printing.^[670] The field of TPL printing related topological photonics and BIC related photonics is still newborn, but rapidly growing with cutting-edge physical concepts.^[671–674] It is expected that the burgeon of topological or BIC photonics will rely more on the TPL based fabrication techniques.

5.6. Quantum Optics and Optical Storage

Quantum optics is a fast-growing field that was evolving from laser development and their miniaturization, via optical combs and metrology, photon entanglement and quantum information processing celebrated in several Nobel prizes. Light-matter interaction in small volumes comparable with wavelength λ^3 , single photon emitters, spin-orbital momentum control and its application in opto-mechanical systems are other traits of this broad field. The application potential of quantum optics is broadly explored in various kinds of sensors and in this particular area of engineering research, the 3D fs-laser printing is becoming increasingly important. Polymerization of micro-optics is a very appropriate topic for the year-2022 of glass (UNESCO). Control of voxel size down to $\approx \lambda^3$ volumes under tight focusing and even stronger localization via ENZ state enhances shallow energy deposition into a skin depth, opens a new toolbox for nano-micro volume modification and fabrication. Micro-optical elements, lenses, photonic crystals, DOEs and their hybrids, circular polarizers, spin-orbital couplers, etc., can all be miniaturized and combined with optical fibers^[474] and imaging devices.^[508,675] Photonic wire bonding (PWB) is an exact example of a 3D laser polymerization technology transfer to solve on-a-chip integration challenges for micro-lasers couple to waveguides and optical circuits. Inherent 3D capability of laser writing has brought new functionalities for tapering polymerized photonic links to single-mode fibers and control of the propagation phase via exact length in the bond.^[558] Collecting light from single-photon emitters is another miniaturization and integration task that can be fulfilled by 3D TPL.^[676] Active opto-electronic elements for focusing and polarization control have been demonstrated using 3D laser polymerization and metasurfaces.^[677]

3D printing speed of sub-wavelength sized voxels is now approaching 10 MHz by implementing combined exposure with light-sheet and DLW.^[190] Printing of nano-emitters on demand at sub-wavelength resolution and to build up 3D structures is also demonstrated showing the principle of photo-chemical control of photo-modification using 3D laser writing.^[678] 3D TPL printing, which started in 1990s with quest for high-resolution is becoming now a highly productive method for quantum optics applications, where utmost demanding precision and

gyroid photonic crystal, bottom panels: the polymer is uniformly coated with a high-n Sb_2Te_3 . Reproduced with permission.^[659] Copyright 2018, Wiley–VCH. i) Robust edge states in photonic Floquet topological insulators. Left: SEM image of the Floquet topological insulator with spiral waveguide array inside. Right: experimental results of light intensity at the edge of the Floquet topological insulator. Reproduced under terms of the CC-BY license.^[662] Copyright 2017, the Authors, published by IOP Publishing. j) Generalized Snell's law at two different photonic artificial gauge fields' interface. Left: fabricated waveguides structures. Right: simulation and experimental results of the refracted and reflected lights in momentum space. Reproduced under terms of the CC-BY license.^[665] Copyright 2020, the Authors, published by Nature Publishing Group. k) OAM dependent Aharonov–Bohm effect in Floquet topological insulators. Incident beam with OAM value equals to 1 repeats the light intensity in a manner like “Talbot effect” instead of dispersion. Reproduced under terms of the CC-BY license.^[667] Copyright 2020, the Authors, published by Nature Publishing Group.

resolution is required for fabrication of micro-optics with high collection efficiency of photons and functioning at low level photon counts (light intensity) within small sub-wavelength volumes. It has a promising industrial future with the incoming quantum computing and quantum communications.^[676]

Similarly, optical data storage also requires the confinement of light-matter interaction in a small volume for high density information memory. Using visible or infrared wavelengths at the diffraction limit, information with density of 10^8 bits cm^{-2} can be stored with conventional 2D optical data storage. TPL enables the possibility to store information in 3D. In an early work, Stricker and Webb experimentally demonstrated the storage density can be as high as 10^{12} bits cm^{-3} with TPL based printing.^[679] They first prepared an ≈ 100 μm thick photopolymer film and irradiated it with ≈ 3 mJ cm^{-2} of UV light to prevent distortion. Then using a 100 femtosecond and ≈ 620 -nm-wavelength laser, 3D stacks of data were written inside the film. The 3D data were read by successively imaging each of the data planes using differential interference contrast microscopy. Later, Cumpston et al. developed a class of π -conjugated initiators that exhibit large TPA cross section, and demonstrated 3D data storage that permits fluorescent and refractive read-out.^[680] These initiators offer low polymerization thresholds, high efficiency for the activation of radical polymerization, which are critical in 3D data storage. Makarov et al. developed a theoretical model of an 3D optical storage system with 100 MHz repetition rate and 100 fs pulse duration in a large number (≈ 1000) of stacked layers.^[681] They demonstrated that with detector shot-noise-limited readout signal-to-noise ratio >4 and minimum 100 MHz data access rate, the least intrinsic TPA cross section $\sigma_2 \approx 10^3$ GM of the chromophores is required. To further increase the TPA efficiency, Yanez et al. reported new photosensitive polymeric systems that has TPA cross sections as high as 1550 GM and demonstrated a storage density capacity of 1.8×10^{13} bits cm^{-3} .^[682] Integrating other optical properties such as different polarization states,^[683] and focal intensities of a writing beam,^[684,685] OAM of light,^[686,687] higher dimensional optical storage is feasible.^[688]

5.7. Dynamic Optics and Optical Robots

3D printing with SRMs is also known as 4D printing. Combining with the features of stimuli-response and nano-/micro-scale TPL fabrication, the produced structures have attracted an increasing research interest in applications of dynamic optics/nanophotonics and optical microrobots.^[689]

The dynamic optic and nanophotonic properties are attributed to the controllable structural deformation under external stimuli.^[690,691] The SMRs are the key to induce such deformations, such as shape memory polymers,^[114] LCE,^[159,692–697] and ionogels have been reported.^[116,698] By now, several kinds of dynamic optic/nanophotonic elements have been developed, and most of them were used for visual effects related applications, such as structural color and hologram. Zhang et al. developed the first shape memory polymer for TPL 4D printing with sub micro feature size (Figure 14a).^[114] Wang et al. reported the dynamical holograms using shape memory polymers. As an improvement to their previous work,^[114] they reported an

improved recipe to enhance the stiffness of the printed shape memory polymer, resulting in 5.2 GPa storage modulus at room temperature. The high stiffness made the material suitable for structures with a high aspect ratio. Nanopillars with different heights were printed to generate the phase difference for transmittance light. The hologram was observed on the printed structure and can be concealed on the deformed state under stress, while recovered by overcoming the van der Waals force after heating. Florea et al. achieved the humidity-responsive structural transformation using a LCE photonic photoresist.^[692] The as-printed LCE are static and can be changed to switchable post-treatment by cleaving the hydrogen bonds (Figure 14b). Later, they further developed a responsive ionogel by using ionic liquids as a solvent in the photoresist,^[116] and demonstrated that the printed structures have different responses to different vapors of isopropanol, ethanol, and water. Pozo et al. also reported a LCE photoresist responsive to temperature (Figure 14c).^[159] Wiresma et al. realized light control of the beam steerer with photo-responsive liquid crystalline network,^[545] which changes from an ordered nematic to a disordered arrangement under suitable irradiation, inducing a global structural change. They produced a grading structure to generate diffraction patterns, and the patterns could be controllable when projecting an extra laser from a tilting angle (Figure 14d). Besides direct printing the responsive materials, TPL can also be used to make solid molds to produce replica using responsive materials. Ruan et al. reported the TPL-fabricated relief structures to produced stretchable PDMS-based replica.^[485]

With the advantages of TPL 3D printing, various microrobots with sizes ranging from hundreds of micrometer to submicron have been fabricated,^[699–701] whose action can be controlled by acoustic, biohybrid, optical, magnetic, chemical, thermal, and electric methods.^[701] For optical controlled ones, also called light-powered microrobots,^[699–702] the commonly used materials for TPL are liquid crystals^[145,703] and poly (N-isopropylacrylamide) (PNIPAM),^[144] of which both can swell and shrink in response to the photothermal effect. Wiersma et al. reported the first light-powered TPL-fabricated microrobot,^[145] which has 1 soft orthogon body and 4 hard cone legs. The body and legs were made of LCE and IP-Dip, respectively by a multistep printing step. Under optical irradiation, this robot can move due to the reversible contraction (up to 20%) behavior of the LCE-based body, which is sensitive to photo-induced local heating (Figure 14e). To control the microrobot walking direction on the polyimide-coated glass is relatively harder than on a clean glass or a grating substrate due to the rough surface of polyimide, which induces significant friction fluctuations. Martella et al. also developed a hand-like microrobot with LCE that can catch small objects under laser irradiation either onto the microrobot itself or the vicinity of the targeting object (Figure 14f).^[703] PNIPAM is also widely used for the optical microrobots. Bastmeyer et al. developed the 3D hetero-microstructures using the responsive PNIPAM and the passive pentaerythritol triacrylate (PETA).^[144] Based on such design principal, they proved that a microbeam made of such a bi-layer structure can be bent in a programmable way under laser irradiation (Figure 14g). Beyond the responsive materials, there are several works reported that the introduction of plasmonic Au nanocrystals to promote both the photothermal and mechanical

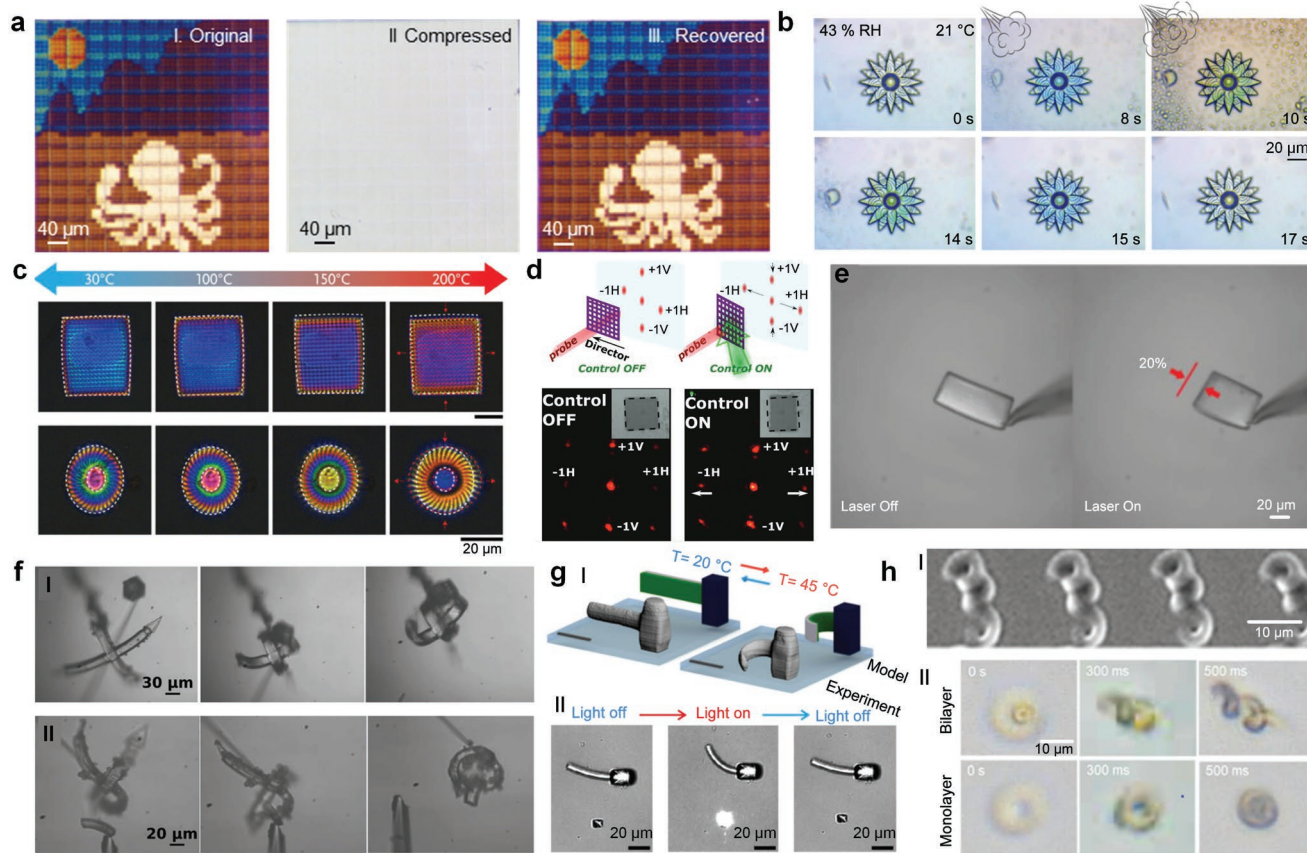


Figure 14. Dynamic optics and optical robots. a) An SMPs structural color demo made of 13×13 patches in its I) original, II) compressed, and III) recovered states. Reproduced under terms of the CC-BY license.^[114] Copyright 2021, the Authors, published by Nature publishing group. b) Micrographs that display the optical response of a printed flower upon exposure to breath and after. Reproduced with permission.^[692] Copyright 2020, American Chemical Society. c) Optical images of LCE printed 3D woodpile (top) and spiral disk (bottom) microstructures' temperature response. Reproduced under terms of the CC-BY license.^[159] Copyright 2022, the Authors, published by Wiley-VCH. d) Operating scheme and optical diffraction pattern with the laser control beam on and off respectively for structured optical structures printed by liquid crystalline networks. Reprinted with permission.^[545] Copyright 2018, Wiley-VCH. e) Optical image of a $60 \times 30 \times 10 \mu\text{m}^3$ with the laser off and on respectively.^[145] Copyright 2015, Wiley-VCH. f) Laser activated grabber. I) The hand is placed close to a microcube, activated with a green laser, then grabbing the microcube from a fiber tip. II) The same effect demonstrated with a LCN made block.^[703] Copyright 2017, Wiley-VCH. g) I) Scheme of bi-material hetero-structures. II) Optical images of a bi-materials beam with light on and off. Reproduced under terms of the CC-BY license.^[144] Copyright 2019, the Authors, published by Nature Publishing Group. h) I) SEM images of bilayer helices containing Au nanocrystals and PNIPAm gel, respectively. II) Phase-contrast images of the original, 300 ms exposed, and 500 ms exposed bilayer helix and soft monolayer helix. Reprinted with permission.^[704] Copyright 2020, American Chemical Society.

performance (Figure 14h),^[704,705] and magnetic nanoparticles could be used for electromagnetic control of the composite photoresist.^[706–710]

6. Challenges and Perspective

Though TPL has been widely used and has inspired various optical applications, its potential is far from fully explored. The advances in modern optics and photonics demand further developments in TPL fabrication techniques, along with the development of functional materials, manufacturing methods, and characterization approaches.^[711,712] The crucial step of TPL is in the light-matter interaction between ultra-short-pulsed lasers and resin, hence a deeper understanding of the underlying mechanisms will help us design unique photopolymers for particular applications.^[150,678,713,714] For example, with

high-efficiency radical quencher^[715] and photoinitiators,^[184,716] also customized monomers, proximity effects can be suppressed and mechanically stable 3D structures with feature size $< 50 \text{ nm}$ are possible, even toward 10 nm for chip-scale applications. To more efficiently modulate light, materials with high RI > 1.7 are required to bring functions comparable with EBL-based 2D metasurface,^[717,718] further minimize the elements,^[719] and also take another spatial degree of freedom into design. Post-processing-based RI improvement methods, such as doping-induced low surface roughness, pyrolysis-induced deformation and enhanced absorption can be avoided. Furthermore, the dispersion engineering is important to extend the applicable wavelength band beyond the visible range to UV, near infrared, and even middle and long infrared.^[470,720–723] However, the RI mismatching during the exposure process should be considered for fine structure fabrication. Photoresists with higher transparency are also required for better optical

performance, for example, IP-Dip shows a tint of light yellow, thus lower transmittance than IP-Visio, while the former is more suitable for high-resolution fabrication. In addition, conducting polymers are promising for various applications such as solar energy, flexible optoelectronics, and bio-optoelectronics. Carbon nano tubes,^[724,725] and silver nanowires^[388] were doped into the photoresist, but the induced scattering and absorption hampered the further use for nanoscale optical applications. With electric conductive polymer precursors,^[726–729] and the nanoscale printing ability of TPL, 3D nanostructures with optical transparency and high conductivity may change the research of photo-electronic circuits. Moreover, biocompatible photoresists based on materials such as chitin,^[730] cellulose^[731] could enable the implantation of 3D printed optical devices. Environment-sensitive and environment-friendly optical elements made of degradable materials like chemo-selectively cleavable photoresists,^[732] light-stabilized dynamic materials,^[733] and exposure degradable bimeane group photoresists,^[734] bring more possibilities for security labels and sensing. Other photo-responsive materials can be used for active optics and optical robots, such as precise medical operations.^[735,736] Furthermore, optical opaque photoresists can enhance the imaging contrast of lens,^[737] while optically clear yet radiopaque photoresists can enhance the contrast under X-ray computed tomography.^[738]

Regarding the femtosecond laser beam, there has been much progress in the development of focus modulation methods in TPL for plenty of applications. However, several challenges remain and much more can be done to unlock the full potential of TPL for optics and photonics.^[739] More developments should focus on the device development industry, as AOE used for focus modulation in TPL require higher resolution (pixel size of SLM or DMD), faster reconfigurable speed, and larger pixel numbers. It can be envisaged that the parallelization of a laser beam with distinct focus intensity can be utilized in more research areas about light-matter interaction, such as two-photon holographic microscopy. Additionally, optimization algorithms to generate the CGH (phase or amplitude pattern) are still needed, though series of work has been done in this field, the power of artificial neural networks or ML needs to be fully utilized for efficient wavefront detection and modulation of the focus in TPL. Further developments are also expected in the material field, where the varied novel materials can be applied for TPL under different focusing conditions,^[174] providing a larger scope for the utilization of focus modulation in TPL.

With the shaping of laser beam,^[740–742] optical elements with super smooth surface can be realized with grayscale lithography by modulating the intensity of laser for each voxel on the surface, avoiding slicing-induced defects.^[267] The local control of beam intensity also provides a powerful tool to change the material properties such as the RI and the transmittance via polymerization ratio, thus introducing inhomogeneous and engineering the interaction between the structure and light.^[470] Tuning the laser exposure dose and polymerization also affects the mechanical properties such as the swelling ratio^[158,743] and modulus,^[361] which are useful for the design and fabrication of active optical devices.^[744–746] For industrial manufacturing, multiple parallel beams with precise alignment, resonant-scanning two-photon microscope,^[747] three-mirror laser scanning

holographic lithography system^[748] have been developed toward high-speed centimeter scale superfine 3D TPL printing.^[749,750] Besides, by choosing appropriate negative or positive photoresists,^[113,481,751–753] the molding process for 2.5D structures can be significantly accelerated by combining with nanoimprinting, stepping forward to wafer-scale manufacturing. Combining one- and two-photon polymerization is also a feasible way for photonic integration.^[754] Moreover, with the recent development of cw laser polymerizable photoresists,^[755–757] cost-effective and high-power 3D TPL printing systems may bring new possibilities for industrial mass production, and also minimization into highly integrated equipment.^[758]

In addition, multimaterial printing is promising as different parts of the structure can be fabricated and integrated within one step for multifunctional applications.^[759] For example, microfluidic chamber can be integrated into the commercial TPL system to inject different resins to the printing plate,^[646] or MEMS stencil patterning can be combined for multimaterial fabrication.^[760,761] Different materials can also be introduced in the post-processing steps, for example, non-transparent parts can be fabricated onto the TPL printed structures by an inkjet printer to form a dark shell and an aperture for integrated miniature spectrometer.^[604] To reduce the usage of materials, printing with a wrapped lens is a simple way while maintaining the high resolution.^[762] Furthermore, other novel techniques like microfluidic-assisted 3D printing,^[501] sacrificial-scaffold-mediated TPL,^[763] and mask-assisted double-sided TPL^[764] could be used for specific optical element fabrications.

For fabricated transparent 3D structures that are < 100 micrometers in size and have characterizable feature sizes of < 1 micrometer, there is still a need for convenient characterization methods. It relates to non-destructive measurements that do not require tampering with samples, such as applying a reflective coating for reflective profilometry or conductive coatings for SEM imaging. Advanced optical methods are gaining attention and are being developed rapidly and for easy use: white light interferometry-based geometry analysis for feature and surface characterization is becoming the tool of choice, while the in-plane resolution still does not fulfil requirements.^[399,765] In addition, advanced microscopy-based wavefront sensor tools are becoming available that can directly measure optical path differences at 1 nm resolution, thus can characterize RI variations in both bulk and surface.^[766–768] obtaining more precise RI than the traditional ellipsometry.^[469] Moreover, internal material properties in terms of birefringence are also becoming accessible.^[769] The general outlook is that advanced tools that can be implemented as augmentations to classical and widespread bright field transmission microscopes will become more widespread. The high speed optical equipment such as optical diffraction tomography,^[770] and X-ray computed tomography^[771] offering non-destructive and 3D characterization of the produced object is also of critical importance for the advancement of the TPL technique.

With the ≈ 25-years development, the application of TPL has been involved in almost all the aspects of optics and photonics, along with the innovation of materials and techniques. From discrete elements to integrated systems,^[772,773] from chip-scale to wafer-scale, the pursuit of structural precision, surface smoothness, bulk uniformity, optical transparency, etc. of

optical elements never ceased. Following the continuous steps on expanding TPL application scenarios, the incoming burst to employ this powerful tool to investigate the light-matter interaction will sustainably invigorate the field, and further accelerate the optical and photonic research.

Acknowledgements

H.W. and W.Z. contributed equally to this work. H.W. and J.K.W.Y. acknowledge the support from the National Research Foundation (NRF) Singapore, under its Competitive Research Programme award NRF-CRP20-2017-0004 and NRF Investigatorship Award NRF-NRFI06-2020-0005, as well as the MTC Programmatic grant M21J9b0085. H.Y. and M.G. acknowledge the support from the Science and Technology Commission of Shanghai Municipality (grant no. 21DZ1100500), the Shanghai Municipal Science and Technology Major Project, the Shanghai Frontiers Science Center Program (2021-2025 No. 20), the Zhangjiang National Innovation Demonstration Zone (grant no. ZJ2019-ZD-005), and China Postdoctoral Research Foundation (grant no. 5B22904001 and 3722904006). D.L. thanks the support from Greece and the European Union (European Social Fund-ESF) through the Operational Programme–Human Resources Development, Education and Lifelong Learning—in the context of the Act “Enhancing Human Resources Research Potential by Undertaking a Doctoral Research” and IKY Scholarship Programme for PhD candidates in the Greek Universities (2022-050-0502-52271). M.F. thanks the grant from European Union under the Horizon 2020 research and innovation program (G.A. No. 964481–IN2SIGHT and 824996–PULSE). D.G. acknowledges the support from European Social Fund (project no 09.3.3-LMT-K712-17-0016) under the grant agreement with the Research Council of Lithuania (LMTLT). M.M. acknowledges the support from LASERLAB-EUROPE grant agreement no. 871124, European Union’s Horizon 2020 research and innovation programme. S.J. is grateful for partial support by the ARC DP190103284 grant.

Conflict of Interest

The authors declare no conflict of interest.

Keywords

3D printing, additive manufacturing, direct laser writing, light-matter interaction, optics and photonics, two-photon polymerization lithography

Received: December 6, 2022

Revised: February 1, 2023

Published online:

- [1] T. D. Ngo, A. Kashani, G. Imbalzano, K. T. Nguyen, D. Hui, *Compos. – B: Eng.* **2018**, *143*, 172.
- [2] S. V. Murphy, A. Atala, *Nat. Biotechnol.* **2014**, *32*, 773.
- [3] Z.-X. Low, Y. T. Chua, B. M. Ray, D. Mattia, I. S. Metcalfe, D. A. Patterson, *J. Membr. Sci.* **2017**, *523*, 596.
- [4] L. Y. Zhou, J. Fu, Y. He, *Adv. Funct. Mater.* **2020**, *30*, 2000187.
- [5] H. Liu, H. Zhang, W. Han, H. Lin, R. Li, J. Zhu, W. Huang, *Adv. Mater.* **2021**, *33*, 2004782.
- [6] X. Liu, J. Tao, J. Liu, X. Xu, J. Zhang, Y. Huang, Y. Chen, J. Zhang, D. Y. Deng, M. Gou, *ACS Appl. Mater. Interfaces* **2019**, *11*, 12209.

- [7] W. Xu, S. Jambhulkar, Y. Zhu, D. Ravichandran, M. Kakarla, B. Vernon, D. G. Lott, J. L. Cornella, O. Shefi, G. Miquelard-Garnier, *Compos. – B: Eng.* **2021**, *223*, 109102.
- [8] C. Yan, P. Jiang, X. Jia, X. Wang, *Nanoscale* **2020**, *12*, 2924.
- [9] M. Hippler, E. D. Lemma, S. Bertels, E. Blasco, C. Barner-Kowollik, M. Wegener, M. Bastmeyer, *Adv. Mater.* **2019**, *31*, 1808110.
- [10] A. Ambrosi, M. Pumera, *Chem. Soc. Rev.* **2016**, *45*, 2740.
- [11] P. Ahangar, M. E. Cooke, M. H. Weber, D. H. Rosenzweig, *Appl. Sci.* **2019**, *9*, 1713.
- [12] A. Bandyopadhyay, K. D. Traxel, S. Bose, *Mater. Sci. Eng. R Rep.* **2021**, *145*, 100609.
- [13] M. Regehy, Y. Garmshausen, M. Reuter, N. F. König, E. Israel, D. P. Kelly, C.-Y. Chou, K. Koch, B. Asfari, S. Hecht, *Nature* **2020**, *588*, 620.
- [14] B. Elder, R. Neupane, E. Tokita, U. Ghosh, S. Hales, Y. L. Kong, *Adv. Mater.* **2020**, *32*, 1907142.
- [15] Y. G. Santos, R. S. de Oliveira, T. V. de Oliveira, M. C. Velho, M. V. Konrad, G. S. da Silva, M. Deon, R. C. Beck, *Adv. Funct. Mater.* **2021**, *31*, 2009691.
- [16] H. Zhan, Y. Nie, Y. Chen, J. M. Bell, Y. Gu, *Adv. Funct. Mater.* **2020**, *30*, 1903841.
- [17] L. Y. Ee, S. F. Y. Li, *Nanoscale Adv.* **2021**, *3*, 1167.
- [18] Y. G. Park, I. Yun, W. G. Chung, W. Park, D. H. Lee, J. U. Park, *Adv. Sci.* **2022**, *9*, 2104623.
- [19] H. Kim, S.-k. Ahn, D. M. Mackie, J. Kwon, S. H. Kim, C. Choi, Y. H. Moon, H. B. Lee, S. H. Ko, *Mater. Today* **2020**, *41*, 243.
- [20] M. Chen, J. Yang, Z. Wang, Z. Xu, H. Lee, H. Lee, Z. Zhou, S. P. Feng, S. Lee, J. Pyo, *Adv. Mater.* **2019**, *31*, 1904073.
- [21] B. Ko, J. Kim, Y. Yang, T. Badloe, J. Park, J. H. Ko, M. Jeong, H. Kang, C. Jung, Y. M. Song, *Adv. Sci.* **2022**, *10*, 2204469.
- [22] G. Yoon, K. Kim, D. Huh, H. Lee, J. Rho, *Nat. Commun.* **2020**, *11*, 2268.
- [23] G. Yoon, K. Kim, S.-U. Kim, S. Han, H. Lee, J. Rho, *ACS Nano* **2021**, *15*, 698.
- [24] I. Kim, G. Yoon, J. Jang, P. Genevet, K. T. Nam, J. Rho, *ACS Photonics* **2018**, *5*, 3876.
- [25] C. Lee, G. Chang, J. Kim, G. Hyun, G. Bae, S. So, J. Yun, J. Seong, Y. Yang, D. Y. Park, S. Jeon, J. Rho, *ACS Photonics* **2022**, <https://doi.org/10.1021/acsp Photonics.2c01324>.
- [26] S. M. Kamali, E. Arbabi, H. Kwon, A. Faraon, *Proc. Natl. Acad. Sci. U.S.A.* **2019**, *116*, 21379.
- [27] W.-G. Kim, J.-M. Lee, Y. Yang, H. Kim, V. Devaraj, M. Kim, H. Jeong, E.-J. Choi, J. Yang, Y. Jang, T. Badloe, D. Lee, J. Rho, J. T. Kim, J.-W. Oh, *Nano Lett.* **2022**, *22*, 4702.
- [28] J. Bae, S. Lee, J. Ahn, J. H. Kim, M. Wajahat, W. S. Chang, S.-Y. Yoon, J. T. Kim, S. K. Seol, J. Pyo, *ACS Nano* **2020**, *14*, 10993.
- [29] W. Jung, Y.-H. Jung, P. V. Pikhitsa, J. Feng, Y. Yang, M. Kim, H.-Y. Tsai, T. Tanaka, J. Shin, K.-Y. Kim, *Nature* **2021**, *592*, 54.
- [30] G. Pakeltis, Z. Hu, A. G. Nixon, E. Mutunga, C. P. Anyanwu, C. A. West, J. C. Idrobo, H. Plank, D. J. Masiello, J. D. Fowlkes, *ACS Appl. Nano Mater.* **2019**, *2*, 8075.
- [31] H. Plank, R. Winkler, C. H. Schwalb, J. Hütner, J. D. Fowlkes, P. D. Rack, I. Utke, M. Huth, *Micromachines* **2019**, *11*, 48.
- [32] R. Winkler, J. D. Fowlkes, P. D. Rack, H. Plank, *J. Appl. Phys.* **2019**, *125*, 210901.
- [33] S. Chen, J. Chen, X. Zhang, Z.-Y. Li, J. Li, *Light Sci. Appl.* **2020**, *9*, 75.
- [34] J. Li, C. Wu, P. K. Chu, M. Gelinsky, *Mater. Sci. Eng. R Rep.* **2020**, *140*, 100543.
- [35] E. Geisler, M. Lecomperre, O. Soppera, *Photonics Res.* **2022**, *10*, 1344.
- [36] S. Park, W. Shou, L. Makatura, W. Matusik, K. K. Fu, *Matter* **2022**, *5*, 43.
- [37] X. Wang, M. Jiang, Z. Zhou, J. Gou, D. Hui, *Compos. – B: Eng.* **2017**, *110*, 442.

- [38] M. Layani, X. Wang, S. Magdassi, *Adv. Mater.* **2018**, *30*, 1706344.
- [39] M. Falahati, P. Ahmadvand, S. Safaei, Y.-C. Chang, Z. Lyu, R. Chen, L. Li, Y. Lin, *Mater. Today* **2020**, *40*, 215.
- [40] E. R. Zhiganshina, M. V. Arsenyev, D. A. Chubich, D. A. Kolymagin, A. V. Pisarenko, D. S. Burkatovsky, E. V. Baranov, A. G. Vitukhnovsky, A. N. Lobanov, R. P. Matital, *Eur. Polym. J.* **2022**, *162*, 110917.
- [41] Y. Yagci, S. Jockusch, N. J. Turro, *Macromolecules* **2010**, *43*, 6245.
- [42] A. Bagheri, J. Jin, *ACS Appl. Polym. Mater.* **2019**, *1*, 593.
- [43] H. Y. Jeong, E. Lee, S.-C. An, Y. Lim, Y. C. Jun, *Nanophotonics* **2020**, *9*, 1139.
- [44] J. Li, M. Purnera, *Chem. Soc. Rev.* **2021**, *50*, 2794.
- [45] G. L. Goh, H. Zhang, T. H. Chong, W. Y. Yeong, *Adv. Electron. Mater.* **2021**, *7*, 2100445.
- [46] M. Pagac, J. Hajnys, Q.-P. Ma, L. Jancar, J. Jansa, P. Stefek, J. Mesicek, *Polymers* **2021**, *13*, 598.
- [47] M. Vaezi, H. Seitz, S. Yang, *J. Adv. Manuf. Technol.* **2013**, *67*, 1721.
- [48] G. Berglund, A. Wisniowiecki, J. Gawedzinski, B. Applegate, T. S. Tkaczyk, *Optica* **2022**, *9*, 623.
- [49] A. Camposeo, L. Persano, M. Farsari, D. Pisignano, *Adv. Opt. Mater.* **2019**, *7*, 1800419.
- [50] X. Zhang, Y. Wang, B. Ding, X. Li, *Small* **2020**, *16*, 1902842.
- [51] K. Jung, N. Corrigan, M. Ciftci, J. Xu, S. E. Seo, C. J. Hawker, C. Boyer, *Adv. Mater.* **2020**, *32*, 1903850.
- [52] C. Liao, A. Wuethrich, M. Trau, *Appl. Mater. Today* **2020**, *19*, 100635.
- [53] M. Carloti, V. Mattoli, *Small* **2019**, *15*, 1902687.
- [54] M. He, Z. Zhang, C. Cao, G. Zhou, C. Kuang, X. Liu, *Laser Photonics Rev.* **2022**, *16*, 2100229.
- [55] Z. Sekkat, S. Kawata, *Laser Photonics Rev.* **2014**, *8*, 1.
- [56] L. Yang, F. Mayer, U. H. Bunz, E. Blasco, M. Wegener, *Light Adv. Manuf.* **2021**, *2*, 17.
- [57] P. Kiefer, V. Hahn, M. Nardi, L. Yang, E. Blasco, C. Barner-Kowollik, M. Wegener, *Adv. Opt. Mater.* **2020**, *8*, 2000895.
- [58] M. Göppert-Mayer, *Ann. Phys.* **1931**, *401*, 273.
- [59] W. Kaiser, C. G. B. Garrett, *Phys. Rev. Lett.* **1961**, *7*, 229.
- [60] H. K. Soong, J. B. Malta, *Am. J. Ophthalmol.* **2009**, *147*, 189.
- [61] S. Maruo, O. Nakamura, S. Kawata, *Opt. Lett.* **1997**, *22*, 132.
- [62] S. Kawata, H.-B. Sun, T. Tanaka, K. Takada, *Nature* **2001**, *412*, 697.
- [63] X. Zhou, Y. Hou, J. Lin, *AIP Adv.* **2015**, *5*, 030701.
- [64] K. Sugioka, Y. Cheng, *Appl. Phys. Rev.* **2014**, *1*, 041303.
- [65] L. Jonušauskas, S. Juodkazis, M. Malinauskas, *J. Opt.* **2018**, *20*, 053001.
- [66] C. N. LaFratta, T. Baldacchini, *Micromachines* **2017**, *8*, 101.
- [67] E. Skliutas, M. Lebedevaite, E. Kabouraki, T. Baldacchini, J. Ostrauskaite, M. Vamvakaki, M. Farsari, S. Juodkazis, M. Malinauskas, *Nanophotonics* **2021**, *10*, 1211.
- [68] S. C. Ligon, R. Liska, J. Stampfl, M. Gurr, R. Mülhaupt, *Chem. Rev.* **2017**, *117*, 10212.
- [69] S. Varapnickas, M. Malinauskas, in *Handbook of Laser Micro- and Nano-Engineering* (Ed: K. Sugioka), Springer, Cham **2020**, p. 1.
- [70] Y. Zhu, T. Tang, S. Zhao, D. Joralmon, Z. Poit, B. Ahire, S. Keshav, A. R. Raje, J. Blair, Z. Zhang, *Addit. Manuf.* **2022**, 102682.
- [71] A. Spangenberg, N. Hobeika, F. Stehlin, J.-P. Malval, F. Wieder, P. Prabhakaran, P. Baldeck, O. Soppera, in *Updates in Advanced Lithography* (Ed: S. Hosaka), IntechOpen, London, UK **2013**, Ch. 2, p. 35.
- [72] V. Harinarayana, Y. Shin, *Opt. Laser Technol.* **2021**, *142*, 107180.
- [73] H.-B. Sun, S. Kawata, *Adv. Polym. Sci.* **2006**, *170*, 169.
- [74] A. J. Otuka, N. B. Tomazio, K. T. Paula, C. R. Mendonça, *Polymers* **2021**, *13*, 1994.
- [75] J. Serbin, M. Gu, *Adv. Mater.* **2006**, *18*, 221.
- [76] X. Zheng, K. Cheng, X. Zhou, J. Lin, X. Jing, *AIP Adv.* **2017**, *7*, 095318.
- [77] E. P. Mottay, *Proc. SPIE* **2021**, *11768*, 1176807.
- [78] M. Han, D. Smith, S. H. Ng, V. Anand, T. Katkus, S. Juodkazis, *Eng. Proc.* **2021**, *11*, 44.
- [79] M. A. Ahmed, *Proc. SPIE* **2021**, *11664*, 1166404.
- [80] N. Hodgson, A. Steinkopff, S. Heming, H. Allegre, H. Haloui, T. S. Lee, M. Laha, J. VanNunen, *Proc. SPIE* **2021**, *11673*, 21.
- [81] L. Wang, Q.-D. Chen, X.-W. Cao, R. Buividas, X. Wang, S. Juodkazis, H.-B. Sun, *Light Sci. Appl.* **2017**, *6*, e17112.
- [82] E. Bonaccorso, *Proc. SPIE* **2021**, *11768*, 11768M.
- [83] J. Maksimovic, J. Hu, S. H. Ng, T. Katkus, G. Seniutinas, T. Pinedo Rivera, M. Stuber, Y. Nishijima, S. John, S. Juodkazis, *Opto-Electron. Adv.* **2022**, *5*, 210086.
- [84] L. Rapp, S. Madden, J. Brand, L. J. Walsh, H. Spallek, O. Zuaite, A. Habeb, T. R. Hirst, A. V. Rode, *Biomed. Opt. Express* **2022**, *13*, 4559.
- [85] D. J. Förster, B. Jäggi, A. Michalowski, B. Neuenschwander, *Materials* **2021**, *14*, 3331.
- [86] M. Malinauskas, A. Žukauskas, S. Hasegawa, Y. Hayasaki, V. Mizeikis, R. Buividas, S. Juodkazis, *Light Sci. Appl.* **2016**, *5*, e16133.
- [87] L. Jonusauskas, D. Gailevicius, S. Rekstyte, T. Baldacchini, S. Juodkazis, M. Malinauskas, *Opt. Express* **2019**, *27*, 15205.
- [88] D. Samsonas, E. Skliutas, A. Čiburys, L. Kontenis, D. Gailevičius, J. Berzinš, D. Narbutis, V. Jukna, M. Vengris, S. Juodkazis, M. Malinauskas, *Nanophotonics* **2023**, <https://doi.org/10.1515/nanoph-2022-0629>.
- [89] J. Bonse, S. Baudach, J. Krüger, W. Kautek, M. Lenzner, *Appl. Phys. A* **2002**, *74*, 19.
- [90] C. S. Nathala, A. Ajami, W. Husinsky, B. Farooq, S. I. Kudryashov, A. Daskalova, I. Bliznakova, A. Assion, *Appl. Phys. A* **2016**, *122*, 107.
- [91] E. G. Gamaly, A. Rode, *Appl. Phys. A* **2018**, *124*, 278.
- [92] Y. Nishijima, S. Morimoto, A. Balčytis, T. Hashizume, R. Matsubara, A. Kubono, N. To, M. Ryu, J. Morikawa, S. Juodkazis, *J. Mater. Chem. C* **2022**, *10*, 451.
- [93] Z.-Z. Li, L. Wang, H. Fan, Y.-H. Yu, Q.-D. Chen, S. Juodkazis, H.-B. Sun, *Light Sci. Appl.* **2020**, *9*, 41.
- [94] S. H. Ng, S. Juodkazis, in *Ultrafast Laser Nanostructuring: The Pursuit of Extreme Scales*, Vol. 239 (Eds: R. Stoian, J. Bonse), Springer, Berlin **2023**, Ch. 25.
- [95] F. H. Dill, *IEEE Trans. Electron Devices* **1975**, *22*, 440.
- [96] P. G. Eliseev, O. N. Krokhin, I. N. Zavestovskaya, *Appl. Surf. Sci.* **2005**, *248*, 313.
- [97] E. G. Gamaly, S. Juodkazis, K. Nishimura, H. Misawa, B. Luther-Davies, L. Hallo, P. Nicolai, V. T. Tikhonchuk, *Phys. Rev. B* **2006**, *73*, 214101.
- [98] E. G. Gamaly, A. V. Rode, B. Luther-Davies, V. T. Tikhonchuk, *Phys. Plasmas* **2002**, *9*, 949.
- [99] E. G. Gamaly, *Femtosecond Laser-Matter Interaction: Theory, Experiments and Applications*, Jenny Stanford Publishing, Dubai **2011**.
- [100] C. Kerse, H. Kalaycıoğlu, P. Elahi, B. Çetin, D. K. Kesim, Ö. Akçaalan, S. Yavaş, M. D. Aşık, B. Öktem, H. Hoogland, *Nature* **2016**, *537*, 84.
- [101] H. Nishiyama, Y. Hirata, in *Lithography* (Ed: M. Wang), InTech, Rijeka **2010**, Ch. 4.
- [102] M. Malinauskas, A. Žukauskas, G. Bičkuskaitė, R. Gadonas, S. Juodkazis, *Opt. Express* **2010**, *18*, 10209.
- [103] J. Fischer, J. B. Mueller, J. Kaschke, T. J. Wolf, A.-N. Unterreiner, M. Wegener, *Opt. Express* **2013**, *21*, 26244.
- [104] N. Murazawa, S. Juodkazis, H. Misawa, K. Kamada, *Mol. Cryst. Liq. Cryst.* **2008**, *489*, 310.
- [105] S. Rekštytė, T. Jonavičius, D. Gailevičius, M. Malinauskas, V. Mizeikis, E. G. Gamaly, S. Juodkazis, *Adv. Opt. Mater.* **2016**, *4*, 1209.
- [106] L. Li, J. T. Fourkas, *Mater. Today* **2007**, *10*, 30.

- [107] S. O'Halloran, A. Pandit, A. Heise, A. Kellett, *Adv. Sci.* **2022**, 2204072, <https://doi.org/10.1002/advs.202204072>.
- [108] D. Kam, A. Olender, A. Rudich, Y. Kan-Tor, A. Buxboim, O. Shoseyov, S. Magdassi, *Adv. Funct. Mater.* **2023**, 2210993, <https://doi.org/10.1002/adfm.202210993>.
- [109] S.-F. Liu, Z.-W. Hou, L. Lin, Z. Li, H.-B. Sun, *Adv. Funct. Mater.* **2023**, <https://doi.org/10.1002/adfm.202211280>.
- [110] M. Farsari, B. N. Chichkov, *Nat. Photon.* **2009**, 3, 450.
- [111] M. Farsari, M. Vamvakaki, B. N. Chichkov, *J. Opt.* **2010**, 12, 124001.
- [112] W. H. Teh, U. Durig, G. Salis, R. Harbers, U. Drechsler, R. F. Mahrt, C. G. Smith, H. J. Guntherodt, *Appl. Phys. Lett.* **2004**, 84, 4095.
- [113] W. Zhou, S. M. Kuebler, K. L. Braun, T. Yu, J. K. Cammack, C. K. Ober, J. W. Perry, S. R. Marder, *Science* **2002**, 296, 1106.
- [114] W. Zhang, H. Wang, H. Wang, J. Y. E. Chan, H. Liu, B. Zhang, Y.-F. Zhang, K. Agarwal, X. Yang, A. S. Ranganath, H. Y. Low, Q. Ge, J. K. W. Yang, *Nat. Commun.* **2021**, 12, 112.
- [115] W. Zhang, H. Wang, A. T. L. Tan, A. Sargur Ranganath, B. Zhang, H. Wang, J. Y. E. Chan, Q. Ruan, H. Liu, S. T. Ha, D. Wang, V. K. Ravikumar, H. Y. Low, J. K. W. Yang, *Nano Lett.* **2022**, 22, 8917.
- [116] C. Delaney, J. Qian, X. Zhang, R. Potyrailo, A. L. Bradley, L. Florea, *J. Mater. Chem. C* **2021**, 9, 11674.
- [117] M. Deubel, G. von Freymann, M. Wegener, S. Pereira, K. Busch, C. M. Soukoulis, *Nat. Mater.* **2004**, 3, 444.
- [118] V. Hahn, T. Messer, N. M. Bojanowski, E. R. Curticean, I. Wacker, R. R. Schroder, E. Blasco, M. Wegener, *Nat. Photon.* **2021**, 15, 932.
- [119] A. Ovsianikov, X. Shizhou, M. Farsari, M. Vamvakaki, C. Fotakis, B. N. Chichkov, *Opt. Express* **2009**, 17, 2143.
- [120] S. Shukla, E. P. Furlani, X. Vidal, M. T. Swihart, P. N. Prasad, *Adv. Mater.* **2010**, 22, 3695.
- [121] A. Vyatskikh, R. C. Ng, B. Edwards, R. M. Briggs, J. R. Greer, *Nano Lett.* **2020**, 20, 3513.
- [122] F. Kotz, A. S. Quick, P. Risch, T. Martin, T. Hoose, M. Thiel, D. Helmer, B. E. Rapp, *Adv. Mater.* **2021**, 33, 2006341.
- [123] X. Wen, B. Zhang, W. Wang, F. Ye, S. Yue, H. Guo, G. Gao, Y. Zhao, Q. Fang, C. Nguyen, *Nat. Mater.* **2021**, 20, 1506.
- [124] I. Cooperstein, S. C. Indukuri, A. Bouketov, U. Levy, S. Magdassi, *Adv. Mater.* **2020**, 32, 2001675.
- [125] Y. Peng, S. Jradi, X. Y. Yang, M. Dupont, F. Hamie, X. Q. Dinh, X. W. Sun, T. Xu, R. Bachelot, *Adv. Mater. Technol.* **2019**, 4, 1800522.
- [126] S. Maruo, S. Kawata, *J. Microelectromechanical Syst.* **1998**, 7, 411.
- [127] C. R. Mendonca, D. S. Correa, F. Marlow, T. Voss, P. Tayalia, E. Mazur, *Appl. Phys. Lett.* **2009**, 95, 250.
- [128] Z. B. Sun, X. Z. Dong, W. Q. Chen, S. Shoji, X. M. Duan, S. Kawata, *Nanotechnology* **2008**, 19, 035611.
- [129] Z. B. Sun, X. Z. Dong, W. Q. Chen, S. Nakanishi, X. M. Duan, S. Kawata, *Adv. Mater.* **2008**, 20, 914.
- [130] X. M. Duan, H. B. Sun, K. Kaneko, S. Kawata, *Thin Solid Films* **2004**, 453, 518.
- [131] T. Bückmann, N. Stenger, M. Kadic, J. Kaschke, A. Frölich, T. Kennerknecht, C. Eberl, M. Thiel, M. Wegener, *Adv. Mater.* **2012**, 24, 2710.
- [132] S. Schweiger, T. Schulze, S. Schlipf, P. Reinig, H. Schenk, *J. Opt. Microscop.* **2022**, 2, 033501.
- [133] M. Schmid, F. Sterl, S. Thiele, A. Herkommer, H. Giessen, *Opt. Lett.* **2021**, 46, 2485.
- [134] T. Gissibl, S. Thiele, A. Herkommer, H. Giessen, *Nat. Photon.* **2016**, 10, 554.
- [135] J. Lolsberg, J. Linkhorst, A. Cinar, A. Jans, A. J. C. Kuehne, M. Wessling, *Lab Chip* **2018**, 18, 1341.
- [136] H. Wang, Y. J. Liu, Q. F. Ruan, H. L. Liu, R. J. H. Ng, Y. S. Tan, H. T. Wang, Y. Li, C. W. Qiu, J. K. W. Yang, *Adv. Opt. Mater.* **2019**, 7, 1900068.
- [137] T. Y. Huang, M. S. Sakar, A. Mao, A. J. Petruska, F. Qiu, X. B. Chen, S. Kennedy, D. Mooney, B. J. Nelson, *Adv. Mater.* **2015**, 27, 6644.
- [138] J. Jang, J. Y. Kim, Y. C. Kim, S. Kim, N. Chou, S. Lee, Y. H. Choung, S. Kim, J. Brugger, H. Choi, J. H. Jang, *Adv. Healthcare Mater.* **2019**, 8, 1900379.
- [139] Q. Ge, A. H. Sakhaei, H. Lee, C. K. Dunn, N. X. Fang, M. L. Dunn, *Sci. Rep.* **2016**, 6, 31110.
- [140] B. Zhang, H. Li, J. Cheng, H. Ye, A. H. Sakhaei, C. Yuan, P. Rao, Y. F. Zhang, Z. Chen, R. Wang, *Adv. Mater.* **2021**, 33, 2101298.
- [141] L. Wang, F. Zhang, S. Du, J. Leng, *Compos. – A: Appl. Sci. Manuf.* **2022**, 162, 107146.
- [142] A. Sydney Gladman, E. A. Matsumoto, R. G. Nuzzo, L. Mahadevan, J. A. Lewis, *Nat. Mater.* **2016**, 15, 413.
- [143] Q. Ge, Z. Chen, J. Cheng, B. Zhang, Y.-F. Zhang, H. Li, X. He, C. Yuan, J. Liu, S. Magdassi, *Sci. Adv.* **2021**, 7, eaba4261.
- [144] M. Hippler, E. Blasco, J. Qu, M. Tanaka, C. Barner-Kowollik, M. Wegener, M. Bastmeyer, *Nat. Commun.* **2019**, 10, 232.
- [145] H. Zeng, P. Wasylczyk, C. Parmeggiani, D. Martella, M. Burrelli, D. S. Wiersma, *Adv. Mater.* **2015**, 27, 3883.
- [146] H. Zeng, H. Zhang, O. Ikkala, A. Priimagi, *Matter* **2020**, 2, 194.
- [147] M. J. Ford, C. P. Ambulo, T. A. Kent, E. J. Markvicka, C. Pan, J. Malen, T. H. Ware, C. Majidi, *Proc. Natl. Acad. Sci. U.S.A.* **2019**, 116, 21438.
- [148] J. Leng, H. Lv, Y. Liu, S. Du, *Appl. Phys. Lett.* **2007**, 91, 144105.
- [149] Q. Ze, X. Kuang, S. Wu, J. Wong, S. M. Montgomery, R. Zhang, J. M. Kovitz, F. Yang, H. J. Qi, R. Zhao, *Adv. Mater.* **2020**, 32, 1906657.
- [150] Z. Chen, D. Zhao, B. Liu, G. Nian, X. Li, J. Yin, S. Qu, W. Yang, *Adv. Funct. Mater.* **2019**, 29, 1900971.
- [151] L. V. Elliott, E. E. Salzman, J. R. Greer, *Adv. Funct. Mater.* **2021**, 31, 2008380.
- [152] C. A. Spiegel, M. Hackner, V. P. Bothe, J. P. Spatz, E. Blasco, *Adv. Funct. Mater.* **2022**, 2110580.
- [153] X. Xia, A. Afshar, H. Yang, C. M. Portela, D. M. Kochmann, C. V. Di Leo, J. R. Greer, *Nature* **2019**, 573, 205.
- [154] H. Zeng, D. Martella, P. Wasylczyk, G. Cerretti, J. C. G. Lavocat, C. H. Ho, C. Parmeggiani, D. S. Wiersma, *Adv. Mater.* **2014**, 26, 2319.
- [155] Y. Guo, J. Zhang, W. Hu, M. T. A. Khan, M. Sitti, *Nat. Commun.* **2021**, 12, 5936.
- [156] A. Münchinger, L.-Y. Hsu, F. Fürtner, E. Blasco, M. Wegener, *Mater. Today* **2022**, 59, 9.
- [157] M. Hippler, K. Weissenbruch, K. Richler, E. D. Lemma, M. Nakahata, B. Richter, C. Barner-Kowollik, Y. Takashima, A. Harada, E. Blasco, *Sci. Adv.* **2020**, 6, eabc2648.
- [158] D. Jin, Q. Chen, T.-Y. Huang, J. Huang, L. Zhang, H. Duan, *Mater. Today* **2020**, 32, 19.
- [159] M. del Pozo, C. Delaney, M. Pilz da Cunha, M. G. Debije, L. Florea, A. P. Schenning, *Small Struct.* **2022**, 3, 2100158.
- [160] T. Zhao, R. Yu, X. Li, B. Cheng, Y. Zhang, X. Yang, X. Zhao, Y. Zhao, W. Huang, *Eur. Polym. J.* **2018**, 101, 120.
- [161] J. Torgersen, X. H. Qin, Z. Q. Li, A. Ovsianikov, R. Liska, J. Stampfl, *Adv. Funct. Mater.* **2013**, 23, 4542.
- [162] J. L. Drury, D. J. Mooney, *Biomaterials* **2003**, 24, 4337.
- [163] D. Wu, Q. D. Chen, L. G. Niu, J. N. Wang, J. Wang, R. Wang, H. Xia, H. B. Sun, *Lab Chip* **2009**, 9, 2391.
- [164] P. J. Su, Q. A. Tran, J. J. Fong, K. W. Eliceiri, B. M. Ogle, P. J. Campagnola, *Biomacromolecules* **2012**, 13, 2917.
- [165] L. P. Cunningham, M. P. Veilleux, P. J. Campagnola, *Opt. Express* **2006**, 14, 8613.
- [166] S. Basu, L. P. Cunningham, G. D. Pins, K. A. Bush, R. Taboada, A. R. Howell, J. Wang, P. J. Campagnola, *Biomacromolecules* **2005**, 6, 1465.
- [167] S. Basu, P. J. Campagnola, *Biomacromolecules* **2004**, 5, 572.

- [168] S. Basu, P. J. Campagnola, *J. Biomed. Mater. Res., Part A* **2004**, *71A*, 359.
- [169] J. D. Pitts, A. R. Howell, R. Taboada, I. Banerjee, J. Wang, S. L. Goodman, P. J. Campagnola, *Photochem. Photobiol.* **2002**, *76*, 135.
- [170] D. Serien, K. Sugioka, *ACS Biomater. Sci. Eng.* **2020**, *6*, 1279.
- [171] J. D. Pitts, P. J. Campagnola, G. A. Epling, S. L. Goodman, *Macromolecules* **2000**, *33*, 1514.
- [172] K. Parkatzidis, E. Kabouraki, A. Selimis, M. Kaliva, A. Ranella, M. Farsari, M. Vamvakaki, *Macromol. Mater. Eng.* **2018**, *303*, 1800458.
- [173] M. Lebedevaite, J. Ostrauskaite, E. Skliutas, M. Malinauskas, *Polymers* **2019**, *11*, 116.
- [174] H. Yu, H. Ding, Q. Zhang, Z. Gu, M. Gu, *Light Adv. Manuf.* **2021**, *2*, 3.
- [175] A. Ovsianikov, S. Muhleder, J. Torgersen, Z. Li, X. H. Qin, S. Van Vlierberghe, P. Dubruel, W. Holthöner, H. Redl, R. Liska, J. Stampfl, *Langmuir* **2014**, *30*, 3787.
- [176] V. Melissinaki, A. A. Gill, I. Ortega, M. Vamvakaki, A. Ranella, J. W. Haycock, C. Fotakis, M. Farsari, F. Claeysens, *Biofabrication* **2011**, *3*, 045005.
- [177] P. S. Timashev, K. N. Bardakova, N. V. Minaev, T. S. Demina, T. A. Mishchenko, E. V. Mitroshina, A. A. Akovantseva, A. A. Koroleva, D. S. Asyutin, L. F. Pimenova, N. A. Konovalov, T. A. Akopova, A. B. Solov'eva, I. V. Mukhina, M. V. Vedunova, B. N. Chichkov, V. N. Bagratashvili, *Prikl. Biokhim. Mikrobiol.* **2016**, *52*, 495.
- [178] M. Lebedevaite, J. Ostrauskaite, E. Skliutas, M. Malinauskas, *J. Appl. Polym. Sci.* **2020**, *137*, 48708.
- [179] M. Lebedevaite, J. Ostrauskaite, *Ind. Crops Prod.* **2021**, *161*, 113210.
- [180] S. Grauzeliene, A. Navaruckiene, E. Skliutas, M. Malinauskas, A. Serra, J. Ostrauskaite, *Polymers* **2021**, *13*, 872.
- [181] G. O. Dias, O. Lecarme, J. Cordeiro, E. Picard, D. Peyrade, *Microelectron. Eng.* **2022**, *257*, 111751.
- [182] B. L. Aekbote, T. Fekete, J. Jacak, G. Vizsnyiczai, P. Ormos, L. Kelemen, *Biomed. Opt. Express* **2016**, *7*, 45.
- [183] V. Mizeikis, K. K. Seet, S. Juodkazis, H. Misawa, *Opt. Lett.* **2004**, *29*, 2061.
- [184] S. M. Kuebler, K. L. Braun, W. H. Zhou, J. K. Cammack, T. Y. Yu, C. K. Ober, S. R. Marder, J. W. Perry, *J. Photochem. Photobiol. A* **2003**, *158*, 163.
- [185] G. Witzgall, R. Vrijen, E. Yablonovitch, V. Doan, B. J. Schwartz, *Opt. Lett.* **1998**, *23*, 1745.
- [186] V. C. Pinto, P. J. Sousa, V. F. Cardoso, G. Minas, *Micromachines* **2014**, *5*, 738.
- [187] L. Sun, H. Zou, S. Sang, *Polym. Eng. Sci.* **2021**, *61*, 2222.
- [188] N. Tsutsumi, N. Sakamoto, R. Nakamura, K. Kinashi, W. Sakai, *J. Laser Appl.* **2017**, *29*, 042010.
- [189] A. Ovsianikov, S. Schlie, A. Ngezahayo, A. Haverich, B. N. Chichkov, *J. Tissue Eng. Regener. Med.* **2007**, *1*, 443.
- [190] V. Hahn, P. Rietz, F. Hermann, P. Müller, C. Barner-Kowollik, T. Schlöder, W. Wenzel, E. Blasco, M. Wegener, *Nat. Photon.* **2022**, *16*, 784.
- [191] D. K. Limberg, J. H. Kang, R. C. Hayward, *J. Am. Chem. Soc.* **2022**, *144*, 5226.
- [192] S. N. Sanders, T. H. Schloemer, M. K. Gangishetty, D. Anderson, M. Seitz, A. O. Gallegos, R. C. Stokes, D. N. Congreve, *Nature* **2022**, *604*, 474.
- [193] V. V. Rocheva, A. V. Koroleva, A. G. Savelyev, K. V. Khaydukov, A. N. Generalova, A. V. Nechaev, A. E. Guller, V. A. Semchishen, B. N. Chichkov, E. V. Khaydukov, *Sci. Rep.* **2018**, *8*, 3663.
- [194] X. Liu, Y. Yang, J. Qiu, *J. Non-Cryst. Sol.* **2022**, *15*, 100114.
- [195] P. Delrot, D. Loterie, C. Moser, in 2021 21st Int. Conf. Solid-State Sensors, Actuators Microsystems (Transducers), IEEE, New Jersey **2021**, p. 397.
- [196] D. Loterie, P. Delrot, C. Moser, *Nat. Commun.* **2020**, *11*, 852.
- [197] P. N. Bernal, M. Bouwmeester, J. Madrid-Wolff, M. Falandt, S. Florczak, N. G. Rodriguez, Y. Li, G. Grossbacher, R. A. Samsom, M. van Wolferen, L. J. W. van der Laan, P. Delrot, D. Loterie, J. Malda, C. Moser, B. Spee, R. Levato, *Adv. Mater.* **2022**, *34*, 2110054.
- [198] J. Madrid-Wolff, A. Boniface, D. Loterie, P. Delrot, C. Moser, *Adv. Sci.* **2022**, *9*, 2105144.
- [199] J. T. Toombs, M. Luitz, C. C. Cook, S. Jenne, C. C. Li, B. E. Rapp, F. Kotz-Helmer, H. K. Taylor, *Science* **2022**, *376*, 308.
- [200] N. Liaros, *Opt. Lett.* **2022**, *47*, 3327.
- [201] M. Farsari, G. Filippidis, C. Fotakis, *Opt. Lett.* **2005**, *30*, 3180.
- [202] Y. Jun, P. Nagpal, D. J. Norris, *Adv. Mater.* **2008**, *20*, 606.
- [203] A. I. Maydykovskiy, E. A. Mamonov, N. V. Mitetelo, S. Soria, T. V. Murzina, *JETP Lett.* **2022**, *115*, 261.
- [204] M. Triplett, L. Kessler, S. Sahota, K. Kampasi, X. Tan, R.-u. Haque, C.-P. Richter, *Proc. SPIE* **2022**, *11935*, 1193502.
- [205] M. A. Brown, K. M. Zappitelli, L. Singh, R. C. Yuan, M. A. Bemrose, V. Brogden, D. J. Miller, S. F. Cogan, T. J. Gardner, *Biorxiv* **2022**, <https://doi.org/10.1101/2022.06.07.495165>.
- [206] B. Lamprecht, A. Ulm, P. Lichtenegger, C. Leiner, W. Nemitz, C. Sommer, *Appl. Opt.* **2022**, *61*, 1863.
- [207] D. Weyers, A. Mistry, K. Niewegłowski, K. Bock, in 2022 IEEE 72nd Electron. Comp. Technol. Conf. (ECTC), IEEE, San Diego, CA, USA **2022**, p. 1919.
- [208] P. Danilevicius, S. Rekštytė, E. Balciunas, A. Kraniuska, R. Jarasiene, R. Sirmenis, D. Baltrikiene, V. Bukelskiene, R. Gadonas, M. Malinauskas, *J. Biomed. Opt.* **2012**, *17*, 081405.
- [209] S. Rekštytė, D. Paipulas, M. Malinauskas, V. Mizeikis, *Nanotechnology* **2017**, *28*, 124001.
- [210] A. Ovsianikov, J. Viertl, B. Chichkov, M. Oubaha, B. MacCraith, I. Sakellari, A. Giakoumaki, D. Gray, M. Vamvakaki, M. Farsari, *ACS Nano* **2008**, *2*, 2257.
- [211] S. Psycharakis, A. Tosca, V. Melissinaki, A. Giakoumaki, A. Ranella, *Biomed. Mater.* **2011**, *6*, 045008.
- [212] J. Mačiulaitis, M. Deveikytė, S. Rekštytė, M. Bratichkov, A. Darinskas, A. Šimbelytė, G. Daunoras, A. Laurinavičienė, A. Laurinavičius, R. Gudas, *Biofabrication* **2015**, *7*, 015015.
- [213] D. Ladika, G. Noirbent, F. Dumur, D. Gigmes, A. Mourka, G. D. Barmparis, M. Farsari, D. Gray, *Appl. Phys. A* **2022**, *128*, 745.
- [214] G. Zyla, A. Kovalev, C. Esen, A. Ostendorf, S. Gorb, *J. Opt. Microsyst.* **2022**, *2*, 031203.
- [215] D. Gailevičius, V. Padolskytė, L. Mikoliūnaitė, S. Šakirzanovas, S. Juodkazis, M. Malinauskas, *Nanoscale Horiz.* **2019**, *4*, 647.
- [216] G. Merkininkaitė, E. Aleksandravičius, M. Malinauskas, D. Gailevičius, S. Šakirzanovas, *Opto-Electron. Adv.* **2022**, *5*, 210077.
- [217] K. Terzaki, N. Vasilantonakis, A. Gaidukeviciute, C. Reinhardt, C. Fotakis, M. Vamvakaki, M. Farsari, *Opt. Mater. Express* **2011**, *1*, 586.
- [218] M. Emons, K. Obata, T. Binhammer, A. Ovsianikov, B. N. Chichkov, U. Morgner, *Opt. Mater. Express* **2012**, *2*, 942.
- [219] E. Balčiūnas, S. J. Baldock, N. Dreižė, M. Grubliauskaitė, S. Coultas, D. L. Rochester, M. Valius, J. G. Hardy, D. Baltrikiene, *Polym. Int.* **2019**, *68*, 1928.
- [220] E. Balciunas, N. Dreize, M. Grubliauskaite, S. Urnikyte, E. Simoliunas, V. Bukelskiene, M. Valius, S. J. Baldock, J. G. Hardy, D. Baltrikiene, *Materials* **2019**, *12*, 3932.
- [221] I. Sakellari, A. Gaidukeviciute, A. Giakoumaki, D. Gray, C. Fotakis, M. Farsari, M. Vamvakaki, C. Reinhardt, A. Ovsianikov, B. N. Chichkov, *Appl. Phys. A* **2010**, *100*, 359.
- [222] I. Sakellari, E. Kabouraki, D. Karanikolopoulos, S. Droulias, M. Farsari, P. Loukakos, M. Vamvakaki, D. Gray, *Nanoscale Adv.* **2019**, *1*, 3413.
- [223] S. K. Saha, B. Au, J. S. Oakdale, *Adv. Eng. Mater.* **2019**, *21*, 1900583.

- [224] E. Kabouraki, A. N. Giakoumaki, P. Danilevicius, D. Gray, M. Vamvakaki, M. Farsari, *Nano Lett.* **2013**, *13*, 3831.
- [225] A. Vyatskikh, S. Delalande, A. Kudo, X. Zhang, C. M. Portela, J. R. Greer, *Nat. Commun.* **2018**, *9*, 593.
- [226] D. W. Yee, M. L. Lifson, B. W. Edwards, J. R. Greer, *Adv. Mater.* **2019**, *31*, 1901345.
- [227] M. Malinauskas, A. Gaidukevičiūtė, V. Purlys, A. Žukauskas, I. Sakellari, E. Kabouraki, A. Candiani, D. Gray, S. Pissadakis, R. Gadonas, *Metamaterials* **2011**, *5*, 135.
- [228] M. Malinauskas, A. Zukauskas, V. Purlys, A. Gaidukevičiūtė, Z. Balevicius, A. Piskarskas, C. Fotakis, S. Pissadakis, D. Gray, R. Gadonas, M. Vamvakaki, M. Farsari, *Opt. Lasers Eng.* **2012**, *50*, 1785.
- [229] M. Oubaha, A. Kavanagh, A. Gorin, G. Bickauskaite, R. Byrne, M. Farsari, R. Winfield, D. Diamond, C. McDonagh, R. Copperwhite, *J. Mater. Chem.* **2012**, *22*, 10552.
- [230] T. Tanaka, A. Ishikawa, S. Kawata, *Appl. Phys. Lett.* **2006**, *88*, 081107.
- [231] S. Shukla, X. Vidal, E. P. Furlani, M. T. Swihart, K. T. Kim, Y. K. Yoon, A. Urbas, P. N. Prasad, *ACS Nano* **2011**, *5*, 1947.
- [232] I. Izquierdo-Lorenzo, S. Jradi, P. M. Adam, *RSC Adv.* **2014**, *4*, 4128.
- [233] E. Blasco, J. Muller, P. Muller, V. Trouillet, M. Schon, T. Scherer, C. Barner-Kowollik, M. Wegener, *Adv. Mater.* **2016**, *28*, 3592.
- [234] R. Nakamura, K. Kinashi, W. Sakai, N. Tsutsumi, *Phys. Chem. Chem. Phys.* **2016**, *18*, 17024.
- [235] Y. A. Liu, Q. Hu, F. Zhang, C. Tuck, D. Irvine, R. Hague, Y. F. He, M. Simonelli, G. A. Rance, E. F. Smith, R. D. Wildman, *Polymers* **2016**, *8*, 325.
- [236] Q. Hu, X. Z. Sun, C. D. J. Parmenter, M. W. Fay, E. F. Smith, G. A. Rance, Y. He, F. Zhang, Y. Liu, D. Irvine, C. Tuck, R. Hague, R. Wildman, *Sci. Rep.* **2017**, *7*, 17150.
- [237] A. Jaiswal, S. Rani, G. P. Singh, S. Saxena, S. Shukla, *Mater. Lett.* **2021**, *304*, 130642.
- [238] F. Kotz, K. Arnold, W. Bauer, D. Schild, N. Keller, K. Sachsenheimer, T. M. Nargang, C. Richter, D. Helmer, B. E. Rapp, *Nature* **2017**, *544*, 337.
- [239] F. Kotz, N. Schneider, A. Striegel, A. Wolfschlagel, N. Keller, M. Worgull, W. Bauer, D. Schild, M. Milich, C. Greiner, D. Helmer, B. E. Rapp, *Adv. Mater.* **2018**, *30*, 1707100.
- [240] R. Ni, B. Qian, C. Liu, X. Liu, J. Qiu, *Opt. Express* **2018**, *26*, 25481.
- [241] C.-L. Tai, W.-L. Hong, Y.-T. Kuo, C.-Y. Chang, M.-C. Niu, M. Karupathevar Ponnusamythevar Ochathevar, C.-L. Hsu, S.-F. Horng, Y.-C. Chao, *ACS Appl. Mater. Interfaces* **2019**, *11*, 30176.
- [242] M. Gastaldi, F. Cardano, M. Zanetti, G. Viscardi, C. Barolo, S. Bordiga, S. Magdassi, A. Fin, I. Roppolo, *ACS Mater. Lett.* **2020**, *3*, 1.
- [243] B. Jia, D. Buso, J. van Embden, J. Li, M. Gu, *Adv. Mater.* **2010**, *22*, 2463.
- [244] A. Marino, J. Barsotti, G. de Vito, C. Filippeschi, B. Mazzolai, V. Piazza, M. Labardi, V. Mattoli, G. Ciofani, *ACS Appl. Mater. Interfaces* **2015**, *7*, 25574.
- [245] J. Chen, K. Zidek, P. Chabera, D. Liu, P. Cheng, L. Nuuttilla, M. J. Al-Marri, H. Lehtivuori, M. E. Messing, K. Han, K. Zheng, T. Pullerits, *J. Phys. Chem. Lett.* **2017**, *8*, 2316.
- [246] T. Ritacco, G. E. Lio, X. L. Xu, A. Broussier, A. Issa, M. Giocondo, R. Bachelot, S. Blaize, C. Couteau, S. Jradi, *ACS Appl. Nano Mater.* **2021**, *4*, 6916.
- [247] A. Jaiswal, S. Rani, G. P. Singh, S. Saxena, S. Shukla, *J. Phys. Photonics* **2021**, *3*, 034021.
- [248] D. G. Moore, L. Barbera, K. Masania, A. R. Studart, *Nat. Mater.* **2020**, *19*, 212.
- [249] H. Zhang, L. Huang, M. Tan, S. Zhao, H. Liu, Z. Lu, J. Li, Z. Liang, *Micromachines* **2022**, *13*, 81.
- [250] B. Tan, K. Venkatakrishnan, A. Makaronets, *Des. Monomers Polym.* **2013**, *16*, 145.
- [251] T. Baldacchini, S. Snider, R. Zadayan, *Opt. Express* **2012**, *20*, 29890.
- [252] H. B. Sun, T. Tanaka, S. Kawata, *Appl. Phys. Lett.* **2002**, *80*, 3673.
- [253] H. B. Sun, K. Takada, M. S. Kim, K. S. Lee, S. Kawata, *Appl. Phys. Lett.* **2003**, *83*, 1104.
- [254] R. J. DeVoe, H. W. Kalweit, C. A. Leatherdale, T. R. Williams, *Proc. SPIE* **2003**, *4797*, 310.
- [255] H. B. Sun, M. Maeda, K. Takada, J. W. M. Chon, M. Gu, S. Kawata, *Appl. Phys. Lett.* **2003**, *83*, 819.
- [256] C. Arnoux, L. A. Perez-Covarrubias, A. Khaldi, Q. Carlier, P. L. Baldeck, K. Heggarty, A. Banyasz, C. Monnereau, *Addit. Manuf.* **2022**, *49*, 102491.
- [257] L. P. Covarrubias, C. Arnoux, Q. Carlier, A. Khaldi, P. Baldeck, K. Heggarty, *Proc. SPIE* **2020**, *11349*, 43.
- [258] A. Žukauskas, M. Malinauskas, E. Brasselet, *Appl. Phys. Lett.* **2013**, *103*, 181122.
- [259] S. Reškštytė, M. Malinauskas, S. Juodkazis, *Opt. Express* **2013**, *21*, 17028.
- [260] E. Polonio-Alcalá, M. Rabionet, A. J. Guerra, M. Yeste, J. Ciurana, T. Puig, *Int. J. Mol. Sci.* **2018**, *19*, 3148.
- [261] M. Malinauskas, P. Danilevičius, S. Juodkazis, *Opt. Express* **2011**, *19*, 5602.
- [262] L. Jonušauskas, D. Gailevičius, L. Mikoliūnaitė, D. Sakalauskas, S. Šakirzanovas, S. Juodkazis, M. Malinauskas, *Materials* **2017**, *10*, 12.
- [263] J. Stampfl, R. Liska, A. Ovsianikov, *Multiphoton Lithography: Techniques, Materials, and Applications*, Wiley, Hoboken **2016**.
- [264] M. Malinauskas, A. Zukauskas, V. Purlys, K. Belazaras, A. Momot, D. Paipulas, R. Gadonas, A. Piskarskas, H. Gilbergs, A. Gaidukevičiūtė, I. Sakellari, M. Farsari, S. Juodkazis, *J. Opt.* **2010**, *12*, 124010.
- [265] J. S. Oakdale, R. F. Smith, J. B. Forien, W. L. Smith, S. J. Ali, L. B. B. Aji, T. M. Willey, J. C. Ye, A. W. van Buuren, M. A. Worthington, S. T. Prisbrey, H. S. Park, P. A. Amendt, T. F. Baumann, J. Biener, *Adv. Funct. Mater.* **2017**, *27*, 1702425.
- [266] Q. Liu, K. Vanmol, S. Lycke, J. Van Erps, P. Vandenabeele, H. Thienpont, H. Ottevaere, *RSC Adv.* **2020**, *10*, 14274.
- [267] T. Aderneuer, O. Fernandez, R. Ferrini, *Opt. Express* **2021**, *29*, 39511.
- [268] A. Butkus, E. Skliutas, D. Gailevičius, M. Malinauskas, *J. Cent. South Univ.* **2022**, *29*, 3270.
- [269] M. D. Turner, M. Saba, Q. M. Zhang, B. P. Cumming, G. E. Schroder-Turk, M. Gu, *Nat. Photon.* **2013**, *7*, 801.
- [270] H. Yu, Q. Zhang, B. P. Cumming, E. Goi, J. H. Cole, H. Luan, X. Chen, M. Gu, *Adv. Sci.* **2021**, *8*, 2100141.
- [271] X. Y. Fang, H. R. Ren, M. Gu, *Nat. Photon.* **2020**, *14*, 102.
- [272] H. Y. Yu, Q. M. Zhang, X. Chen, H. T. Luan, M. Gu, *Adv. Photonics* **2022**, *4*, 034002.
- [273] R. D. Simmonds, P. S. Salter, A. Jesacher, M. J. Booth, *Opt. Express* **2011**, *19*, 24122.
- [274] B. P. Cumming, M. D. Turner, G. E. Schroder-Turk, S. Debbarma, B. Luther-Davies, M. Gu, *Opt. Express* **2014**, *22*, 689.
- [275] E. H. Waller, M. Renner, G. von Freymann, *Opt. Express* **2012**, *20*, 24949.
- [276] B. P. Cumming, S. Debbarma, B. Luther-Davis, M. Gu, *Opt. Express* **2013**, *21*, 19135.
- [277] L. Yang, D. D. Qian, C. Xin, Z. J. Hu, S. Y. Ji, D. Wu, Y. L. Hu, J. W. Li, W. H. Huang, J. R. Chu, *Appl. Phys. Lett.* **2017**, *110*, 221103.
- [278] J. Kato, N. Takeyasu, Y. Adachi, H. B. Sun, S. Kawata, *Appl. Phys. Lett.* **2005**, *86*, 044102.
- [279] X. P. Li, Y. Y. Cao, N. Tian, L. Fu, M. Gu, *Optica* **2015**, *2*, 567.
- [280] G. Lee, S. H. Song, C. H. Oh, P. S. Kim, *Opt. Lett.* **2004**, *29*, 2539.
- [281] L. Yang, A. El-Tamer, U. Hinze, J. W. Li, Y. L. Hu, W. H. Huang, J. R. Chu, B. N. Chichkoy, *Opt. Lasers Eng.* **2015**, *70*, 26.
- [282] B. Mills, J. A. Grant-Jacob, M. Feinaeugle, R. W. Eason, *Opt. Express* **2013**, *21*, 14853.

- [283] P. Török, P. Varga, Z. Laczik, G. Booker, *J. Opt. Soc. Am. A* **1995**, *12*, 325.
- [284] A. Marcinkevičius, V. Mizeikis, S. Juodkasis, S. Matsuo, H. Misawa, *Appl. Phys. A* **2003**, *76*, 257.
- [285] Q. Sun, H. B. Jiang, Y. Liu, Y. H. Zhou, H. Yang, Q. H. Gong, *J. Opt. A-Pure Appl. Opt.* **2005**, *7*, 655.
- [286] M. J. Booth, M. A. A. Neil, T. Wilson, *J. Microscopy-Oxford* **1998**, *192*, 90.
- [287] H. B. Ding, Q. M. Zhang, H. C. Gu, X. J. Liu, L. T. Sun, M. Gu, Z. Z. Gu, *Adv. Funct. Mater.* **2020**, *30*, 1901760.
- [288] M. J. Booth, M. Schwertner, T. Wilson, M. Nakano, Y. Kawata, M. Nakabayashi, S. Miyata, *Appl. Phys. Lett.* **2006**, *88*, 031109.
- [289] N. Bischof, J. Guan, M. J. Booth, P. S. Salter, *Appl. Phys. A* **2019**, *125*, 364.
- [290] P. S. Salter, M. J. Woolley, S. M. Morris, M. J. Booth, J. A. J. Fells, *Opt. Lett.* **2018**, *43*, 5993.
- [291] S. Stallinga, *J. Opt. Soc. Am. A* **2001**, *18*, 2846.
- [292] G. Zhou, A. Jesacher, M. Booth, T. Wilson, A. Rodenas, D. Jaque, M. Gu, *Opt. Express* **2009**, *17*, 17970.
- [293] P. Karpinski, V. Shvedov, W. Krolikowski, C. Hnatovsky, *Opt. Express* **2016**, *24*, 7456.
- [294] M. J. Booth, *Light Sci. Appl.* **2014**, *3*, e165.
- [295] P. S. Salter, Z. Iqbal, M. J. Booth, *Int. J. Optomechanics* **2013**, *7*, 1.
- [296] P. S. Salter, M. Baum, I. Alexeev, M. Schmidt, M. J. Booth, *Opt. Express* **2014**, *22*, 17644.
- [297] C. Mauclair, A. Mermillod-Blondin, N. Huot, E. Audouard, R. Stoian, *Opt. Express* **2008**, *16*, 5481.
- [298] C. C. Tartan, P. S. Salter, T. D. Wilkinson, M. J. Booth, S. M. Morris, S. J. Elston, *RSC Adv.* **2017**, *7*, 507.
- [299] M. Manousidaki, D. G. Papazoglou, M. Farsari, S. Tzortzakos, *Opt. Lett.* **2020**, *45*, 85.
- [300] L. Kelemen, P. Ormos, G. Vizsnyiczai, *J. Eur. Opt. Soc.-Rapid Publ.* **2011**, *6*, 11029.
- [301] P. Somers, Z. Liang, J. E. Johnson, B. W. Boudouris, L. Pan, X. Xu, *Light Sci. Appl.* **2021**, *10*, 199.
- [302] M. Ams, G. Marshall, D. Spence, M. Withford, *Opt. Express* **2005**, *13*, 5676.
- [303] D. Pan, S. Liu, J. Li, J. Ni, C. Xin, S. Ji, Z. Lao, C. Zhang, B. Xu, R. Li, *Adv. Funct. Mater.* **2022**, *32*, 2106917.
- [304] J. Ni, S. Liu, Y. Chen, G. Hu, Y. Hu, W. Chen, J. Li, J. Chu, C.-W. Qiu, D. Wu, *Nano Lett.* **2022**, *22*, 9013.
- [305] L. Liu, D. Yang, W. Wan, H. Yang, Q. Gong, Y. Li, *Nanophotonics* **2019**, *8*, 1087.
- [306] H. Yu, Q. Zhang, M. Gu, *Opt. Express* **2018**, *26*, 32111.
- [307] Y. Cheng, K. Sugioka, K. Midorikawa, M. Masuda, K. Toyoda, M. Kawachi, K. Shihoyama, *Opt. Lett.* **2003**, *28*, 55.
- [308] P. S. Salter, A. Jesacher, J. B. Spring, B. J. Metcalf, N. Thomas-Peter, R. D. Simmonds, N. K. Langford, I. A. Walsley, M. J. Booth, *Opt. Lett.* **2012**, *37*, 470.
- [309] Y. Liao, J. Qi, P. Wang, W. Chu, Z. Wang, L. Qiao, Y. Cheng, *Sci. Rep.* **2016**, *6*, 28790.
- [310] J. Qi, P. Wang, Y. Liao, W. Chu, Z. M. Liu, Z. H. Wang, L. L. Qiao, Y. Cheng, *Opt. Mater. Express* **2016**, *6*, 2554.
- [311] G. Cerullo, R. Osellame, S. Taccheo, M. Marangoni, D. Polli, R. Ramponi, P. Laporta, S. De Silvestri, *Opt. Lett.* **2002**, *27*, 1938.
- [312] R. R. Thomson, A. S. Bockelt, E. Ramsay, S. Beecher, A. H. Greenaway, A. K. Kar, D. T. Reid, *Opt. Express* **2008**, *16*, 12786.
- [313] A. R. De La Cruz, A. Ferrer, W. Gawelda, D. Puerto, M. G. Sosa, J. Siegel, J. Solis, *Opt. Express* **2009**, *17*, 20853.
- [314] E. Goi, B. S. Mashford, B. P. Cumming, M. Gu, *Adv. Opt. Mater.* **2016**, *4*, 226.
- [315] B. K. Wang, Q. M. Zhang, M. Gu, *Opt. Mater. Express* **2020**, *10*, 3174.
- [316] M. D. Turner, G. E. Schroder-Turk, M. Gu, *Opt. Express* **2011**, *19*, 10001.
- [317] H. Yu, *Masters Thesis*, RMIT University, Melbourne **2019**.
- [318] M. Saba, M. D. Turner, K. Mecke, M. Gu, G. E. Schroder-Turk, *Phys. Rev. B* **2013**, *88*, 245116.
- [319] J. A. Dolan, B. D. Wilts, S. Vignolini, J. J. Baumberg, U. Steiner, T. D. Wilkinson, *Adv. Opt. Mater.* **2015**, *3*, 12.
- [320] H. Ren, G. Briere, X. Fang, P. Ni, R. Sawant, S. Heron, S. Chenot, S. Veizan, B. Damilano, V. Brandli, S. A. Maier, P. Genevet, *Nat. Commun.* **2019**, *10*, 2986.
- [321] B. Mills, D. Kundys, M. Farsari, S. Mailis, R. W. Eason, *Appl. Phys. A* **2012**, *108*, 651.
- [322] S. J. Zhang, Y. Li, Z. P. Liu, J. L. Ren, Y. F. Xiao, H. Yang, Q. H. Gong, *Appl. Phys. Lett.* **2014**, *105*, 061101.
- [323] L. Li, R. R. Gattass, E. Gershgoren, H. Hwang, J. T. Fourkas, *Science* **2009**, *324*, 910.
- [324] T. F. Scott, B. A. Kowalski, A. C. Sullivan, C. N. Bowman, R. R. McLeod, *Science* **2009**, *324*, 913.
- [325] Z. Gan, Y. Cao, R. A. Evans, M. Gu, *Nat. Commun.* **2013**, *4*, 2061.
- [326] J. Hering, E. H. Waller, G. Von Freymann, *Opt. Express* **2016**, *24*, 28500.
- [327] T. J. Gould, D. Burke, J. Bewersdorf, M. J. Booth, *Opt. Express* **2012**, *20*, 20998.
- [328] H. Yu, W. Shao, Q. Zhang, F. D. Salim, M. Gu, in *2019 Conf. Lasers Electro Opt. Europe Europ. Quant. Electron. Conf. IEEE*, Munich, Germany **2019**, p 1.
- [329] L. Jiang, P. J. Liu, X. L. Yan, N. Leng, C. C. Xu, H. Xiao, Y. F. Lu, *Opt. Lett.* **2012**, *37*, 2781.
- [330] S. Matsuo, S. Juodkasis, H. Misawa, *Appl. Phys. A* **2005**, *80*, 683.
- [331] N. J. Jenness, K. D. Wulff, M. S. Johannes, M. J. Padgett, D. G. Cole, R. L. Clark, *Opt. Express* **2008**, *16*, 15942.
- [332] M. Yamaji, H. Kawashima, J. Suzuki, S. Tanaka, *Appl. Phys. Lett.* **2008**, *93*, 041116.
- [333] Z. Kuang, D. Liu, W. Perrie, S. Edwardson, M. Sharp, E. Fearon, C. Dearden, K. Watkins, *Appl. Surf. Sci.* **2009**, *255*, 6582.
- [334] C. S. Lim, M. H. Hong, Y. Lin, G. X. Chen, A. S. Kumar, M. Rahman, L. S. Tan, J. Y. Fuh, G. C. Lim, *J. Mater. Process. Technol.* **2007**, *192*, 328.
- [335] R. Di Leonardo, F. Ianni, G. Ruocco, *Opt. Express* **2007**, *15*, 1913.
- [336] R. W. Gerchberg, *Optik* **1972**, *35*, 237.
- [337] M. Sakakura, T. Sawano, Y. Shimotsuna, K. Miura, K. Hirao, *Opt. Express* **2010**, *18*, 12136.
- [338] J. Bengtsson, *Appl. Opt.* **1994**, *33*, 6879.
- [339] H. Ren, H. Lin, X. Li, M. Gu, *Opt. Lett.* **2014**, *39*, 1621.
- [340] A. Jesacher, M. J. Booth, *Opt. Express* **2010**, *18*, 21090.
- [341] E. H. Waller, G. von Freymann, *Opt. Express* **2013**, *21*, 21708.
- [342] Z. Y. Zhang, C. C. Zhang, Y. L. Hu, C. W. Wang, J. W. Li, Y. H. Su, J. R. Chu, D. Wu, *Appl. Phys. Lett.* **2016**, *109*, 021109.
- [343] K. Obata, J. Koch, U. Hinze, B. N. Chichkov, *Opt. Express* **2010**, *18*, 17193.
- [344] H. Lin, B. Jia, M. Gu, *Opt. Lett.* **2011**, *36*, 406.
- [345] B. Sun, P. S. Salter, C. Roider, A. Jesacher, J. Strauss, J. Heberle, M. Schmidt, M. J. Booth, *Light Sci. Appl.* **2018**, *7*, 17117.
- [346] S. Hasegawa, Y. Hayasaki, *Opt. Lett.* **2011**, *36*, 2943.
- [347] K. L. Włodarczyk, J. J. J. Kaakkunen, P. Vahimaa, D. P. Hand, *Appl. Phys. A* **2014**, *116*, 111.
- [348] S. Hasegawa, H. Ito, H. Toyoda, Y. Hayasaki, *Opt. Express* **2016**, *24*, 18513.
- [349] Q. Geng, D. Wang, P. Chen, S.-C. Chen, *Nat. Commun.* **2019**, *10*, 2179.
- [350] C. Maibohm, O. F. Silvestre, J. Borme, M. Sinou, K. Heggarty, J. B. Nieder, *Sci. Rep.* **2020**, *10*, 8740.
- [351] L. Zhang, B. Liu, C. Wang, C. Xin, R. Li, D. Wang, L. Xu, S. Fan, J. Zhang, C. Zhang, *Nano Lett.* **2022**, *22*, 5277.

- [352] G. Vizsnyczai, L. Kelemen, P. Ormos, *Opt. Express* **2014**, *22*, 24217.
- [353] L. Yang, J. W. Li, Y. L. Hu, C. C. Zhang, Z. X. Lao, W. H. Huang, J. R. Chu, *Opt. Commun.* **2014**, *331*, 82.
- [354] Y. C. Li, T. F. Yeh, H. C. Huang, H. Y. Chang, C. Y. Lin, L. C. Cheng, C. Y. Chang, H. Teng, S. J. Chen, *Opt. Express* **2014**, *22*, 19726.
- [355] G. Zhu, J. van Howe, M. Durst, W. Zipfel, C. Xu, *Opt. Express* **2005**, *13*, 2153.
- [356] D. Oron, Y. Silberberg, *Opt. Express* **2005**, *13*, 9903.
- [357] K. S. Lee, D. Y. Yang, S. H. Park, R. H. Kim, *Polym. Adv. Technol.* **2006**, *17*, 72.
- [358] N. Rohbeck, R. Ramachandramoorthy, D. Casari, P. Schurch, T. E. J. Edwards, L. Schilinsky, L. Philippe, J. Schwiedrzik, J. Michler, *Mater. Des.* **2020**, *195*, 108977.
- [359] L. Pertoldi, V. Zega, C. Comi, R. Osellame, *J. Appl. Phys.* **2020**, *128*, 175102.
- [360] E. D. Lemma, F. Rizzi, T. Dattoma, B. Spagnolo, L. Sileo, A. Quattieri, M. De Vittorio, F. Pisanello, *IEEE Trans. Nanotechnol.* **2016**, *16*, 23.
- [361] L. J. Jiang, Y. S. Zhou, W. Xiong, Y. Gao, X. Huang, L. Jiang, T. Baldacchini, J.-F. Silvain, Y. F. Lu, *Opt. Lett.* **2014**, *39*, 3034.
- [362] J. S. Oakdale, J. Ye, W. L. Smith, J. Biener, *Opt. Express* **2016**, *24*, 27077.
- [363] Y. Liu, J. Campbell, O. Stein, L. Jiang, J. Hund, Y. Lu, *Nanomaterials* **2018**, *8*, 498.
- [364] M. Sun, H. Cheng, P. Golvari, S. M. Kuebler, X. Yu, M. Zhang, *Addit. Manuf.* **2022**, *60*, 103241.
- [365] Y. Bougdid, Z. Sekkat, *Sci. Rep.* **2020**, *10*, 10409.
- [366] L. Yang, A. Munchinger, M. Kadic, V. Hahn, F. Mayer, E. Blasco, C. Barner-Kowollik, M. Wegener, *Adv. Opt. Mater.* **2019**, *7*, 1901040.
- [367] M. G. Guney, G. K. Fedder, *J. Micromech. Microeng.* **2016**, *26*, 105011.
- [368] A. Butkutė, L. Čekanavičius, G. Rimšelis, D. Gailevičius, V. Mizeikis, A. Melninkaitis, T. Baldacchini, L. Jonušauskas, M. Malinauskas, *Opt. Lett.* **2020**, *45*, 13.
- [369] S. K. Saha, C. Divin, J. A. Cuadra, R. M. Panas, *J. Micro Nano-Manuf.* **2017**, *5*, 031002.
- [370] H. Wang, H. Wang, W. Zhang, J. K. W. Yang, *ACS Nano* **2020**, *14*, 10452.
- [371] A.-I. Bunea, N. del Castillo Iniesta, A. Droumpali, A. E. Wetzel, E. Engay, R. Taborski, *Micro* **2021**, *1*, 164.
- [372] Z. F. Rad, P. D. Prewett, G. J. Davies, *Addit. Manuf.* **2022**, *56*, 102953.
- [373] T. Onanuga, *Masters Thesis*, Friedrich-Alexander-Universität Erlangen-Nürnberg (FAU), Nurnberg **2019**.
- [374] Q. Hu, G. A. Rance, G. F. Trindade, D. Pervan, L. Jiang, A. Foerster, L. Turyanska, C. Tuck, D. J. Irvine, R. Hague, R. D. Wildman, *Addit. Manuf.* **2022**, *51*, 102575.
- [375] F. Glöckler, D. Müller, F. Erb, K.-E. Gottschalk, A. Kienle, *Opt. Mater. Express* **2019**, *9*, 2327.
- [376] E. M. Harnisch, T. Venek, S. Nohr, N. Konig, R. Schmitt, *Opt. Mater. Express* **2019**, *9*, 269.
- [377] T. Zandrini, N. Liaros, L. Jiang, Y. Lu, J. Fourkas, R. Osellame, T. Baldacchini, *Opt. Mater. Express* **2019**, *9*, 2601.
- [378] M. Hasan, S. Blair, *Opt. Mater. Express* **2022**, *12*, 895.
- [379] N. Lang, S. Enns, J. Hering, G. von Freymann, *Opt. Express* **2022**, *30*, 28805.
- [380] X. Y. Lee, S. K. Saha, S. Sarkar, B. Giera, *Addit. Manuf.* **2020**, *36*, 101444.
- [381] H.-B. Sun, T. Suwa, K. Takada, R. P. Zaccaria, M.-S. Kim, K.-S. Lee, S. Kawata, *Appl. Phys. Lett.* **2004**, *85*, 3708.
- [382] D.-Y. Yang, S. H. Park, T. W. Lim, H.-J. Kong, S. W. Yi, H. K. Yang, K.-S. Lee, *Appl. Phys. Lett.* **2007**, *90*, 013113.
- [383] T. Tanaka, H. B. Sun, S. Kawata, *Appl. Phys. Lett.* **2002**, *80*, 312.
- [384] C. Y. Liao, M. Bouriauand, P. L. Baldeck, J. C. Leon, C. Masclet, T. T. Chung, *Appl. Phys. Lett.* **2007**, *91*, 033108.
- [385] S.-H. Park, K. H. Kim, T. W. Lim, D.-Y. Yang, K.-S. Lee, *Microelectron. Eng.* **2008**, *85*, 432.
- [386] K. Ueno, S. Juodkazis, T. Shibuya, Y. Yokota, V. Mizeikis, K. Sasaki, H. Misawa, *J. Am. Chem. Soc.* **2008**, *130*, 6928.
- [387] A. Sundaramurthy, P. J. Schuck, N. R. Conley, D. P. Fromm, G. S. Kino, W. Moerner, *Nano Lett.* **2006**, *6*, 355.
- [388] Y. Liu, W. Xiong, Y. Lu, X. Huang, H. Liu, L. S. Fan, L. Jiang, J.-F. Silvain, Y. F. Lu, *Int. J. Extreme Manuf.* **2019**, *1*, 025001.
- [389] J. Purto, A. Verch, P. Rogin, R. Hensel, *Microelectron. Eng.* **2018**, *194*, 45.
- [390] X. G. Shang, N. Wang, Z. M. Wang, H. Q. Jiang, Y. F. Jia, N. J. Zhou, M. Qiu, *Appl. Phys. Lett.* **2022**, *120*, 171107.
- [391] J. Bauer, A. G. Izzard, Y. F. Zhang, T. Baldacchini, L. Valdevit, *Opt. Express* **2020**, *28*, 20362.
- [392] F. Mayer, D. Ryklin, I. Wacker, R. Curticean, M. Calkovsky, A. Niemeyer, Z. Dong, P. A. Levkin, D. Gerthsen, R. R. Schroder, M. Wegener, *Adv. Mater.* **2020**, *32*, 2002044.
- [393] J. Arai, *J. Appl. Electrochem.* **2002**, *32*, 1071.
- [394] J.-G. Park, S.-H. Lee, J.-S. Ryu, Y.-K. Hong, T.-G. Kim, A. A. Busnaina, *J. Electrochem. Soc.* **2006**, *153*, G811.
- [395] H. Namatsu, K. Yamazaki, K. Kurihara, *Microelectron. Eng.* **1999**, *46*, 129.
- [396] Y. Liu, O. Stein, J. H. Campbell, L. Jiang, N. Petta, Y. Lu, *SPIE Nanosci. Eng.* **2017**, *10354*, 103541U.
- [397] L. Jiang, J. Campbell, Y. Lu, T. Bernat, N. Petta, *Fusion Sci. Technol.* **2016**, *70*, 295.
- [398] H. E. Bennett, J. O. Porteus, *J. Opt. Soc. Am.* **1961**, *51*, 123.
- [399] T. Gissibl, S. Thiele, A. Herkommer, H. Giessen, *Nat. Commun.* **2016**, *7*, 11763.
- [400] M. Malinauskas, M. Farsari, A. Piskarskas, S. Juodkazis, *Phys. Rep.* **2013**, *533*, 1.
- [401] M. Malinauskas, V. Purylys, M. Rutkauskas, R. Gadonas, *Proc. SPIE* **7204**, **2009**, 84.
- [402] K. Takada, H.-B. Sun, S. Kawata, *Appl. Phys. Lett.* **2005**, *86*, 071122.
- [403] M. Malinauskas, G. Bičkauskaitė, M. Rutkauskas, D. Paipulas, V. Purylys, R. Gadonas, *Lith. J. Phys.* **2010**, *50*, 75.
- [404] D. Wu, S.-Z. Wu, L.-G. Niu, Q.-D. Chen, R. Wang, J.-F. Song, H.-H. Fang, H.-B. Sun, *Appl. Phys. Lett.* **2010**, *97*, 031109.
- [405] S. Wang, Y. Yu, H. Liu, K. T. P. Lim, B. M. Srinivasan, Y. W. Zhang, J. K. W. Yang, *Nano Futures* **2018**, *2*, 025006.
- [406] H. Xia, J. Wang, Y. Tian, Q.-D. Chen, X.-B. Du, Y.-L. Zhang, Y. He, H.-B. Sun, *Adv. Mater.* **2010**, *22*, 3204.
- [407] S. H. Park, S. H. Lee, D.-Y. Yang, H. J. Kong, K.-S. Lee, *Appl. Phys. Lett.* **2005**, *87*, 154108.
- [408] R. Guo, S. Xiao, X. Zhai, J. Li, A. Xia, W. Huang, *Opt. Express* **2006**, *14*, 810.
- [409] H. Wang, H. Wang, Q. Ruan, Y. S. Tan, C.-W. Qiu, J. K. W. Yang, *ACS Nano* **2021**, *15*, 10185.
- [410] Y.-L. Zhang, Q.-D. Chen, H. Xia, H.-B. Sun, *Nano Today* **2010**, *5*, 435.
- [411] Z. D. Popovic, R. A. Sprague, G. A. Neville Connell, *Appl. Opt.* **1988**, *27*, 1281.
- [412] F. T. O'Neill, J. T. Sheridan, *Optik* **2002**, *113*, 405.
- [413] K. Kim, K.-W. Jang, J.-K. Ryu, K.-H. Jeong, *Light Sci. Appl.* **2020**, *9*, 28.
- [414] M. Wang, W. Yu, T. Wang, X. Han, E. Gu, X. Li, *RSC Adv.* **2015**, *5*, 35311.
- [415] A. Schleunitz, V. A. Guzenko, M. Messerschmidt, H. Atasoy, R. Kirchner, H. Schiff, *Nano Converg.* **2014**, *1*, 7.
- [416] R. Kirchner, H. Schiff, *Mater. Sci. Semicond.* **2019**, *92*, 58.
- [417] R. Kirchner, A. Schleunitz, R. Zhang, H. Schiff, *J. Photopolym. Sci. Technol.* **2020**, *32*, 799.
- [418] R. Kirchner, N. Chidambaram, M. Altana, H. Schiff, *Proc. SPIE* **2017**, *10095*, 8.

- [419] H. Schiff, N. Chidambaram, M. Altana, R. Kirchner, *Proc. SPIE* **2017**, 10144, 51.
- [420] R. Kirchner, N. Chidambaram, H. Schiff, *Opt. Eng.* **2018**, 57, 041403.
- [421] H. Schiff, R. Kirchner, N. Chidambaram, M. Altana, *Proc. SPIE* **2018**, 10456, 39.
- [422] N. Chidambaram, R. Kirchner, R. Fallica, L. Yu, M. Altana, H. Schiff, *Adv. Mater. Technol.* **2017**, 2, 1700018.
- [423] C. Arnoux, T. Konishi, E. Van Elslande, E.-A. Poutougnigni, J.-C. Mulatier, L. Khrouz, C. Bucher, E. Dumont, K. Kamada, C. Andraud, *Macromolecules* **2020**, 53, 9264.
- [424] Y. Bougdid, I. Maouli, A. Rahmouni, K. Mochizuki, I. Bennani, M. Halim, Z. Sekkat, *J. Micromech. Microeng.* **2019**, 29, 035018.
- [425] J. Fischer, M. Wegener, *Laser Photonics Rev.* **2013**, 7, 22.
- [426] L. Zheng, K. Kurselis, A. El-Tamer, U. Hinze, C. Reinhardt, L. Overmeyer, B. Chichkov, *Nanoscale Res. Lett.* **2019**, 14, 134.
- [427] T. Ding, J. Mertens, A. Lombardi, O. A. Scherman, J. J. Baumberg, *ACS Photonics* **2017**, 4, 1453.
- [428] L. Jonušauskas, M. Lau, P. Gruber, B. Gökce, S. Barcikowski, M. Malinauskas, A. Ovsianikov, *Nanotechnology* **2016**, 27, 154001.
- [429] Y. Wang, S. Wang, S. Zhang, O. A. Scherman, J. J. Baumberg, T. Ding, H. Xu, *Nano Res.* **2018**, 11, 6384.
- [430] F. Kameche, W. Heni, S. Telitel, D. Ge, L. Vidal, F. Dumur, D. Gigmes, J. Lalevee, S. Marguet, L. Douillard, *Mater. Today* **2020**, 40, 38.
- [431] F. Kameche, W. Heni, S. Telitel, L. Vidal, S. Marguet, L. Douillard, C. Fiorini-Debuisschert, R. Bachelot, O. Soppera, *J. Phys. Chem. C* **2021**, 125, 8719.
- [432] Y. Liu, H. Wang, J. Ho, R. C. Ng, R. J. H. Ng, V. H. Hall-Chen, E. H. H. Koay, Z. Dong, H. Liu, C.-W. Qiu, J. R. Greer, J. K. W. Yang, *Nat. Commun.* **2019**, 10, 4340.
- [433] Z. Gan, M. D. Turner, M. Gu, *Sci. Adv.* **2016**, 2, 1600084.
- [434] J. Fischer, M. Wegener, *Opt. Mater. Express* **2011**, 1, 614.
- [435] I. Sakellari, E. Kabouraki, D. Gray, V. Purlys, C. Fotakis, A. Pikulin, N. Bityurin, M. Vamvakaki, M. Farsari, *ACS Nano* **2012**, 6, 2302.
- [436] C. Cao, Y. Qiu, L. Guan, Z. Wei, Z. Yang, L. Zhan, D. Zhu, C. Ding, X. Shen, X. Xia, *ACS Appl. Mater. Interfaces* **2022**, 14, 31332.
- [437] G. E. Lio, A. Ferraro, T. Ritacco, D. M. Aceti, A. De Luca, M. Giocondo, R. Caputo, *Adv. Mater.* **2021**, 33, 2008644.
- [438] Q.-Q. Liu, Y.-Y. Zhao, M.-L. Zheng, X.-M. Duan, *Appl. Phys. Lett.* **2017**, 111, 223102.
- [439] G. Zyla, A. Kovalev, M. Grafen, E. L. Gurevich, C. Esen, A. Ostendorf, S. Gorb, *Sci. Rep.* **2017**, 7, 17622.
- [440] G. Zyla, A. Kovalev, S. Heisterkamp, C. Esen, E. L. Gurevich, S. Gorb, A. Ostendorf, *Opt. Mater. Express* **2019**, 9, 2630.
- [441] H. Gu, X. Liu, Z. Mu, Q. Wang, H. Ding, X. Du, Z. Gu, *ACS Appl. Mater. Interfaces* **2021**, 13, 60648.
- [442] H. K. Raut, H. Wang, Q. Ruan, H. Wang, J. G. Fernandez, J. K. Yang, *Nano Lett.* **2021**, 21, 8602.
- [443] G. Seniutinas, A. Weber, C. Padeste, I. Sakellari, M. Farsari, C. David, *Microelectron. Eng.* **2018**, 191, 25.
- [444] C. Conci, E. Jacchetti, L. Sironi, L. Gentili, G. Cerullo, R. Osellame, G. Chirico, M. T. Raimondi, *Adv. Opt. Mater.* **2022**, 10, 2101103.
- [445] M. Malinauskas, D. Baltriukiene, A. Kraniauskas, P. Danilevicius, R. Jarsiene, R. Sirmenis, A. Zukauskas, E. Balciunas, V. Purlys, R. Gadonas, *Appl. Phys. A* **2012**, 108, 751.
- [446] A. Žukauskas, G. Batavičiūtė, M. Ščiuka, Z. Balevičius, A. Melninkaitis, M. Malinauskas, *Opt. Mater.* **2015**, 39, 224.
- [447] E. Kabouraki, V. Melissinaki, A. Yadav, A. Melninkaitis, K. Tourlouki, T. Tachtsidis, N. Kehagias, G. D. Barmparis, D. G. Papazoglou, E. Rafailou, *Nanophotonics* **2021**, 10, 3759.
- [448] A. E. G. Merkininkaitė, S. Varapnickas, D. Gailevicius, S. Sakirzanovas, M. Malinauskas, in *Ultrafast Laser Nanostructuring – The Pursuit of Extreme Scales* (Eds: R. Stoian, J. Bonse), Springer, Berlin **2023**.
- [449] J. Bauer, A. Schroer, R. Schwaiger, O. Kraft, *Nat. Mater.* **2016**, 15, 438.
- [450] F. Jin, J. Liu, Y.-Y. Zhao, X.-Z. Dong, M.-L. Zheng, X.-M. Duan, *Nat. Commun.* **2022**, 13, 1357.
- [451] M. Sharipova, T. Baluyan, K. Abrashitova, G. Kulagin, A. Petrov, A. Chizhov, T. Shatalova, D. Chubich, D. Kolymagin, A. Vitukhnovsky, *Opt. Mater. Express* **2021**, 11, 371.
- [452] P. Serles, M. Haché, J. Tam, A. Maguire, T. Li, G. Wang, K. Sebastian, J. Lou, C. Jia, P. M. Ajayan, *Carbon* **2023**, 201, 161.
- [453] D. Jang, L. R. Meza, F. Greer, J. R. Greer, *Nat. Mater.* **2013**, 12, 893.
- [454] A. Ovsianikov, A. Ostendorf, B. Chichkov, *Appl. Surf. Sci.* **2007**, 253, 6599.
- [455] T. A. Pham, D. P. Kim, T. W. Lim, S. H. Park, D. Y. Yang, K. S. Lee, *Adv. Funct. Mater.* **2006**, 16, 1235.
- [456] J. Li, B. Jia, M. Gu, *Opt. Express* **2008**, 16, 20073.
- [457] J. Winczewski, M. Herrera, C. Cabriel, I. Izeddin, S. Gabel, B. Merle, A. Susarrey Arce, H. Gardeniers, *Adv. Opt. Mater.* **2022**, 10, 2102758.
- [458] A. Bertoncini, C. Liberale, *IEEE Photon. Technol. Lett.* **2018**, 30, 1882.
- [459] S. Thiele, K. Arzenbacher, T. Gissibl, H. Giessen, A. M. Herkommer, *Sci. Adv.* **2017**, 3, e1602655.
- [460] S. Varapnickas, S. Chandran Thodika, F. Moroté, S. Juodkazis, M. Malinauskas, E. Basselet, *Appl. Phys. Lett.* **2021**, 118, 151104.
- [461] Z. Y. Hu, Y. L. Zhang, C. Pan, J. Y. Dou, Z. Z. Li, Z. N. Tian, J. W. Mao, Q. D. Chen, H. B. Sun, *Nat. Commun.* **2022**, 13, 5634.
- [462] A. Žukauskas, M. Malinauskas, C. Reinhardt, B. N. Chichkov, R. Gadonas, *Appl. Opt.* **2012**, 51, 4995.
- [463] C. Liberale, G. Cojoc, P. Candeloro, G. Das, F. Gentile, F. De Angelis, E. Di Fabrizio, *IEEE Photon. Technol. Lett.* **2010**, 22, 474.
- [464] K. Obata, A. El-Tamer, L. Koch, U. Hinze, B. N. Chichkov, *Light Sci. Appl.* **2013**, 2, e116.
- [465] S. Ristok, S. Thiele, A. Toulouse, A. M. Herkommer, H. Giessen, *Opt. Mater. Express* **2020**, 10, 2370.
- [466] A. Žukauskas, G. Batavičiūtė, M. Ščiuka, T. Jukna, A. Melninkaitis, M. Malinauskas, *Opt. Mater. Express* **2014**, 4, 1601.
- [467] A. Accardo, M. C. Blatché, R. Courson, I. Loubinoux, C. Thibault, L. Malaquin, C. Vieu, *Small* **2017**, 13, 1700621.
- [468] T. Abele, T. Messer, K. Jahnke, M. Hippler, M. Bastmeyer, M. Wegener, K. Göpfrich, *Adv. Mater.* **2022**, 34, 2106709.
- [469] T. Gissibl, S. Wagner, J. Sykora, M. Schmid, H. Giessen, *Opt. Mater. Express* **2017**, 7, 2293.
- [470] S. Dottermusch, D. Busko, M. Langenhorst, U. W. Paetzold, B. S. Richards, *Opt. Lett.* **2019**, 44, 29.
- [471] X. Porte, N. U. Dinc, J. Moughames, G. Panusa, C. Juliano, M. Kadic, C. Moser, D. Brunner, D. Psaltis, *Optica* **2021**, 8, 1281.
- [472] A. Žukauskas, I. Matulaitienė, D. Paipulas, G. Niaura, M. Malinauskas, R. Gadonas, *Laser Photonics Rev.* **2015**, 9, 706.
- [473] D. Gonzalez-Hernandez, S. Varapnickas, G. Merkininkaitė, A. Čiburys, D. Gailevičius, S. Šakirzanovas, S. Juodkazis, M. Malinauskas, *Photonics* **2021**, 8, 577.
- [474] D. Gonzalez-Hernandez, S. Varapnickas, A. Bertoncini, C. Liberale, M. Malinauskas, *Adv. Opt. Mater.* **2023**, 11, 2201701.
- [475] S. Peng, R. Zhang, V. H. Chen, E. T. Khabiboulline, P. Braun, H. A. Atwater, *ACS Photonics* **2016**, 3, 1131.
- [476] A. Ledermann, L. Cademartiri, M. Hermatschweiler, C. Toninelli, G. A. Ozin, D. S. Wiersma, M. Wegener, G. Von Freymann, *Nat. Mater.* **2006**, 5, 942.
- [477] M. Hermatschweiler, A. Ledermann, G. A. Ozin, M. Wegener, G. von Freymann, *Adv. Funct. Mater.* **2007**, 17, 2273.
- [478] A. Frölich, J. Fischer, T. Zebrowski, K. Busch, M. Wegener, *Adv. Mater.* **2013**, 25, 3588.

- [479] A. C. Lamont, M. A. Restaino, A. T. Alsharhan, Z. Liu, D. X. Hammer, R. D. Sochol, A. Agrawal, *Opt. Mater. Express* **2020**, *10*, 2757.
- [480] M. S. Rill, C. Plet, M. Thiel, I. Staude, G. Von Freymann, S. Linden, M. Wegener, *Nat. Mater.* **2008**, *7*, 543.
- [481] J. K. Gansel, M. Thiel, M. S. Rill, M. Decker, K. Bade, V. Saile, G. von Freymann, S. Linden, M. Wegener, *Science* **2009**, *325*, 1513.
- [482] L. Chen, K. A. Morgan, G. A. Alzaidy, C.-C. Huang, Y.-L. D. Ho, M. P. Taverne, X. Zheng, Z. Ren, Z. Feng, I. Zeimpekis, *ACS Photonics* **2019**, *6*, 1248.
- [483] C. Delaney, N. Geoghegan, H. Ibrahim, M. O'Loughlin, B. J. Rodriguez, L. Florea, S. M. Kelleher, *ACS Appl. Polym. Mater.* **2020**, *2*, 3632.
- [484] P. Schürch, R. Ramachandramoorthy, L. Pethö, J. Michler, L. Philippe, *Appl. Mater. Today* **2020**, *18*, 100472.
- [485] Q. Ruan, W. Zhang, H. Wang, J. Y. E. Chan, H. Wang, H. Liu, D. Fan, Y. Li, C. W. Qiu, J. K. Yang, *Adv. Mater.* **2022**, *34*, 2108128.
- [486] Q. Wang, H. N. Chan, H. Wu, *J. Appl. Polym. Sci.* **2022**, *139*, e52655.
- [487] N. Tétreault, G. von Freymann, M. Deubel, M. Hermatschweiler, F. Pérez-Willard, S. John, M. Wegener, G. A. Ozin, *Adv. Mater.* **2006**, *18*, 457.
- [488] F. Seiboth, A. Kubec, A. Schropp, S. Niese, P. Gawlitza, J. Garvoet, V. Galbierz, S. Achilles, S. Patjens, M. E. Stuckelberger, C. David, C. G. Schroer, *Opt. Express* **2022**, *30*, 31519.
- [489] U. T. Sanli, H. Ceylan, I. Bykova, M. Weigand, M. Sitti, G. Schutz, K. Keskinbora, *Adv. Mater.* **2018**, *30*, 1802503.
- [490] M. Jiang, S. Song, Y. Li, X. Zeng, L. Zhu, M. Zhang, S. Wang, X. Li, Y. Cao, *Opt. Lett.* **2021**, *46*, 356.
- [491] A. Kyriazis, K. Vanmol, G. Belay, H. Thienpont, J. Van Erps, *Proc. SPIE* **2022**, *12135*, 30.
- [492] S. Lightman, M. Bin-Nun, G. Bar, G. Hurvitz, R. Gvishi, *Appl. Opt.* **2022**, *61*, 1434.
- [493] J. C. Zhou, P. T. Lin, *Opt. Laser Technol.* **2022**, *156*, 108509.
- [494] J. Wang, C. Cai, K. Wang, J. Wang, *Opt. Lett.* **2022**, *47*, 5766.
- [495] J. Yu, Z. Bai, G. Zhu, C. Fu, Y. Li, S. Liu, C. Liao, Y. Wang, *Opt. Express* **2020**, *28*, 38127.
- [496] S. Lightman, G. Hurvitz, R. Gvishi, A. Arie, *Optica* **2017**, *4*, 605.
- [497] S. Lightman, O. Porat, G. Hurvitz, R. Gvishi, *Opt. Lett.* **2022**, *47*, 5248.
- [498] B. Bai, H. Wei, X. Yang, D. Mengu, A. Ozcan, *arXiv preprint arXiv:2212.12873*, **2022**.
- [499] E. Goi, S. Schoenhardt, M. Gu, *Nat. Commun.* **2022**, *13*, 7531.
- [500] J. Li, S. Thiele, B. C. Quirk, R. W. Kirk, J. W. Verjans, E. Akers, C. A. Bursill, S. J. Nicholls, A. M. Herkommer, H. Giessen, R. A. McLaughlin, *Light Sci. Appl.* **2020**, *9*, 124.
- [501] B. Dai, L. Zhang, C. Zhao, H. Bachman, R. Becker, J. Mai, Z. Jiao, W. Li, L. Zheng, X. Wan, T. J. Huang, S. Zhuang, D. Zhang, *Nat. Commun.* **2021**, *12*, 6458.
- [502] C. R. Ocier, C. A. Richards, D. A. Bacon-Brown, Q. Ding, R. Kumar, T. J. Garcia, J. van de Groep, J. H. Song, A. J. Cyphersmith, A. Rhode, A. N. Perry, A. J. Littlefield, J. Zhu, D. Xie, H. Gao, J. F. Messinger, M. L. Brongersma, K. C. Toussaint Jr., L. L. Goddard, P. V. Braun, *Light Sci. Appl.* **2020**, *9*, 196.
- [503] S. Thiele, C. Pruss, A. M. Herkommer, H. Giessen, *Opt. Express* **2019**, *27*, 35621.
- [504] H. Ren, J. Jang, C. Li, A. Aigner, M. Plidschun, J. Kim, J. Rho, M. A. Schmidt, S. A. Maier, *Nat. Commun.* **2022**, *13*, 4183.
- [505] F. Balli, M. Sultan, S. K. Lami, J. T. Hastings, *Nat. Commun.* **2020**, *11*, 3892.
- [506] A. Asadollahbaik, S. Thiele, K. Weber, A. Kumar, J. Drozella, F. Sterl, A. M. Herkommer, H. Giessen, J. Fick, *ACS Photonics* **2019**, *7*, 88.
- [507] J.-J. Xu, W.-G. Yao, Z.-N. Tian, L. Wang, K.-M. Guan, Y. Xu, Q.-D. Chen, J.-A. Duan, H.-B. Sun, *IEEE Photon. Technol. Lett.* **2015**, *27*, 2465.
- [508] Z. Hong, P. Ye, D. A. Loy, R. Liang, *Adv. Sci.* **2022**, *9*, 2105595.
- [509] A. Bertocini, S. P. Laptinok, L. Genchi, V. P. Rajamanickam, C. Liberale, *J. Biophotonics* **2020**, *14*, 202000219.
- [510] J. Li, S. Thiele, R. W. Kirk, B. C. Quirk, A. Hoogendoorn, Y. C. Chen, K. Peter, S. J. Nicholls, J. W. Verjans, P. J. Psaltis, C. Bursill, A. M. Herkommer, H. Giessen, R. A. McLaughlin, *Small* **2022**, *18*, 2107032.
- [511] Z. He, Y. H. Lee, D. Chanda, S. T. Wu, *Opt. Express* **2018**, *26*, 21184.
- [512] M. A. Tadayon, I. Pavlova, K. M. Martyniuk, A. Mohanty, S. P. Roberts, F. Barbosa, C. A. Denny, M. Lipson, *Sci. Rep.* **2018**, *8*, 10756.
- [513] P. I. Dietrich, R. J. Harris, M. Blaicher, M. K. Corrigan, T. M. Morris, W. Freude, A. Quirrenbach, C. Koos, *Opt. Express* **2017**, *25*, 18288.
- [514] A. Mikhaylov, S. Reich, A. Plech, M. Zakharova, V. Vlnieska, D. Kunka, in *SPIE Optics + Optoelectronics*, Vol. 11032, SPIE, Prague, Czech Republic **2019**.
- [515] W. Yuan, L.-H. Li, W.-B. Lee, C.-Y. Chan, *Chin. J. Mech. Eng.* **2018**, *31*, 16.
- [516] L. Yan, D. Yang, Q. Gong, Y. Li, *Micromachines* **2020**, *11*, 112.
- [517] D. Wu, Q.-D. Chen, L.-G. Niu, J. Jiao, H. Xia, J.-F. Song, H.-B. Sun, *IEEE Photon. Technol. Lett.* **2009**, *21*, 1535.
- [518] K.-H. Jeong, J. Kim, L. P. Lee, *Science* **2006**, *312*, 557.
- [519] Z. C. Ma, X. Y. Hu, Y. L. Zhang, X. Q. Liu, Z. S. Hou, L. G. Niu, L. Zhu, B. Han, Q. D. Chen, H. B. Sun, *Adv. Funct. Mater.* **2019**, *29*, 1903340.
- [520] B. Du, H. Zhang, J. Xia, J. Wu, H. Ding, G. Tong, *J. Phys. Chem. A* **2020**, *124*, 7211.
- [521] S. Coelho, J. Baek, J. Walsh, J. Justin Gooding, K. Gaus, *Nat. Commun.* **2022**, *13*, 647.
- [522] G. Roberts, C. Ballew, I. Foo, P. Hon, A. Faraon, in *Conf. Lasers Elect. Opt.*, Optica Publishing Group, San Jose, California **2022**, p. FM5H2.
- [523] M. Khorasaninejad, W. T. Chen, R. C. Devlin, J. Oh, A. Y. Zhu, F. Capasso, *Science* **2016**, *352*, 1190.
- [524] C. Roques-Carmes, Z. Lin, R. E. Christiansen, Y. Salamin, S. E. Kooi, J. D. Joannopoulos, S. G. Johnson, M. Soljačić, *ACS Photonics* **2022**, *9*, 43.
- [525] S. Thiele, T. Gissibl, H. Giessen, A. M. Herkommer, *Opt. Lett.* **2016**, *41*, 3029.
- [526] M. Plidschun, H. Ren, J. Kim, R. Forster, S. A. Maier, M. A. Schmidt, *Light Sci. Appl.* **2021**, *10*, 57.
- [527] R. Thomas, J. Li, S. Ladak, D. Barrow, P. M. Smowton, *Opt. Express* **2018**, *26*, 13436.
- [528] P. I. Dietrich, M. Blaicher, I. Reuter, M. Billah, T. Hoose, A. Hofmann, C. Caer, R. Dangel, B. Offrein, U. Troppenz, M. Moehrle, W. Freude, C. Koos, *Nat. Photon.* **2018**, *12*, 241.
- [529] G. Cojoc, C. Liberale, P. Candeloro, F. Gentile, G. Das, F. De Angelis, E. Di Fabrizio, *Microelectron. Eng.* **2010**, *87*, 876.
- [530] K. Yanny, N. Antipa, W. Liberti, S. Dehaeck, K. Monakhova, F. L. Liu, K. Shen, R. Ng, L. Waller, *Light Sci. Appl.* **2020**, *9*, 171.
- [531] B. Lee, *Opt. Fiber Technol.* **2003**, *9*, 57.
- [532] D. J. Richardson, J. M. Fini, L. E. Nelson, *Nat. Photon.* **2013**, *7*, 354.
- [533] J. Trisno, H. Wang, J. K. Yang, *Int. J. Extreme Manuf.* **2020**, *3*, 015301.
- [534] J. Bürger, V. Schalles, J. Kim, B. Jang, M. Zeisberger, J. Gargiulo, L. S. de Menezes, M. A. Schmidt, S. A. Maier, *ACS Photonics* **2022**, *9*, 3012.
- [535] C. Xiong, C. Liao, Z. Li, K. Yang, M. Zhu, Y. Zhao, Y. Wang, *Front. Mater.* **2020**, *7*, 586496.
- [536] Z. Li, C. Liao, J. Song, Y. Wang, F. Zhu, Y. Wang, X. Dong, *Photonics Res.* **2016**, *4*, 197.

- [537] M. Hou, K. Yang, J. He, X. Xu, S. Ju, K. Guo, Y. Wang, *Opt. Express* **2018**, 26, 23770.
- [538] J. Zhao, S. Q. Cao, C. R. Liao, Y. Wang, G. J. Wang, X. Z. Xu, C. L. Fu, G. W. Xu, J. R. Lian, Y. P. Wang, *Sens. Actuators, B* **2016**, 230, 206.
- [539] Z. Y. Li, C. R. Liao, J. Wang, Z. L. Li, P. Zhou, Y. Wang, Y. P. Wang, *J. Lightwave Technol.* **2019**, 37, 1241.
- [540] A. Bogucki, Ł. Zinkiewicz, W. Pacuski, P. Wasylczyk, P. Kossacki, *Opt. Express* **2018**, 26, 11513.
- [541] C. Lin, C. Liao, Y. Zhang, L. Xu, Y. Wang, C. Fu, K. Yang, J. Wang, J. He, Y. Wang, *Lab Chip* **2018**, 18, 595.
- [542] Z. Li, C. Liao, D. Chen, J. Song, W. Jin, G. D. Peng, F. Zhu, Y. Wang, J. He, Y. Wang, *Opt. Express* **2017**, 25, 17105.
- [543] Z. P. Liu, X. F. Jiang, Y. Li, Y. F. Xiao, L. Wang, J. L. Ren, S. J. Zhang, H. Yang, Q. H. Gong, *Appl. Phys. Lett.* **2013**, 102, 221108.
- [544] Z. N. Tian, X. W. Cao, W. G. Yao, P. X. Li, Y. H. Yu, G. Li, Q. D. Chen, H. B. Sun, *IEEE Photon. Technol. Lett.* **2016**, 28, 2299.
- [545] S. Nocentini, D. Martella, C. Parmeggiani, S. Zanotto, D. S. Wiersma, *Adv. Opt. Mater.* **2018**, 6, 1800167.
- [546] C. Jain, A. Braun, J. Gargiulo, B. Jang, G. Li, H. Lehmann, S. A. Maier, M. A. Schmidt, *ACS Photonics* **2018**, 6, 649.
- [547] Y. Tian, Y. L. Zhang, J. F. Ku, Y. He, B. B. Xu, Q. D. Chen, H. Xia, H. B. Sun, *Lab Chip* **2010**, 10, 2902.
- [548] J. Wang, Y. He, H. Xia, L. G. Niu, R. Zhang, Q. D. Chen, Y. L. Zhang, Y. F. Li, S. J. Zeng, J. H. Qin, B. C. Lin, H. B. Sun, *Lab Chip* **2010**, 10, 1993.
- [549] B. Spagnolo, V. Brunetti, G. Lemenager, E. De Luca, L. Sileo, T. Pellegrino, P. Paolo Pompa, M. De Vittorio, F. Pisanello, *Sci. Rep.* **2015**, 5, 10531.
- [550] F. Schiappelli, R. Kumar, M. Prasciolu, D. Cojoc, S. Cabrini, M. De Vittorio, G. Visimberga, A. Gerardino, V. Degiorgio, E. Di Fabrizio, *Microelectron. Eng.* **2004**, 73–74, 397.
- [551] S. Cabrini, C. Liberale, D. Cojoc, A. Carpentiero, M. Prasciolu, S. Mora, V. Degiorgio, F. De Angelis, E. Di Fabrizio, *Microelectron. Eng.* **2006**, 83, 804.
- [552] H. M. Presby, A. F. Benner, C. A. Edwards, *Appl. Opt.* **1990**, 29, 2692.
- [553] M. Wakaki, Y. Komachi, G. Kanai, *Appl. Opt.* **1998**, 37, 627.
- [554] G. Kostovski, U. Chinnsamy, S. Jayawardhana, P. R. Stoddart, A. Mitchell, *Adv. Mater.* **2011**, 23, 531.
- [555] Y. Kanamori, M. Okochi, K. Hane, *Opt. Express* **2013**, 21, 322.
- [556] T. Gissibl, M. Schmid, H. Giessen, *Optica* **2016**, 3, 448.
- [557] Z. W. Xie, S. F. Feng, P. J. Wang, L. S. Zhang, X. Ren, L. Cui, T. R. Zhai, J. Chen, Y. L. Wang, X. K. Wang, W. F. Sun, J. S. Ye, P. Han, P. J. Klar, Y. Zhang, *Adv. Opt. Mater.* **2015**, 3, 1232.
- [558] M. Blaicher, M. R. Billah, J. Kemal, T. Hoose, P. Marin-Palomo, A. Hofmann, Y. Kutuvantavida, C. Kieninger, P.-I. Dietrich, M. Lauer mann, *Light Sci. Appl.* **2020**, 9, 71.
- [559] J. Feldmann, N. Youngblood, M. Karpov, H. Gehring, X. Li, M. Stappers, M. Le Gallo, X. Fu, A. Lukashchuk, A. S. Raja, *Nature* **2021**, 589, 52.
- [560] A. Bertoncini, C. Liberale, *Optica* **2020**, 7, 1487.
- [561] T. Baghdasaryan, K. Vanmol, H. Thienpont, F. Berghmans, T. Geernaert, J. Van Erps, *J. Phys. Photonics* **2021**, 3, 045001.
- [562] A. Eich, T. C. Spiekermann, H. Gehring, L. Sommer, J. R. Bankwitz, P. P. Schrunner, J. A. Preuß, S. Michaelis de Vasconcellos, R. Bratschitsch, W. H. Pernice, *ACS Photonics* **2022**, 9, 551.
- [563] H. Gehring, A. Eich, C. Schuck, W. H. P. Pernice, *Opt. Lett.* **2019**, 44, 5089.
- [564] H. Gehring, M. Blaicher, W. Hartmann, P. Varytis, K. Busch, M. Wegener, W. H. P. Pernice, *APL Photonics* **2019**, 4, 010801.
- [565] M. Sartison, K. Weber, S. Thiele, L. Bremer, S. Fischbach, T. Herzog, S. Kolatschek, S. Reitzenstein, A. Herkommer, P. Michler, S. L. Portalupi, H. Giessen, *Light Adv. Manuf.* **2021**, 2, 6.
- [566] P. Maier, Y. Xu, M. Trappen, M. Lauer mann, A. Henniger-Ludwig, H. Kapim, T. Kind, P.-I. Dietrich, A. Weber, M. Blaicher, *arXiv preprint arXiv:2208.11005*, **2022**.
- [567] M. Trappen, M. Blaicher, P.-I. Dietrich, C. Dankwart, Y. Xu, T. Hoose, M. R. Billah, A. Abbasi, R. Baets, U. Troppenz, *Opt. Express* **2020**, 28, 37996.
- [568] P. I. Dietrich, G. Goring, M. Trappen, M. Blaicher, W. Freude, T. Schimmel, H. Holscher, C. Koos, *Small* **2020**, 16, 1904695.
- [569] D. Grobnić, S. J. Mihailov, J. Ballato, P. D. Dragic, *Optica* **2015**, 2, 313.
- [570] M. Majumder, T. K. Gangopadhyay, A. K. Chakraborty, K. Dasgupta, D. K. Bhattacharya, *Sens. Actuator A Phys.* **2008**, 147, 150.
- [571] G. Yin, Y. Wang, C. Liao, B. Sun, Y. Liu, S. Liu, Q. Wang, K. Yang, J. Tang, X. Zhong, *IEEE Photon. Technol. Lett.* **2014**, 27, 375.
- [572] X. Zhong, Y. Wang, J. Qu, C. Liao, S. Liu, J. Tang, Q. Wang, J. Zhao, K. Yang, Z. Li, *Opt. Lett.* **2014**, 39, 5463.
- [573] C. R. Liao, K. M. Yang, J. Wang, Z. Y. Bai, Z. S. Gan, Y. P. Wang, *IEEE Photon. Technol. Lett.* **2019**, 31, 971.
- [574] C. Li, C. Liao, J. Wang, Z. Gan, Y. Wang, *Polymers* **2018**, 10, 1192.
- [575] V. Melissinaki, M. Farsari, S. Pissadakis, *IEEE J. Sel. Top. Quantum Electron.* **2014**, 21, 344.
- [576] A. J. Thompson, M. Power, G. Z. Yang, *Opt. Express* **2018**, 26, 14186.
- [577] M. Li, Y. Liu, X. L. Zhao, R. X. Gao, Y. Li, S. L. Qu, *Sens. Actuator A Phys.* **2017**, 260, 29.
- [578] F. Hou, Y. Zhan, S. Feng, J. Ye, X. Wang, W. Sun, Y. Zhang, *Opt. Express* **2022**, 30, 25277.
- [579] Q. Liu, Y. Zhan, S. Zhang, S. Feng, X. Wang, W. Sun, J. Ye, Y. Zhang, *Opt. Express* **2020**, 28, 11730.
- [580] S. Zhang, S. J. Tang, S. Feng, Y. F. Xiao, W. Cui, X. Wang, W. Sun, J. Ye, P. Han, X. Zhang, *Adv. Opt. Mater.* **2019**, 7, 1900602.
- [581] Y. Qi, S. Zhang, S. Feng, X. Wang, W. Sun, J. Ye, P. Han, Y. Zhang, in *Int. Conf. Opt. Inst. Technol. SPIE*, Beijing, China **2018**, 203.
- [582] K. Markiewicz, P. Wasylczyk, *Opt. Express* **2019**, 27, 8440.
- [583] B. Wang, Q. Zhang, X. Chen, H. Luan, M. Gu, *J. Microsc.* **2020**, 288, 87.
- [584] D. Palima, A. R. Bañas, G. Vizsnyiczai, L. Kelemen, P. Ormos, J. Glückstad, *Opt. Express* **2012**, 20, 2004.
- [585] H. Gao, G. F. Chen, P. Xing, J. W. Choi, H. Y. Low, D. T. Tan, *Adv. Opt. Mater.* **2020**, 8, 2000613.
- [586] A. Nestic, M. Blaicher, E. Orlandini, T. Olariu, M. Paszkiewicz, F. Negrodo, P. Kraft, M. Sukhova, A. Hofmann, W. Dörfler, *arXiv preprint arXiv:2201.09807*, **2022**.
- [587] G. Panusa, N. U. Dinc, D. Psaltis, *Opt. Express* **2022**, 30, 2564.
- [588] G. Panusa, Y. Pu, J. Wang, C. Moser, D. Psaltis, *Polymers* **2020**, 12, 2485.
- [589] A. Nestic, M. Blaicher, T. Hoose, A. Hofmann, M. Lauer mann, Y. Kutuvantavida, M. Nöllenburg, S. Randel, W. Freude, C. Koos, *Opt. Express* **2019**, 27, 17402.
- [590] R. M. Adão, T. L. Alves, C. Maibohm, B. Romeira, J. B. Nieder, *Opt. Express* **2022**, 30, 9623.
- [591] A. Grabulosa, X. Porte, E. Jung, J. Moughames, M. Kadic, D. Brunner, *arXiv preprint arXiv:2208.09767*, **2022**.
- [592] M. Nawrot, Ł. Zinkiewicz, B. Włodarczyk, P. Wasylczyk, *Opt. Express* **2013**, 21, 31919.
- [593] H. Wang, Q. Ruan, H. Wang, S. D. Rezaei, K. T. P. Lim, H. Liu, W. Zhang, J. Trisno, J. Y. E. Chan, J. K. W. Yang, *Nano Lett.* **2021**, 21, 4721.
- [594] K. T. P. Lim, H. Liu, Y. Liu, J. K. W. Yang, *Nat. Commun.* **2019**, 10, 25.
- [595] J. Purto, P. Rogin, A. Verch, V. E. Johansen, R. Hensel, *Nanomaterials* **2019**, 9, 1495.
- [596] J. Y. E. Chan, Q. Ruan, R. J. H. Ng, C.-W. Qiu, J. K. W. Yang, *ACS Nano* **2019**, 13, 14138.

- [597] J. Y. E. Chan, Q. Ruan, M. Jiang, H. Wang, H. Wang, W. Zhang, C.-W. Qiu, J. K. W. Yang, *Nat. Commun.* **2021**, *12*, 3728.
- [598] J. Y. E. Chan, Q. Ruan, H. Wang, H. Wang, H. Liu, Z. Yan, C.-W. Qiu, J. K. W. Yang, *Nano Lett.* **2022**, *22*, 8189.
- [599] X. Cao, Y. Du, Y. Guo, G. Hu, M. Zhang, L. Wang, J. Zhou, Q. Gao, P. Fischer, J. Wang, S. Stavrakis, A. deMello, *Adv. Mater.* **2022**, *34*, 2109161.
- [600] H. Liu, H. Wang, H. Wang, J. Deng, Q. Ruan, W. Zhang, O. A. M. Abdelraouf, N. S. S. Ang, Z. Dong, J. K. W. Yang, H. Liu, *ACS Nano* **2022**, *16*, 8244.
- [601] A. E. Goodling, S. Nagelberg, B. Kaehr, C. H. Meredith, S. I. Cheon, A. P. Saunders, M. Kolle, L. D. Zarzar, *Nature* **2019**, *566*, 523.
- [602] Y. Guo, H. Shahsavani, M. Sitti, *Adv. Opt. Mater.* **2020**, *8*, 1902098.
- [603] B. Liu, B. Dong, C. Xin, C. Chen, L. Zhang, D. Wang, Y. Hu, J. Li, L. Zhang, D. Wu, *Small* **2022**, *2022*, 2204630.
- [604] A. Toulouse, J. Drozella, S. Thiele, H. Giessen, A. Herkommer, *Light Adv. Manuf.* **2021**, *2*, 2.
- [605] Y. Xiao, S. Wei, J. Xu, R. Ma, X. Liu, X. Zhang, T. H. Tao, H. Li, Z. Wang, L. You, Z. Wang, *ACS Photonics* **2022**, *9*, 3450.
- [606] S. K. Saha, D. Wang, V. H. Nguyen, Y. Chang, J. S. Oakdale, S.-C. Chen, *Science* **2019**, *366*, 105.
- [607] J. Von Neumann, E. Wigner, *Phys. Z* **1929**, *30*, 465.
- [608] D. R. Herrick, *Physica B+C* **1976**, *85*, 44.
- [609] C. W. Hsu, B. Zhen, A. D. Stone, J. D. Joannopoulos, M. Soljačić, *Nat. Rev. Mater.* **2016**, *1*, 16048.
- [610] K. Koshelev, G. Favraud, A. Bogdanov, Y. Kivshar, A. Fratallocchi, *Nanophotonics* **2019**, *8*, 725.
- [611] D. C. Marinica, A. G. Borisov, S. V. Shabanov, *Phys. Rev. Lett.* **2008**, *100*, 183902.
- [612] Y. Plotnik, O. Peleg, F. Dreisow, M. Heinrich, S. Nolte, A. Szameit, M. Segev, *Phys. Rev. Lett.* **2011**, *107*, 183901.
- [613] B. Zhen, C. W. Hsu, L. Lu, A. D. Stone, M. Soljačić, *Phys. Rev. Lett.* **2014**, *113*, 257401.
- [614] K. Koshelev, S. Kruk, E. Melik-Gaykazyan, J.-H. Choi, A. Bogdanov, H.-G. Park, Y. Kivshar, *Science* **2020**, *367*, 288.
- [615] A. Tittl, A. Leitis, M. Liu, F. Yesilkoy, D.-Y. Choi, D. N. Neshev, Y. S. Kivshar, H. Altug, *Science* **2018**, *360*, 1105.
- [616] F. Yesilkoy, E. R. Arvelo, Y. Jahani, M. Liu, A. Tittl, V. Cevher, Y. Kivshar, H. Altug, *Nat. Photon.* **2019**, *13*, 390.
- [617] Z. Dong, Z. Mahfoud, R. Paniagua-Domínguez, H. Wang, A. I. Fernández-Domínguez, S. Gorelik, S. T. Ha, F. Tjiptharsono, A. I. Kuznetsov, M. Bosman, J. K. W. Yang, *Light Sci. Appl.* **2022**, *11*, 20.
- [618] M.-S. Hwang, H.-C. Lee, K.-H. Kim, K.-Y. Jeong, S.-H. Kwon, K. Koshelev, Y. Kivshar, H.-G. Park, *Nat. Commun.* **2021**, *12*, 4135.
- [619] N. Bernhardt, K. Koshelev, S. J. U. White, K. W. C. Meng, J. E. Fröch, S. Kim, T. T. Tran, D.-Y. Choi, Y. Kivshar, A. S. Solntsev, *Nano Lett.* **2020**, *20*, 5309.
- [620] Y. Zhou, H. Zheng, I. I. Kravchenko, J. Valentine, *Nat. Photon.* **2020**, *14*, 316.
- [621] Y. Liang, K. Koshelev, F. Zhang, H. Lin, S. Lin, J. Wu, B. Jia, Y. Kivshar, *Nano Lett.* **2020**, *20*, 6351.
- [622] A. Aigner, A. Tittl, J. Wang, T. Weber, Y. Kivshar, S. A. Maier, H. Ren, *Sci. Adv.* **2022**, *8*, eadd4816.
- [623] Y. Liang, H. Lin, K. Koshelev, F. Zhang, Y. Yang, J. Wu, Y. Kivshar, B. Jia, *Nano Lett.* **2021**, *21*, 1090.
- [624] Y. Liang, H. Lin, S. Lin, J. Wu, W. Li, F. Meng, Y. Yang, X. Huang, B. Jia, Y. Kivshar, *Nano Lett.* **2021**, *21*, 8917.
- [625] S. I. Azzam, V. M. Shalae, A. Boltasseva, A. V. Kildishev, *Phys. Rev. Lett.* **2018**, *121*, 253901.
- [626] R. Mermet-Lyaudoz, F. Dubois, N.-V. Hoang, E. Drouard, L. Berguiga, C. Seassal, X. Letartre, P. Viktorovitch, H. S. Nguyen, *arXiv preprint arXiv:1905.03868*, **2019**, <https://doi.org/10.48550/arXiv.1905.03868>.
- [627] V. G. Kravets, A. V. Kabashin, W. L. Barnes, A. N. Grigorenko, *Chem. Rev.* **2018**, *118*, 5912.
- [628] L. Lu, J. D. Joannopoulos, M. Soljačić, *Nat. Photon.* **2014**, *8*, 821.
- [629] A. B. Khanikaev, G. Shvets, *Nat. Photon.* **2017**, *11*, 763.
- [630] T. Ozawa, H. M. Price, A. Amo, N. Goldman, M. Hafezi, L. Lu, M. C. Rechtsman, D. Schuster, J. Simon, O. Zilberberg, I. Carusotto, *Rev. Mod. Phys.* **2019**, *91*, 015006.
- [631] H. Wang, S. K. Gupta, B. Xie, M. Lu, *Front. Optoelectron.* **2020**, *13*, 50.
- [632] M. Kim, Z. Jacob, J. Rho, *Light Sci. Appl.* **2020**, *9*, 130.
- [633] J. Schulz, S. Vaidya, C. Jörg, *APL Photonics* **2021**, *6*, 080901.
- [634] D. V. Zhirihin, Y. S. Kivshar, *Small Sci.* **2021**, *1*, 2100065.
- [635] H. Price, Y. Chong, A. Khanikaev, H. Schomerus, L. J. Maczewsky, M. Kremer, M. Heinrich, A. Szameit, O. Zilberberg, Y. Yang, B. Zhang, A. Alù, R. Thomale, I. Carusotto, P. St-Jean, A. Amo, A. Dutt, L. Yuan, S. Fan, X. Yin, C. Peng, T. Ozawa, A. Blanco-Redondo, *J. Phys. Photonics* **2022**, *4*, 032501.
- [636] L.-H. Wu, X. Hu, *Phys. Rev. Lett.* **2015**, *114*, 223901.
- [637] F. Alpegiani, L. Kuipers, *Optica* **2019**, *6*, 96.
- [638] Y. Ota, F. Liu, R. Katsumi, K. Watanabe, K. Wakabayashi, Y. Arakawa, S. Iwamoto, *Optica* **2019**, *6*, 786.
- [639] L. He, Z. Addison, E. J. Mele, B. Zhen, *Nat. Commun.* **2020**, *11*, 3119.
- [640] F. Dreisow, M. Heinrich, A. Szameit, S. Döring, S. Nolte, A. Tünnermann, S. Fahr, F. Lederer, *Opt. Express* **2008**, *16*, 3474.
- [641] G. Siroki, P. A. Huidobro, V. Giannini, *Phys. Rev. B* **2017**, *96*, 041408.
- [642] Y. Ota, R. Katsumi, K. Watanabe, S. Iwamoto, Y. Arakawa, *Commun. Phys.* **2018**, *1*, 86.
- [643] S. Longhi, *Opt. Lett.* **2014**, *39*, 5892.
- [644] E. Lustig, M.-I. Cohen, R. Bekenstein, G. Harari, M. A. Bandres, M. Segev, *Phys. Rev. A* **2017**, *96*, 041804.
- [645] J. Noh, W. A. Benalcazar, S. Huang, M. J. Collins, K. P. Chen, T. L. Hughes, M. C. Rechtsman, *Nat. Photon.* **2018**, *12*, 408.
- [646] F. Mayer, S. Richter, J. Westhauser, E. Blasco, C. Barner-Kowollik, M. Wegener, *Sci. Adv.* **2019**, *5*, eaau9160.
- [647] Y. Chen, X. Chen, X. Ren, M. Gong, G.-c. Guo, *Phys. Rev. A* **2021**, *104*, 023501.
- [648] J. Schulz, C. Jörg, G. von Freymann, *Opt. Express* **2022**, *30*, 9869.
- [649] X.-L. Zhang, F. Yu, Z.-G. Chen, Z.-N. Tian, Q.-D. Chen, H.-B. Sun, G. Ma, *Nat. Photon.* **2022**, *16*, 390.
- [650] L. Lu, L. Fu, J. D. Joannopoulos, M. Soljačić, *Nat. Photon.* **2013**, *7*, 294.
- [651] L. Lu, Z. Wang, D. Ye, L. Ran, L. Fu, J. D. Joannopoulos, M. Soljačić, *Science* **2015**, *349*, 622.
- [652] L. Lu, C. Fang, L. Fu, S. G. Johnson, J. D. Joannopoulos, M. Soljačić, *Nat. Phys.* **2016**, *12*, 337.
- [653] R. Bekenstein, Y. Kabessa, Y. Sharabi, O. Tal, N. Engheta, G. Eisenstein, A. J. Agranat, M. Segev, *Nat. Photon.* **2017**, *11*, 664.
- [654] J. Noh, S. Huang, D. Leykam, Y. D. Chong, K. P. Chen, Mikael C. Rechtsman, *Nat. Phys.* **2017**, *13*, 611.
- [655] A. Cerjan, S. Huang, M. Wang, K. P. Chen, Y. Chong, M. C. Rechtsman, *Nat. Photon.* **2019**, *13*, 623.
- [656] A. Kottaram Amrithanath, H. Wei, S. Krishnaswamy, in *SPIE BiOS, Vol. 10895*, SPIE, San Francisco, CA, USA **2019**.
- [657] L.-C. Wang, Y. Chen, M. Gong, F. Yu, Q.-D. Chen, Z.-N. Tian, X.-F. Ren, H.-B. Sun, *Phys. Rev. Lett.* **2022**, *129*, 173601.
- [658] S. Vaidya, J. Noh, A. Cerjan, C. Jörg, G. von Freymann, M. C. Rechtsman, *Phys. Rev. Lett.* **2020**, *125*, 253902.
- [659] E. Goi, Z. Yue, B. P. Cumming, M. Gu, *Laser Photonics Rev.* **2018**, *12*, 1700271.
- [660] M. C. Rechtsman, J. M. Zeuner, Y. Plotnik, Y. Lumer, D. Podolsky, F. Dreisow, S. Nolte, M. Segev, A. Szameit, *Nature* **2013**, *496*, 196.
- [661] A. Szameit, S. Nolte, *J. Phys. B* **2010**, *43*, 163001.

- [662] C. Jörg, F. Letscher, M. Fleischhauer, G. v. Freymann, *New J. Phys.* **2017**, *19*, 083003.
- [663] S. Mukherjee, A. Spracklen, M. Valiente, E. Andersson, P. Öhberg, N. Goldman, R. R. Thomson, *Nat. Commun.* **2017**, *8*, 13918.
- [664] Z. Fedorova, C. Jörg, C. Dauer, F. Letscher, M. Fleischhauer, S. Eggert, S. Linden, G. von Freymann, *Light Sci. Appl.* **2019**, *8*, 63.
- [665] M.-I. Cohen, C. Jörg, Y. Lumer, Y. Plotnik, E. H. Waller, J. Schulz, G. von Freymann, M. Segev, *Light Sci. Appl.* **2020**, *9*, 200.
- [666] S. Mukherjee, M. Di Liberto, P. Öhberg, R. R. Thomson, N. Goldman, *Phys. Rev. Lett.* **2018**, *121*, 075502.
- [667] C. Jörg, G. Queraltó, M. Kremer, G. Pelegrí, J. Schulz, A. Szameit, G. von Freymann, J. Mompart, V. Ahufinger, *Light Sci. Appl.* **2020**, *9*, 150.
- [668] J. Schulz, *Masters Thesis*, Technische Universität Kaiserslautern, Kaiserslautern **2018**.
- [669] A. Bayazeed, *Masters Thesis*, Technische Universität Kaiserslautern, Kaiserslautern **2020**.
- [670] A. Landowski, J. Gutsche, S. Guckenbiehl, M. Schönberg, G. v. Freymann, A. Widera, *APL Photonics* **2020**, *5*, 016101.
- [671] Y. Song, Y. Monceaux, S. Bittner, K. Chao, H. M. R. de la Cruz, C. Lafargue, D. Decanini, B. Dietz, J. Zyss, A. Grigis, *Phys. Rev. Lett.* **2021**, *127*, 203901.
- [672] X. Lin, W. Zhou, Y. Liu, F. J. Shu, C. L. Zou, C. Dong, C. Wei, H. Dong, C. Zhang, J. Yao, *Small* **2022**, *18*, 2202812.
- [673] J. Wang, S. Valligatla, Y. Yin, L. Schwarz, M. Medina-Sánchez, S. Baunack, C. H. Lee, R. Thomale, S. Li, V. M. Fomin, L. Ma, O. G. Schmidt, *Nat. Photon.* **2023**, *17*, 120.
- [674] N. Dai, S. Liu, Z. Ren, Y. Cao, J. Ni, D. Wang, L. Yang, Y. Hu, J. Li, J. Chu, D. Wu, *ACS Nano* **2023**, *17*, 1541.
- [675] Z.-Y. Hu, Y.-L. Zhang, C. Pan, J.-Y. Dou, Z.-Z. Li, Z.-N. Tian, J.-W. Mao, Q.-D. Chen, H.-B. Sun, *Nat. Commun.* **2022**, *13*, 5634.
- [676] J. A. Preuß, H. Gehring, R. Schmidt, L. Jin, D. Wendland, J. Kern, W. H. P. Pernice, S. M. de Vasconcellos, R. Bratschitsch, *Nano Lett.* **2023**, *23*, 407.
- [677] J. Karst, Y. Lee, M. Floess, M. Ubl, S. Ludwigs, M. Hentschel, H. Giessen, *Nat. Commun.* **2022**, *13*, 7183.
- [678] S.-F. Liu, Z.-W. Hou, L. Lin, F. Li, Y. Zhao, X.-Z. Li, H. Zhang, H.-H. Fang, Z. Li, H.-B. Sun, *Science* **2022**, *377*, 1112.
- [679] J. H. Strickler, W. W. Webb, *Opt. Lett.* **1991**, *16*, 1780.
- [680] B. H. Cumpston, S. P. Ananthavel, S. Barlow, D. L. Dyer, J. E. Ehrlich, L. L. Erskine, A. A. Heikal, S. M. Kuebler, I.-Y. S. Lee, D. McCord-Maughon, *Nature* **1999**, *398*, 51.
- [681] N. Makarov, A. Rebane, M. Drobizhev, H. Wolleb, H. Spahnov, *J. Opt. Soc. Am. B* **2007**, *24*, 1874.
- [682] C. O. Yanez, C. D. Andrade, S. Yao, G. Luchita, M. V. Bondar, K. D. Belfield, *ACS Appl. Mater. Interfaces* **2009**, *1*, 2219.
- [683] P. Zijlstra, J. W. Chon, M. Gu, *Nature* **2009**, *459*, 410.
- [684] D. Ganic, D. Day, M. Gu, *Opt. Lasers Eng.* **2002**, *38*, 433.
- [685] J. Zhang, M. Gecevicius, M. Beresna, P. G. Kazansky, *Phys. Rev. Lett.* **2014**, *112*, 033901.
- [686] N. Bozinovic, Y. Yue, Y. Ren, M. Tur, P. Kristensen, H. Huang, A. E. Willner, S. Ramachandran, *Science* **2013**, *340*, 1545.
- [687] C. D. Stanciu, F. Hansteen, A. V. Kimel, A. Kirilyuk, A. Tsukamoto, A. Itoh, T. Rasing, *Phys. Rev. Lett.* **2007**, *99*, 047601.
- [688] M. Gu, X. Li, Y. Cao, *Light Sci. Appl.* **2014**, *3*, e177.
- [689] C. Deng, Y. Liu, X. Fan, B. Jiao, Z. Zhang, M. Zhang, F. Chen, H. Gao, L. Deng, W. Xiong, *Adv. Funct. Mater.* **2023**, 2211473, <https://doi.org/10.1002/adfm.202211473>.
- [690] S. Daqiqeh Rezaei, Z. Dong, J. You En Chan, J. Trisno, R. J. H. Ng, Q. Ruan, C.-W. Qiu, N. A. Mortensen, J. K. W. Yang, *ACS Photonics* **2021**, *8*, 18.
- [691] L. Tenbrake, A. Faßbender, S. Hofferberth, S. Linden, H. Pfeifer, *arXiv preprint arXiv:2212.13532*, **2022**, <https://doi.org/10.48550/arXiv.2212.13532>.
- [692] M. Del Pozo, C. Delaney, C. W. M. Bastiaansen, D. Diamond, A. Schenning, L. Florea, *ACS Nano* **2020**, *14*, 9832.
- [693] Y. Guo, H. Shahsavan, M. Sitti, *Adv. Mater.* **2020**, *32*, 2002753.
- [694] A. Münchinger, V. Hahn, D. Beutel, S. Woska, J. Monti, C. Rockstuhl, E. Blasco, M. Wegener, *Adv. Mater. Technol.* **2022**, *7*, 2100944.
- [695] Z. He, G. Tan, D. Chanda, S.-T. Wu, *Opt. Express* **2019**, *27*, 11472.
- [696] J. Monti, A. Concellón, R. Dong, M. Simmler, A. Münchinger, C. Huck, P. Tegeder, H. Nirschl, M. Wegener, C. O. Osuji, *ACS Appl. Mater. Interfaces* **2022**, *14*, 33746.
- [697] Y. Shi, P. S. Salter, M. Li, R. A. Taylor, S. J. Elston, S. M. Morris, D. D. Bradley, *Adv. Funct. Mater.* **2021**, *31*, 2007493.
- [698] Z.-C. Ma, Y.-L. Zhang, B. Han, X.-Y. Hu, C.-H. Li, Q.-D. Chen, H.-B. Sun, *Nat. Commun.* **2020**, *11*, 4536.
- [699] F. Rajabzadi, L. Schwarz, M. Medina-Sánchez, O. G. Schmidt, *Prog. Mater. Sci.* **2021**, *120*, 100808.
- [700] M. Y. Khalid, Z. U. Arif, R. Noroozi, A. Zolfagharian, M. Bodaghi, *J. Manuf. Process.* **2022**, *81*, 759.
- [701] A.-I. Bunea, D. Martella, S. Nocentini, C. Parmeggiani, R. Taboryski, D. S. Wiersma, *Adv. Intell. Syst.* **2021**, *3*, 2000256.
- [702] G. Adam, A. Benouhiba, K. Rabenoroso, C. Clévy, D. J. Cappelleri, *Adv. Intell. Syst.* **2021**, *3*, 2000216.
- [703] D. Martella, S. Nocentini, D. Nuzhdin, C. Parmeggiani, D. S. Wiersma, *Adv. Mater.* **2017**, *29*, 1704047.
- [704] A. Nishiguchi, H. Zhang, S. Schweizerhof, M. F. Schulte, A. Mourran, M. Möller, *ACS Appl. Mater. Interfaces* **2020**, *12*, 12176.
- [705] L. Chen, Y. Dong, C.-Y. Tang, L. Zhong, W.-C. Law, G. C. P. Tsui, Y. Yang, X. Xie, *ACS Appl. Mater. Interfaces* **2019**, *11*, 19541.
- [706] P. Fischer, D. Sanz-Hernández, R. Streubel, A. Fernández-Pacheco, *APL Mater.* **2020**, *8*, 010701.
- [707] M. K. Al Mamoori, L. Keller, J. Pieper, S. Barth, R. Winkler, H. Plank, J. Müller, M. Huth, *Materials* **2018**, *11*, 289.
- [708] L. Keller, M. K. Al Mamoori, J. Pieper, C. Gspan, I. Stockem, C. Schröder, S. Barth, R. Winkler, H. Plank, M. Pohlitz, *Sci. Rep.* **2018**, *8*, 6160.
- [709] Z. Xiong, C. Zheng, F. Jin, R. Wei, Y. Zhao, X. Gao, Y. Xia, X. Dong, M. Zheng, X. Duan, *Sens. Actuators, B* **2018**, *274*, 541.
- [710] G. Williams, M. Hunt, B. Boehm, A. May, M. Taverne, D. Ho, S. Giblin, D. Read, J. Rarity, R. Allenspach, *Nano Res.* **2018**, *11*, 845.
- [711] F. Han, S. Gu, A. Klimas, N. Zhao, Y. Zhao, S.-C. Chen, *Science* **2022**, *378*, 1325.
- [712] K. Li, Z.-J. Luo, H. Jiao, Z. Gan, *Nanoscale Adv.* **2023**, *5*, 1299.
- [713] J.-F. Xing, M.-L. Zheng, X.-M. Duan, *Chem. Soc. Rev.* **2015**, *44*, 5031.
- [714] Y. Zhang, Y. Su, Y. Zhao, Z. Wang, C. Wang, *Small* **2022**, *18*, 2200514.
- [715] S. H. Park, T. W. Lim, D. Y. Yang, R. H. Kim, K. S. Lee, *Macromol. Res.* **2006**, *14*, 559.
- [716] J. F. Xing, X. Z. Dong, W. Q. Chen, X. M. Duan, N. Takeyasu, T. Tanaka, S. Kawata, *Appl. Phys. Lett.* **2007**, *90*, 131106.
- [717] A. Kneidinger, P. Schuster, C. Thanner, M. Eibelhuber, *Proc. SPIE* **2022**, 12135, 61.
- [718] R. Khaleghi Qusheh Bolagh, A. Salimi, K. Kabiri, A. Pourali, *J. Appl. Polym. Sci.* **2023**, *140*, e53375.
- [719] M. Schmid, D. Ludescher, H. Giessen, *Opt. Mater. Express* **2019**, *9*, 4564.
- [720] M. Reynoso, I. Gaudi, P. Measor, *Opt. Mater. Express* **2021**, *11*, 3392.
- [721] L. Rodriguez, H.-Y. Ahn, K. D. Belfield, *Opt. Express* **2009**, *17*, 19617.
- [722] D. B. Fullager, G. D. Boreman, T. Hofmann, *Opt. Mater. Express* **2017**, *7*, 888.
- [723] R. Ketchum, P. Alcaraz, P.-A. Blanche, *Opt. Mater. Express* **2022**, *12*, 3152.
- [724] U. Staudinger, G. Zyla, B. Krause, A. Janke, D. Fischer, C. Esen, B. Voit, A. Ostendorf, *Microelectron. Eng.* **2017**, *179*, 48.

- [725] Y. Liu, W. Xiong, L. Jiang, Y. Zhou, Y. Lu, *SPIE Proc.* **2016**, 9738, 973808.
- [726] K. Kurselis, R. Kiyani, V. N. Bagratashvili, V. K. Popov, B. N. Chichkov, *Opt. Express* **2013**, 21, 31029.
- [727] C. Zhang, H. Zheng, J. Sun, Y. Zhou, W. Xu, Y. Dai, J. Mo, Z. Wang, *Adv. Mater.* **2022**, 34, 2105996.
- [728] H. Yuk, B. Lu, S. Lin, K. Qu, J. Xu, J. Luo, X. Zhao, *Nat. Commun.* **2020**, 11, 1604.
- [729] O. Dadras-Toussi, M. Khorrami, A. S. C. Louis Sam Titus, S. Majd, C. Mohan, M. R. Abidian, *Adv. Mater.* **2022**, 34, 2200512.
- [730] D. T. Meiers, M. Rothhammer, M. Maier, C. Zollfrank, G. von Freymann, *arXiv preprint arXiv:2211.01193*, **2022**, <https://doi.org/10.1002/adem.202201688>.
- [731] M. Rothhammer, D. T. Meiers, M. Maier, G. von Freymann, C. Zollfrank, *arXiv preprint arXiv:2211.01271*, **2022**, <https://doi.org/10.48550/arXiv.2211.01271>.
- [732] D. Gräfe, A. Wickberg, M. M. Zieger, M. Wegener, E. Blasco, C. Barner-Kowollik, *Nat. Commun.* **2018**, 9, 2788.
- [733] S. C. Gauci, M. Gernhardt, H. Frisch, H. A. Houck, J. P. Blinco, E. Blasco, B. T. Tuten, C. Barner-Kowollik, *Adv. Funct. Mater.* **2022**, 2206303, <https://doi.org/10.1002/adfm.202206303>.
- [734] M. Gernhardt, V. X. Truong, C. Barner-Kowollik, *Adv. Mater.* **2022**, 34, 2203474.
- [735] S. Nocentini, D. Martella, C. Parmeggiani, D. S. Wiersma, *Adv. Opt. Mater.* **2019**, 7, 1900156.
- [736] H. S. Kang, S. Yang, *Light Adv. Manuf.* **2022**, 3, 3.
- [737] M. D. Schmid, A. Toulouse, S. Thiele, S. Mangold, A. M. Herkommer, H. Giessen, *Adv. Funct. Mater.* **2022**, 2211159, <https://doi.org/10.1002/adfm.202211159>.
- [738] S. K. Saha, J. S. Oakdale, J. A. Cuadra, C. Divin, J. Ye, J.-B. Forien, L. B. Bayu Aji, J. Biener, W. L. Smith, *ACS Appl. Mater. Interfaces* **2018**, 10, 1164.
- [739] Z. P. Yu, H. H. Li, T. T. Zhong, J. H. Park, S. F. Cheng, C. M. Woo, Q. Zhao, J. Yao, Y. Y. Zhou, X. Z. Huang, W. R. Pang, H. Yoon, Y. C. Shen, H. L. Liu, Y. J. Zheng, Y. Park, L. V. Wang, P. X. Lai, *Innovation* **2022**, 3, 100292.
- [740] G. Konstantinou, A. Boniface, D. Loterie, E. Kakkava, D. Psaltis, C. Moser, *Opt. Lasers Eng.* **2023**, 160, 107232.
- [741] S. Singer, Y. Xu, S. T. Skacel, Y. Bao, H. Zwickel, P. Maier, L. Freter, P.-I. Dietrich, M. Kaschel, C. Menzel, *Opt. Express* **2022**, 30, 46564.
- [742] D. Zhu, L. Xu, C. Ding, Z. Yang, Y. Qiu, C. Cao, H. He, J. Chen, M. Tang, L. Zhan, *Adv. Photonics* **2022**, 4, 066002.
- [743] R. Li, D. Jin, D. Pan, S. Ji, C. Xin, G. Liu, S. Fan, H. Wu, J. Li, Y. Hu, *ACS Nano* **2020**, 14, 5233.
- [744] J. Jang, K. Kang, N. Raeis-Hosseini, A. Ismukhanova, H. Jeong, C. Jung, B. Kim, J. Y. Lee, I. Park, J. Rho, *Adv. Opt. Mater.* **2020**, 8, 1901932.
- [745] M. Umar, D. Son, S. Arif, M. Kim, S. Kim, *ACS Appl. Mater. Interfaces* **2020**, 12, 55231.
- [746] C. Lv, X.-C. Sun, H. Xia, Y.-H. Yu, G. Wang, X.-W. Cao, S.-X. Li, Y.-S. Wang, Q.-D. Chen, Y.-D. Yu, *Sens. Actuators, B* **2018**, 259, 736.
- [747] B. W. Pearre, C. Michas, J.-M. Tsang, T. J. Gardner, T. M. Otchy, *Addit. Manuf.* **2019**, 30, 100887.
- [748] M. Pisanello, D. Zheng, A. Balena, F. Pisano, M. De Vittorio, F. Pisanello, *PLoS One* **2022**, 17, e0265678.
- [749] H. Wang, J. Wen, Z. Yan, M. T. Q. Sun, C. Ma, Z. Wang, L. Zhan, X. Zhang, C. Cao, X. Shen, C. Ding, C. Kuang, *Chin. J. Lasers* **2022**, 49, 2202009.
- [750] W. Chu, Y. Tan, P. Wang, J. Xu, W. Li, J. Qi, Y. Cheng, *Adv. Mater. Technol.* **2018**, 3, 1700396.
- [751] W. Xiong, Y. S. Zhou, X. N. He, Y. Gao, M. Mahjouri-Samani, L. Jiang, T. Baldacchini, Y. F. Lu, *Light Sci. Appl.* **2012**, 1, e6.
- [752] H.-Z. Cao, M.-L. Zheng, X.-Z. Dong, F. Jin, Z.-S. Zhao, X.-M. Duan, *Appl. Phys. Lett.* **2013**, 102, 201108.
- [753] J. Kaschke, M. Wegener, *Nanophotonics* **2016**, 5, 510.
- [754] A. Grabulosa, J. Moughames, X. Porte, D. Brunner, *Nanophotonics* **2022**, 11, 1591.
- [755] Z. Luo, D. Wang, K. Li, D. Zhong, L. Xue, Z. Gan, C. Xie, *J. Phys. Chem. Lett.* **2023**, 14, 709.
- [756] V. Hahn, N. M. Bojanowski, P. Rietz, F. Feist, M. Kozłowska, W. Wenzel, E. Blasco, S. Bräse, C. Barner-Kowollik, M. Wegener, *ACS Photonics* **2023**, 10, 24.
- [757] N. M. Bojanowski, A. Vranic, V. Hahn, P. Rietz, T. Messer, J. Brückel, C. Barner-Kowollik, E. Blasco, S. Bräse, M. Wegener, *Adv. Funct. Mater.* **2022**, 2212482, <https://doi.org/10.1002/adfm.202212482>.
- [758] P. Mueller, M. Thiel, M. Wegener, *Opt. Lett.* **2014**, 39, 6847.
- [759] S. van Kesteren, X. Shen, M. Aldeghi, L. Isa, *Adv. Mater.* **2023**, 2207101, <https://doi.org/10.1002/adma.202207101>.
- [760] J. B. Reeves, R. K. Jayne, L. Barrett, A. E. White, D. J. Bishop, *Nanoscale* **2019**, 11, 3261.
- [761] S. Puce, E. Sciurti, F. Rizzi, B. Spagnolo, A. Qualtieri, M. De Vittorio, U. Staufer, *Micro Nano Eng.* **2019**, 2, 70.
- [762] A. Toulouse, S. Thiele, K. Hirzel, M. Schmid, K. Weber, M. Zyrianova, H. Giessen, A. M. Herkommer, M. Heymann, *Opt. Mater. Express* **2022**, 12, 3801.
- [763] K. Liu, H. Ding, S. Li, Y. Niu, Y. Zeng, J. Zhang, X. Du, Z. Gu, *Nat. Commun.* **2022**, 13, 4563.
- [764] M. Tan, L. Huang, Z. Xiong, H. Zhang, Y. Liu, Z. Lu, Z. Liang, H. Liu, *Opt. Lasers Eng.* **2023**, 161, 107328.
- [765] V. F. Paz, M. Emons, K. Obata, A. Ovsianikov, S. Peterhänsel, K. Frenner, C. Reinhardt, B. Chichkov, U. Morgner, W. Osten, *J. Laser Appl.* **2012**, 24, 042004.
- [766] A. Abou Khalil, W. Gebremichael, Y. Petit, L. Canioni, *Opt. Commun.* **2021**, 485, 126731.
- [767] A. Abou Khalil, J.-P. Bérubé, S. Danto, J.-C. Desmoulin, T. Cardinal, Y. Petit, R. Vallée, L. Canioni, *Sci. Rep.* **2017**, 7, 11124.
- [768] S. Khadir, D. Andrén, R. Verre, Q. Song, S. Monneret, P. Genevet, M. Käll, G. Baffou, *ACS Photonics* **2021**, 8, 603.
- [769] M. Ryu, R. Honda, A. Cernescu, A. Vailionis, A. Balčytis, J. Vongsvivut, J.-L. Li, D. P. Linklater, E. P. Ivanova, V. Mizeikis, *Beilstein J. Nanotechnol.* **2019**, 10, 922.
- [770] Y. He, Q. Shao, S.-c. Chen, R. Zhou, *Addit. Manuf.* **2022**, 60, 103293.
- [771] S. Fritzsche, G.-R. Jaenisch, L. Pavasarytė, A. Funk, *Appl. Sci.* **2022**, 12, 10488.
- [772] M. Schmid, S. Thiele, A. Herkommer, H. Giessen, *Opt. Lett.* **2023**, 48, 131.
- [773] A. Grabulosa, J. Moughames, X. Porte, M. Kadic, D. Brunner, *arXiv preprint arXiv:2301.00983*, **2023**.



Hao Wang received his Bachelor (2012) and Ph.D. (2017) degrees from Harbin Institute of Technology, China. In 2016, he studied in École Polytechnique Fédérale de Lausanne, Switzerland. He joined Singapore University of Technology and Design in 2017, and currently is appointed as a senior research fellow. His research focuses on optics and photonics, metasurface, nanofabrication technologies, 3D printing, structural colors, and related applications.



Wang Zhang received his B.Sc. and M.Sc. degrees in Mechanical Engineering from Hunan University, and a Ph.D. degree from Singapore University of Technology and Design (2022). He is now a research fellow at SUTD. His main research interests lie in additive manufacturing of functional materials at the submicron scale, with potential applications in different areas such as nanophotonics, sensors, and mechanics.



Dimitra Ladika is a Ph.D. candidate at the Materials Science and Technology Department of the University of Crete, Greece. She received her M. Sc (2018) in “Photonics and Nanoelectronics” from the Department of Physics, University of Crete, and B. Sc. in Physics (2016) from University of Patras, Greece. She joined the research group of Dr. Maria Farsari at FORTH/IESL in 2017 and started her Ph. D in 2019 with the research about fabrication of nanophotonic devices, multiphoton polymerization, and nonlinear characterization of novel photosensitive materials. She was awarded an IKY scholarship from Greece and the European Union in 2022.



Haoyi Yu received his M.Sc. From Nankai University (2015) and was awarded a Ph.D. (2020) from RMIT university in Australia. Currently he is appointed as a research fellow at the Institute of Photonic Chips, in University of Shanghai for Science and Technology. His research interests include nanophotonics, artificial neural networks, and biophotonics. He has published over 10 research works in such journals as *Advanced Science*, *Light: Science and Application*, and *Advanced Photonics*.



Hongtao Wang is currently pursuing his Ph.D. degree at Singapore University of Technology and Design and National University of Singapore in the SUTD-NUS Joint PhD program. He received his B.S. degree from Beijing Institute of Technology, China (2015) and his MSc. degree from the same Institute in 2018. In 2017, he was a visiting student at the Center for Micro-Photonics, Swinburne University of Technology, Australia. His interests are in structural colors, orbital angular momentum, nanofabrication technologies, and related applications.



Cheng-Feng Pan received his B.Sc. degree in Optoelectronic Information Science & Engineering from Nanjing University of Science and Technology in 2020, and M.Sc. degree in Electrical and Computer Engineering from National University of Singapore in 2021. He is currently a joint Ph.D. student at Singapore University of Technology and Design and National University of Singapore. His research interest focuses on inverse design in nano optics, imaging optics, structure color, and nanofabrication.



Tomohiro Mori is a visiting research scientist at the Singapore University of Technology and Design from the Industrial Technology Center of Wakayama, Japan. He received his Ph.D. (2017) from Kagawa University, Japan, and previously worked at Nitto Denko Corporation from 2007 to 2013 in the fields of polymer design and stretching technology for optical films. His current research interests are photon upconversion materials, nanofabrication, and structural colors.



Maria Farsari is a Research Director at FORTH/IESL (joined in 2003). She is one of the first to develop laser-based 3D micro/nano printing, a field she first got involved in at Sussex University in 1997. She has pioneered the use of laser-made 3D scaffolds for cell growth and tissue engineering. Her research interests are light-enabled additive manufacturing, multiphoton lithography, and currently focus on architected materials for biomedical applications. She was an optical scientist in DeLaRue Holographics, and a founder of the Dublin-based company Xsil Ltd., a company specializing in the development of precision laser systems and robotics.



Mangirdas Malinauskas defended Ph.D. in 2010 at Vilnius University, Laser Research Center—“Laser Fabrication of Functional 3D Polymeric Micro/Nanostructures”, supervisor Prof. R. Gadonas. During career he has done traineeships at LZH (Prof. B.N. Chichkov) and IESL-FORTH (Dr. M. Farsari). In 2019–2022 a specially appointed Professor at Tokyo Institute of Technology (Japan), group of Prof. J. Morikawa. Currently he investigates fundamentals of laser 3D micro-/nano-structuring of cross-linkable materials for applications in micro-optics, nano-optics (photonics), and biomedicine at VU LRC. Laboratory funding is acquired via National, European, and worldwide (NATO, US Army) schemes. Optica Fellow in 2022.



Saulius Juodkazis is Professor of Nanophotonics and Director of Nanotechnology facility he established in 2011 at Swinburne University of Technology, Melbourne, Australia. He received his Ph.D. (cotutelle) in experimental physics and material sciences jointly from Vilnius University, Lithuania, and Lyon-I University, France. His current interests are in the fields of light-matter interaction occurring in small space (nanoscale) and time (femtosecond) domains. His research focuses on applying principles of light-field enhancement and its spectral control for applications in micro-optics, solid-state lighting, and solar energy conversion. He is Fellow of Optica and the International Society for Optics and Photonics (SPIE).



Min Gu is Executive Chancellor of the University Council and Distinguished Professor of University of Shanghai for Science and Technology. He was Associate Deputy Vice-Chancellor at RMIT University and a Laureate Fellow of the Australian Research Council. He is Fellow of the Australian Academy of Science and the Australian Academy of Technological Sciences and Engineering, and Foreign Fellow of the Chinese Academy of Engineering. He was awarded the Einstein Professorship, the W. H. (Beattie) Steel Medal, the Ian Wark Medal, the Boas Medal, the Victoria Prize for Science and Innovation, the Dennis Gabor Award, and the Emmett N. Leith Medal.



Joel K. W. Yang received his M.Sc. (2005) and Ph.D. (2009) degrees from the Massachusetts Institute of Technology. He is an Associate Professor in Singapore University of Technology and Design and holds a joint appointment as Principal Scientist I at the Institute of Materials Research and Engineering of A*STAR. His research interests include nanoplasmonics, 2D and 3D printed nano optical design elements, and sub-10-nm resolution lithography. He is Optica Fellow, NRF Investigator, and A*STAR Investigator. His accolades include the IPS Nanotechnology Medal and Prize, MIT Technology Review TR35 award, and the Singapore Young Scientist Award.